Why So Colourful? On the Optical Properties of Silicon Nanocrystals

by

Regina Sinelnikov

A thesis submitted in partial fulfillment of the requirements for the degree of

Doctor of Philosophy

Department of Chemistry
University of Alberta

Abstract

Owing to their rich, tailorable surface chemistry, low toxicity, and elemental abundance, silicon nanocrystals (SiNCs) present an attractive alternative to fluorescent organic dyes and traditional quantum dots for bioimaging, optoelectronics, and chemical sensors. These applications capitalize on the optical properties of SiNCs, which are not fully understood. Thus, the aim of this thesis was to gain a fundamental insight into the optical response of SiNCs and the factors that affect it. Size, surface chemistry, oxidation, and attachment of conjugated surface groups were taken into consideration when evaluating factors influencing the photoluminescence (PL) of SiNCs.

First, temperature-dependent steady-state and time-resolved PL measurements of SiNCs of different sizes and surface functionalities were carried out. A general emission mechanism based on the observed phenomena was proposed, suggesting that surface groups play a crucial role in SiNC PL. Next, the effect of oxidation on the stability of the SiNC optical response was evaluated. The convergence of the SiNC PL to the same region of the visible spectrum, regardless of the initial SiNC PL, was postulated to occur due to the formation of surface suboxide species. Lastly, the effect of interfacing SiNCs with conjugated surface groups was explored. Scanning tunneling spectroscopy revealed the formation of in-gap states, which accounted for the observed red-shift in SiNC PL, thus illustrating another way to tune SiNC PL via surface chemistry.

Overall, the research presented in this thesis demonstrated the intricate relationship that exists between size and surface when it comes to SiNC optical response, which should be taken into consideration for any future application design.

Preface

This thesis is an original work by Regina Sinelnikov. The research was conducted under the supervision of Professor Jonathan G. C. Veinot at the Department of Chemistry, University of Alberta.

Chapter 2 of this thesis has been published as Sinelnikov, R.; Dasog, M.; Beamish, J.; Meldrum, A.; and Veinot, J. G. C. "Revisiting an Ongoing Debate: What Role Do Surface Groups Play in Silicon Nanocrystal Photoluminescence?" *ACS Photonics* **2017**, *4* (8), 1920–1929. M. Dasog and myself conceptualized the project. I was responsible for the material synthesis, data collection and analysis, as well as the manuscript composition. The technical apparatus for temperature-dependent measurements was designed by A. Meldrum and myself, with the assistance of J. Beamish. Dasog, M. contributed to manuscript edits. A. Meldrum and J. G. C. Veinot J. G. C. were the supervisory authors and were involved with manuscript composition.

A section of Chapter 4 involving the mid-gap states was published as Angı, A.; Sinelnikov, R.; Meldrum, A.; Veinot, J. G. C.; Balberg, I.; Azulay, D.; Millo, O.; Rieger, B. "Photoluminescence through In-gap States in Phenylacetylene Functionalized Silicon Nanocrystals" *Nanoscale* **2016**, *8*, 7849–7853. A. Angı, from the Technical University of Munich, designed the project and performed most of the experiments, data analysis, and manuscript composition. I assisted with some of the material synthesis, TEM and PL lifetime characterization, and data analysis, as well as manuscript edits. I. Balberg, D. Azulay, and O. Millo at the Hebrew University of Jerusalem performed STM and STS measurements and contributed to manuscript composition. J. G. C. Veinot and A. Meldrum contributed to manuscript edits. B. Rieger was the supervisory author and was involved with manuscript edits.

Dedicated to my family.

Acknowledgements

The following thesis is the culmination of a five-year journey that I could not have completed without the help and support of many people. Indeed, it took a village to produce this brain-child and I am forever grateful for my wonderful community.

First and foremost, I would like to thank my research supervisor Dr. Jonathan G. C. Veinot for letting me spread my research wings but reeling me back in when I strayed too far. Your constant support, encouragement, and belief in me was invaluable. Thank you for teaching me the power of the written word and how to properly convey my scientific message. Second, I would like to thank my mentor, Dr. Mita Dasog. Thank you for taking me under your wing and guiding me throughout my research years at the U of A. You were and remain a constant source of inspiration and awe for me, thank you for being the best role-model and mentor one can ask for. Next, I would like to extend my gratitude to Dr. Al Meldrum for welcoming a newbie chemist into a physics lab and letting me play with lasers. Your passion and dedication to science is truly infectious. Thank you to my supervisory committee: Dr. Juli Gibbs and Dr. Rylan Lundgren for providing valuable feedback throughout my PhD years and Dr. Sarah Styler for joining my examining committee. Dr. Kalaichelvi Saravanamuttu, it was an honor and a true joy to have you as my external examiner.

The work presented in this thesis could not have been realized without the help of the support staff at the University of Alberta. Without further ado, my everlasting gratitude to the following people: Dr. Wayne Moffat and Jennifer Jones (Analytical Services), Greg Popowich (TEM), Dr. Kai Cui (HR-TEM), Dr. Anqiang He and Dr. Shihong Xu (XPS), Mike Xia (AQY), Kim Do (electronic shop), Jason Dibbs (glass shop), Don Mullin (He refrigerator), Paul Crothers and Dieter Starke (machine fabrication), and Anita Weiler (graduate student assistant and all around badass). To the vivacious Dr. Anna Jordan, thank you for donating your time and expertise to proofreading my thesis.

Thank you to the wonderful Veinot group family, former and present group members included. You made our work environment so welcoming and fun. It was a pleasure to come to work with such a talented group of people every day. Special thanks to Dr. Leah Coumont, Dr. Zhenyu (Kevin) Yang, Dr. Christina Gonzalez, Dr. Lida Hadidi, Dr. Morteza Javadi, Dr. Muhammad Iqbal, Dr. Tapas Purkait, Dr. Hosnay

Mobarok, Dr. Angelique Faramous, Dr. Philippe Kitschke, and Dr. Muhammad Amirul Islam. Your guidance, insights, and comments were invaluable to me. My wonderful office mates: Kelsey Deutsch, Alyx Thiessen, Christopher Jay Robidillo, and Haoyang (Emmett) Yu, thanks for being such a good distraction. Maybe without you I would have finished this thesis sooner. And to my sister from another mister and fellow newly minted doctor, Dr. Maraym Aghajamali, words cannot describe how grateful I am to have had you beside me every step of the way. Your warmth, support, and love of life is contagious.

Outside of the Veinot group, I would like to thank the whole ATUMS family. It was a pleasure to meet such a diverse group of people and I have enjoyed your company during the student exchanges and the annual meetings. Particularly, I would like to thank Leah Veinot and Sergei Vagin for facilitating my research exchange in Germany, and Dr. Marc Tornow and Simon Pfaehler for welcoming me to your lab. Dr. Arzu Angı, Dr. Tobias Helbich, Dr. Alina Lyuleeva, Reka Csiki, Markus Pschenitza, and Marc Kloberg thank you for being such amazing collaborators and company. Stephen Lane, Kirsty Gardner, and William Morrish thank you for adopting me into your physics family and showing me the way in your lab.

I would like to also thank the people and groups that kept me sane throughout these rigorous years. The amazing teams of The University of Alberta Nanotechnology Group, Lets Talk Science, and UAlberta WIC I was proud and honored to be part of your groups and all the impactful outreach we have accomplished. For moral support, I would like to thank Kate Powers, Kim Hyson, Dr. Olena Shynkaruk, Dr. Abishek Kannan Iyer, Dr. Melanie Lui, Dr. Anton Oliynyk, and Evelyn Asiedu. To my wonderful roommates over the past year, Dr. Aleksandra Popowich and Chester, thank you for making this past year bearable.

Lastly, but most importantly, I would like to thank my amazing, generous, and loving family. Thank you for always believing in me. I hope to one day become even half of the person you believe me to be.

Table of Contents

List of Tables

List of Figures

List of Schemes

List of Abbreviations

AIBN	Azobisisobutyronitrile
AQY	Absolute quantum yield
a.u.	Arbitrary units
CB	Conduction band
DFT	Density functional theory
DI	Deionized
DOS	Density of states
E_g	Band-gap energy
EI-MS	Electron ionization mass spectrometry
EMA	Effective mass approximation
EPM	Empirical pseudopotential method
ETB	Empirical tight-binding model
FTIR	Fourier transform infrared
FWHM	Full width at half maximum
HF	Hydrofluoric acid
H-SiNCs	Hydride-terminated silicon nanocrystals
HSQ	Hydrogen silsesquioxane
HPLC	High-performance liquid chromatography
LASER	Light amplification by stimulated emission of radiation

LED	Light-emitting diode
MIBK	Methyl isobutyl ketone
NC	Nanocrystal
NMR	Nuclear magnetic resonance
PL	Photoluminescence
PMT	Photomultiplier tube
QC	Quantum confinement
QD	Quantum dot
QY	Quantum yield
rpm	Revolutions per minute
R-SiNCs	Alkyl-passivated silicon nanocrystals
RT	Room temperature
SiNC	Silicon nanocrystal
SiNP	Silicon nanoparticle
SRO	Silicon-rich oxide
STM	Scanning tunneling microscopy
STS	Scanning tunneling spectroscopy
TEM	Transmission electron microscopy
THF	Tetrahydrofuran
TRPL	Time-resolved photoluminescence
UV	Ultraviolet
UV-vis	Ultraviolet-visible (spectroscopy)
VB	Valence band
X-SiNCs	Halide-terminated silicon nanocrystals
XPS	X-ray photoelectron spectroscopy

Chapter 1

Introduction

1.1 Nanomaterials

In his famous lecture: "there's plenty of room at the bottom" Dr. Richard Feynman challenged the scientific community to realize the potential of nanoscience.[3] A burgeoning area of research, nanoscience involves the study of materials and phenomena in the nanoscale (1–100 nm in at least one dimension) and has attracted the interest of chemists, physicists, biologists, and engineers alike. With a promise to address several of mankind's challenges in healthcare, energy conversion and storage, and technology, the synthesis and application of nanomaterials is a rapidly evolving area of research.

1.1.1 Quantum Confinement Effect

One of the most fascinating phenomena of nanomaterials is the quantum confinement (QC) effect, which describes the change in the energy band structure of a material as a result of size reduction from bulk to nanoscale.[4–7] More specifically, when electrons and holes are spatially confined to one or more dimensions due to size constraints, quantization of the energy levels is observed. As a result, nanomaterials exhibit size-dependent properties. The dimensions at which QC effects manifest themselves are material dependent and can be related to the bulk Bohr radius, a_B, of an exciton,[8] given by:

$$a_B = \frac{\hbar^2 \epsilon}{\mu e^2} \tag{1.1}$$

where $\hbar$ is the reduced Planck's constant, ϵ is the material dielectric constant, μ is the reduced mass of the electron-hole pair, and e is the elementary charge. When a material approaches in size its Bohr exciton radius, QC effects become more pronounced, leading to an increase in band gap energies and blue-shift in absorption and emission spectra. An additional consequence of QC effects is the disruption in the continuity of the electronic density of states (DOS), leading to discrete energy levels in one or more dimensions. Quantum dots (QD) exhibit confinement in all three dimensions, thus displaying atomic-like energy levels. QDs also are known as "artificial atoms" or semiconductor nanoparticles. Materials with spatial confinement in two dimensions are known as quantum wires. Lastly, confinement in one plane results in a quantum well, where carriers are free to move in two dimensions.[9,10] The QC effect on the DOS of materials going from bulk to QD is summarized in Figure 1.1.

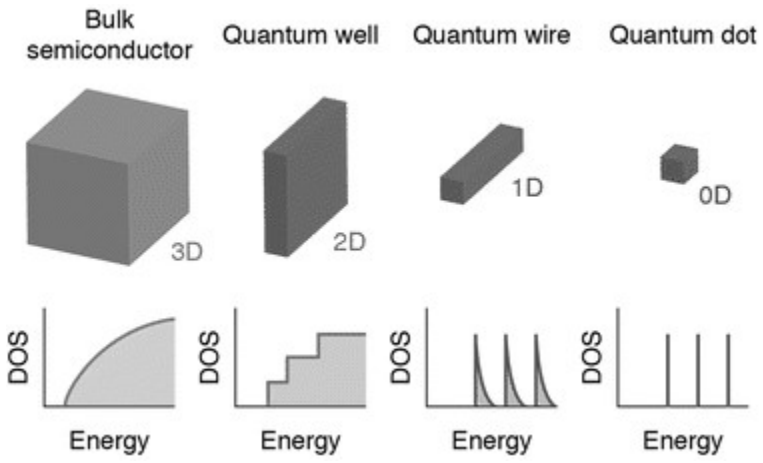

Figure 1.1: *The electronic density of states of a semiconductor as a function of dimension. Adapted with permission from ref 8.*

1.1.2 Quantum Dots

Starting with the seminal work of Rossetti et al.[11,12] demonstrating size-dependent optical properties of CdS QDs, the scientific community has dedicated great efforts to the synthesis and control over the photodynamics of various QDs. Over the past four decades, QDs from II-VI compounds (e.g., ZnS, HgS, CdE, E=S, Se, Te),[13–16] III-V compounds (e.g., InP, GaN, GaAs),[17–19] IV-VI compounds (e.g., SnS, PbE, E=S, Se, Te),[20–23] group IV (e.g., Si, Ge, Sn)[24–26] semiconductors, and even core-shell structures

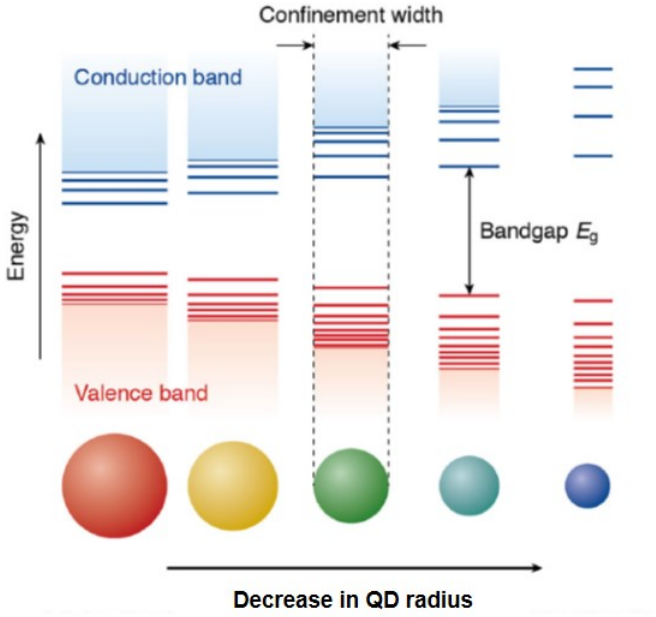

Figure 1.2: *Schematic representation of the QD band gap as a function of size. Adapted with permission from ref 8.*

(e.g., CdSe@ZnS)[27] and alloy QD (e.g., AlGaN, Cu_2ZnSnS_4, CuInSe)[28–30] have been synthesized. More recently, lead halide perovskite ($CsPbX_3$, X = Cl, Br, and I)[31] and carbon-based[32] QDs also have been investigated.

One underlying commonality among all QD materials is their size-dependent properties, particularly the observed increase in band gap energy upon decrease in particle size (Figure 1.2). One early correlation between particle size and band gap is the effective mass approximation (EMA), which draws the analogy between the QD exciton and the quantum mechanical particle-in-a-box problem. Further expansion of the model, accounting for the Coulombic attraction between an electron and a hole, resulted in a model expressed as follows:[33,34]

$$E_{g(QD)} = E_{g(bulk)} + \frac{h^2}{8R^2}\left(\frac{1}{m_e} + \frac{1}{m_h}\right) - \frac{1.8e^2}{4\pi\epsilon_0\epsilon R} \tag{1.2}$$

where E_g is the band gap of the bulk or QD semiconductor, h is Planck's constant, R is the QD radius, and m_e and m_h are the effective masses of the electron and hole, respectively. This equation relates the inverse relationship between the QD band gap and its radius and accounts for material dependency (dielectric constant). While the

model assumes a perfectly spherical QD, it has been employed successfully to predict the optical band gap of various QDs. However, as will be discussed in Section 1.3, the optical properties of QDs in general and SiQDs particularly are more complex and cannot be explained simply with the EMA model.

Nonetheless, the exquisite optical properties of QDs, such as narrow, size-tunable emission, full rendition of the visible spectrum, photo- and thermal stability, and high efficiency, make them very appealing active materials for a multitude of applications.[9]

1.2 Silicon Nanocrystals

Silicon nanocrystals (SiNCs), a fascinating subclass of QDs, boast full visible light colour emission, rich surface chemistry, and compatibility with existing electronics industry.[24,35,36] Moreover, an advantage silicon has over many other QDs is its abundance (second most abundant element in Earth's crust), low toxicity, and emission in the solid-state.

1.2.1 Theoretical Background

Bulk silicon is known to be an indirect semiconductor, where the minimum of the conduction band (CB) and the maximum of the valance band (VB) do not align in k-space (Figure 1.3a).[37] Consequently, a phonon (lattice vibration) must be absorbed or emitted in order for an optical transition to occur (conservation of lattice momentum). The probability for phonon–electron coupling is low; as a result, under standard conditions, bulk Si is non-emissive.[38] However, the observation of visible, room-temperature emission from nanocrystalline and porous silicon suggests that the band structure picture is different in the nanoscale.[39–42]

The confinement of an electron and hole in real space (the nanocrystal) leads to an increased uncertainty of the crystal momentum and broadening of the exciton wavevector in k-space. Thus, the tails of the electron and hole (exciton) wavefunctions overlap, allowing for non-phonon assisted direct transition (Figure 1.3b–c), also known as "quasi-direct" recombination. The breakdown of the k-conservation rule has been calculated theoretically[43] and observed experimentally for silicon by Kovalev et al.[44] Interestingly, an increase in the ratio of zero phonon- to phonon-assisted transitions with decreasing crystal size was observed, suggesting that the smaller the nanocrystal

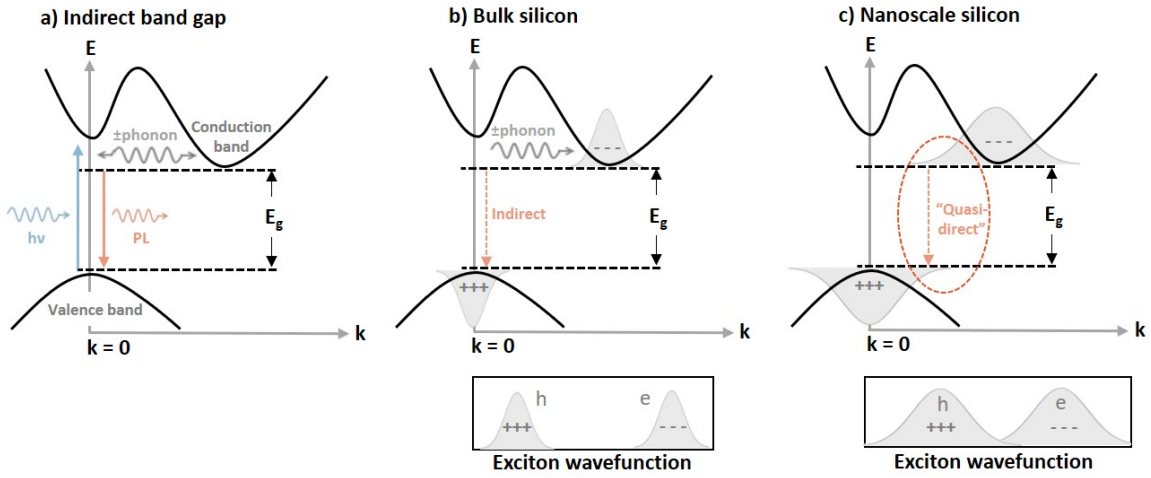

Figure 1.3: *Simplified band structure diagram of an indirect band gap semiconductor (a). Corresponding exciton wavefunctions of bulk (b) and nanoscale silicon (c) illustrating wavefunction broadening leading to "quasi-direct" band gap in SiNCs.*

size, the more "quasi-direct" its band gap. Another ramification of the silicon band gap transitioning from indirect to "quasi-direct" is the decrease in radiative lifetime. Bulk silicon exhibits millisecond lifetimes due to the slow, phonon-assisted radiative recombination.[45] In the nanoscale, shorter lifetimes ranging from hundreds of microseconds for large SiNCs to single digit values for smaller NCs are predicted.[7,46] This has been shown experimentally for both porous silicon[47,48] and SiNCs.[49] Direct band gap transitions in SiNCs, associated with nanosecond lifetime, have been predicated theoretically for small nanocrystals (∼1 nm).[50] Experimentally, nanosecond lifetimes have been observed for SiNCs and are proposed to occur due to tensile-strain[51,52] or an electronegative capping/environment, which changes the silicon band structure to become more direct in nature.[53] However, it is still unclear whether the origin of the observed emission is arising from the silicon core or is due to surface states.

1.2.2 Synthesis of Silicon Nanocrystals

Over the past two decades, a multitude of synthetic routes have been established for rendering free-standing SiQDs. These methods can be classified broadly into four different classes: i) physical methods, ii) gas-phase, iii) solution-phase, and iv) solid-state based methods. The resulting SiQDs are commonly crystalline in nature (SiNCs) or amorphous (SiNPs).

Following the discovery of porous silicon and the observation of PL from silicon nano-domains, several top-down approaches have been developed for the formation of SiNPs. These physical approaches include laser ablation,[54,55] ion-implantation,[56–58] ultrasonication,[59–61] and ball milling.[62] However, most of these methods render particles with poor size control. Gas-phase synthesis of SiNCs generally involves the pyrolysis of silanes using a pulsed laser[63–66] or nonthermal (cold) plasma.[67,68] Various chemical vapour deposition approaches also have been utilized to produce SiNPs from silane precursors.[69–71] Modification of the latter method afforded full-visible-spectrum emission from SiNCs.[72] The most common approach to solution-based synthesis of SiNCs involves the reduction of silanes or their derivatives using Na,[73] Zintl salts,[74] Na(naphthalide),[75] or $LiAlH_4$.[76,77] More recently, microwave-assisted[78] and photochemical[79] one-pot synthesis methods have been utilized to produce silicon-containing NPs. However, solution-based approaches have been known to produce SiNPs with PL predominantly in the blue-region of the visible spectrum, irrespective of size.

Lastly, solid-state approaches generally employ the thermal processing of silicon containing precursors, such as silicon-rich oxides (SROs)[80,81] or sol-gel derived Si-rich polymers.[82–84] Under high temperature and/or reducing conditions, these silicon precursors are reduced to SiNCs embedded in the silica matrix; these can be liberated by HF or HNO_3 treatment. Hydrogen silsesquioxane (HSQ) is a commercially available SRO precursor used to produce SiNCs in a silica-like matrix upon annealing under reducing conditions and high temperatures.[85] Varying the annealing temperature between 1100 and 1400 °C affords size control from 3 to 90 nm.[86] Control over the size of SiNCs is crucial for any discussion revolving around size-dependent PL, therefore, the HSQ method is used in this work.

1.3 Optical Properties of Silicon Nanocrystals

The scope and complexity of silicon photonics is a captivating area of study that has dominated the field ever since room temperature emission from porous silicon was observed. Questions regarding the origin of SiNC luminescence, effect of crystal size, and various surface groups, as well as strategies for improvement of SiNCs quantum efficiency are all active areas of research. The findings to date with respect to these fundamental questions are summarized below.

1.3.1 Size Effect

As was discussed in Section 1.1.1, QC effects can play a role in tuning the absorption and emission of nanoscale materials by changing the band gap energy. Theoretical models correlating SiNC size with band gap energy include the EMA model, the empirical tight-binding (ETB) model,[46,87] and the empirical pseudopotential method (EPM).[88] Unfortunately, none of these methods are able to describe experimental results satisfactorily, as was demonstrated by Garrido et al.[89] One major shortfall is the limitation in describing surface defects, stress, and interface.[90]

To date, size-dependent PL (as determined by PL band maximum) has been demonstrated for SiNCs produced via the HSQ method and nonthermal plasma;[72,86] the latter remains as the only method to exhibit a full visible spectrum based on nanocrystal size (Figure 1.4). The possibility that SiNC emission greater than 2.1 eV is a result of QC has been disputed by Wen et al. and was attributed to surface related states.[91] SiNCs derived from HSQ or cold plasma exhibit microsecond lifetimes, suggesting that the radiative recombination is still indirect in nature. More recently, however, short (nanosecond) lifetimes also have been detected in the same systems.[92,93] Yang et al. attributed the short lifetimes to oxidation defects from incomplete passivation of the silicon surface.[92] Brown et al. suggested that the fast decay originates from minigaps forming within the conduction and valence bands of small (2–3 nm) SiNCs.[93]

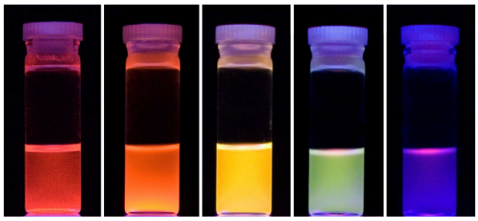

Figure 1.4: *Full visible spectrum emission from variable size SiNCs prepared by nonthermal plasma.*

The effect of particle size also comes into play when considering the quantum yields (QY) of SiNCs. Defined as the ratio of the number of emitted photons to the number of absorbed photons, QY is an important figure of merit when evaluating luminescent materials. A meticulous study carried out by Mastronardi et al. on size-selected particles revealed the trend in the SiNCs QY with size; QY decreased from 43% for 2 nm SiNCs to just 5% for 1 nm SiNCs.[49] This trend was attributed to an increase in

non-radiative pathways for smaller particles arising from surface defects and breakdown of crystallinity. In a more recent report, the increase in nonradiative decay for smaller nanocrystals was explained by a finite confinement model.[94] As the nanocrystal size decreases, the probability of finding an electron or hole outside the nanocrystal increases, either of which can recombine nonradiatively.

1.3.2 Surface Effects

The nature of the SiNC surface has been shown to be just as important as its size in terms of optical response. Most synthetic routes to producing SiNCs render particles that are hydride-, halide-, or suboxide-terminated. However, in order to increase photostability and solution processability, SiNCs are passivated generally with various organic ligands through covalent bonding. The effect of common surface termination on the optical response of SiNCs is summarized below.

H-termination. Generally, the negligible role that hydrogen atoms play in the optical response of SiNCs has been accepted, and hydride terminated SiNCs (H-SiNCs) are treated as reference materials for QC effects.[95] H-SiNCs have been shown to have microsecond lifetimes and PL quantum yields anywhere from 3.2% to 52%.[96,97] However, H-SiNCs have poor solution dispersibility and are prone to oxidation; thus, surface passivation is necessary.

C-termination. Similar to the case of H-SiNCs, the effect of SiNCs passivation with non aromatic carbon-based ligands (R-SiNCs) on their optical response is considered minimal.[98,99] The most common route to functionalization of SiNCs with alkenes or alkynes is via hydrosilylation, which involves the addition of Si–H across an unsaturated bond. A multitude of routes to initiate hydrosilylation have been reported, including thermal,[100] photochemical,[101] catalytical,[102–104] and via radical initiation,[105–107] some of which are summarized in Scheme 1.1. Thermal hydrosilylation is one of the most commonly used functionalization methods, largely due to its effective surface coverage and ability to use the ligand as both the solvent and reactant.[106] However, thermal hydrosilylation requires high-boiling point ligands and/or solvents, which can withstand the reaction conditions (100–190 °C). In addition, Yang et al. showed thermal hydrosilylation leads to oligomerization,[100] creating an insulating layer that can be problematic for optoelectronic applications where charge transfer is required.[108] Thus, over the past decade, multiple alternative hydrosilylation routes on SiNCs have been

explored.

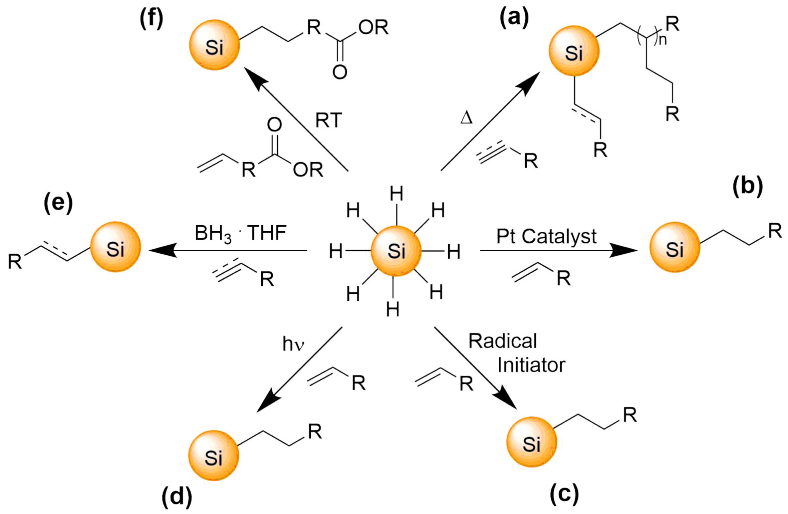

Scheme 1.1: *Schematic for common hydrosilylation methods for H-SiNCs: a) thermal, b) platinum-catalyzed, c) radical-initiated, d) photochemical, e) Lewis acid catalyzed, f) ligand self-catalyzed.*

Room-temperature hydrosilylation can be catalyzed by metal (H_2PtCl_6, Scheme 1.1b)[76,77] or Lewis acid catalysts (BH_3·THF, Scheme 1.1e), which eliminates the need for high boiling point ligands and presents greater surface group tolerance.[102] However, compared to thermal hydrosilylation, poorer surface coverage is afforded by these methods, leading to surface oxidation. In addition, trace metal impurities have been implicated in degradation of the optical response of SiNCs.[109] A catalyst free hydrosilylation method that is carried also out at room temperature is photochemical hydrosilylation (Scheme 1.1d).[101] The reaction can be done in a neat solution of the reactant, however, SiNCs larger than 5 nm are not as effectively passivated as smaller particles, and reaction times can be quite long (18 h).[110] Interestingly, SiNCs functionalized via photochemical hydrosilylation had higher QY compared to those functionalized via thermal hydrosilylation.[92] An alternative room temperature hydrosilylation method that requires bifunctional alkenes with distal polar moieties, was introduced by Yu et al. (Scheme 1.1f).[111] While a reaction that proceeds with no external stimuli is appealing, the long duration of the reaction (12–120 h) and the poor surface coverage detract from its allure. In addition, significant oxidation of the surface was observed, as well as lower reactivity for larger SiNCs.

Radical-initiated hydrosilylation has been explored extensively as an alternative

for thermal hydrosilylation (Scheme 1.1c). Höhlein et al. reported a room temperature hydrosilylation that was initiated by diazonium salts.[105] The reaction proceeded relatively quickly (2 h) and diverse surface group tolerance was demonstrated. However, complete surface coverage was not achieved, leading to oxidation. A follow up study with diaryliodonium salts demonstrated greater nanocrystal size tolerance and potential for in-situ ring-opening polymerization.[107] Traditional radical initiators such as azobisisobutyronitrile (AIBN) and benzoyl peroxide were also used to induce hydrosilylation on the surface of silicon in the presence of various alkenes and alkyens.[106] The reactions were carried out at the decomposition temperature of the radical used. Good monolayer passivation of SiNCs of various sizes was reported for radical-initiated hydrosilylation.

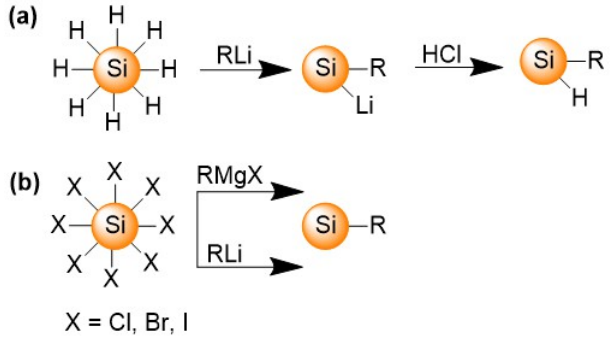

Scheme 1.2: *Schematic for alternative functionalization methods of SiNCs using organolithium and Grignard reagents.*

While hydrosilylation is the most common method for SiNC surface passivation and the formation of Si–C linkages, it is not the only one. Höhlein et al. demonstrated H-SiNCs can be directly reacted with organolithium reagents via Si–Si bond cleavage and the formation of a labile Si–Li surface species (Scheme 1.2a).[112] The silicon surface can be then further reacted with an additional surface group, to form mixed SiNC surface, or quenched by hydrochloric acid. In a recent report, R-SiNCs passivated by the organolithium method exhibited better QYs and external quantum efficiency in LED devices compared to their analogous R-SiNCs passivated by radical-initiated hydrosilylation.[113] Suggesting that even the functionalization method employed can play a role in the optical response of SiNCs. Another pathway for the passivation of SiNCs with alkyl groups involves the reaction of halide-terminated SiNCs (X-SiNCs, X=Cl, Br, I) with Grignard or organolithium reagents (Scheme 1.2b).[114–116] The resulting R-SiNCs

exhibit blue PL and nanosecond lifetimes, regardless of size, as a result of oxynitride and oxychloride species (vide infra).

One common characteristic of all the methods summarized thus far is the increased photostability of the resulting R-SiNCs.[117] Generally, the photodynamics of SiNCs do not change upon functionalization. However, the picture changes if other heteroatoms exist in the system.

N-termination. Early in the history of SiNCs, a disparity between solution-based methods and other methods has been observed with respect to the optical properties of the resulting SiNCs. Solution-based methods rendered SiNCs with emission in the blue region of the visible spectrum and nanosecond lifetimes.[65,75,76] Originally believed to be due to a direct band gap transition in small SiNCs, it was shown later that the blue emission was associated with nitrogen based impurities.[118] Direct functionalization of SiNCs with alkylamines or arylamines results in emission spanning from blue to yellow, depending on the ligand.[78,119–121] The origin of this emission was attributed to a charge transfer from the Si core to an oxynitride related surface state.[121]

O-termination. The formation of Si–O linkages can be achieved by reacting X-SiNCs with alcohols at room-temperature, as was demonstrated by Bley[74] and Shirahata[122] (Scheme 1.3a). Reaction of X-SiNCs with methanol rendered methoxy terminated SiNCs, which degraded over time and lost their PL, most likely due to oxidation. Further reaction of the methoxy-SiNCs with octyltrichlorosilane led to the formation of cross-linked siloxane corona around the SiNC core and stabilization of the PL (Scheme 1.3b).[123] Similar surface coverage was obtained by first reacting H-SiNCs with nitric acid, followed by the addition of trimethoxy(octadecyl)silane (Scheme 1.3b).[66] Since Si–H bonds can add across carbonyls (C=O), aldehydes and ketones have been used to hydrosilylate H-SiNCs to form Si–O linkages under microwave and/or thermal treatment (Scheme 1.3d–e).[124,125] For red-emitting SiNCs, a blue-shift in PL maximum was reported when particles were passivated with oxygen containing groups, such as alkoxy groups, CO_2, and trioctylphosphine oxide.[117,124] As will be discussed in the next section, the optical properties of SiNCs change upon oxidation, so the observed PL maximum changes may be related to partial oxidation of the SiNCs.

Halide-termination. The effect of halides on the optical response of SiNCs is not apparent immediately. As discussed above, halide-terminated SiNCs have been used extensively as platforms for further functionalization with organolithium or Grignard reagents,[114,126,127] however, the former are hard to isolate and study on their own. In

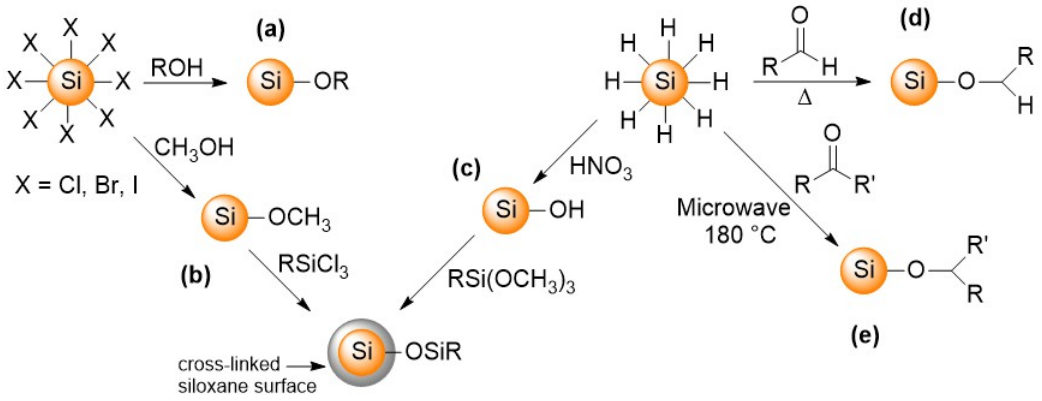

Scheme 1.3: *Schematic for routes to form Si–O linkages with halide-terminated SiNCs (a–b) and hydride-terminated SiNCs (c–e).*

2015, Dasog and co-workers showed that chlorination, bromination, or iodination of SiNCs results in etching of the silicon surface and quenching of the PL.[128] However, upon further reaction with Grignard reagents the PL was recovered. Interestingly, the resulting colour emission varied depending on the halide used. SiNCs derived from chloride exhibited blue PL, those derived from iodide appeared to oxidize and exhibit yellow PL, irrespective of crystal size, while those derived from bromide maintained core emission. In a related study, *N*-bromosuccinimide was used to brominate and then passivate the surface of SiNCs. The original SiNC PL was preserved in this case as well.[129] Another interesting consequence of surface halides is their effect on QY. DFT calculations of SiNCs passivated with chlorides (and other heteroatoms) suggest that at low concentrations of chloride higher recombination rates are expected and, as a result, higher QYs.[130] Experimentally, improved QY were observed for alkyl passivated SiNCs with trace amounts of halides compared to those without halogens present.[103,104]

Table 1.1: *Summary of observed SiNC PL and Possible Culprits*

PL Colour	Possible Culprits
Blue	Size (QC); oxynitride surface state;[118] oxychloride surface state[128]
Blue-green	Oxycarbide;[117] conjugated oxynitride groups[119,120]
Yellow	Size (QC);[85] conjugated oxynitride groups;[131] silicon suboxides[117]
Orange	Size (QC);[132] silicon suboxides[117]
Red-near IR	Size (QC)[86]

Surface chemistry plays an important role in the optical response of SiNCs. Table 1.1 summarizes the observed SiNC PL emission colours and possible culprits affecting it. A nice demonstration of the profound effect various surface ligands can have on the colour emission of SiNCs was reported by Dasog et al.[117] (Figure 1.5), where SiNCs of the same size (and preparation method) were passivated with different ligands, resulting in colour emission spanning the visible spectrum.

Figure 1.5: *SiNCs passivated (from left to right) by dodecylamine, acetal, diphenylamine, trioctylphosphine oxide, and dodecyl under UV illumination. Reprinted with permission from ref. 115. Copyright ©2014 American Chemical Society.*

1.3.3 Temperature Dependence

Low-temperature studies of SiNCs can provide insight into their optical response and help distinguish between surface and core effects. Band gap expansion at low temperatures, $E_g(T)$, is a well-known phenomenon in bulk semiconductors[133,134] and often is described by the modified Varshni model:

$$E_g(T) = E_{g,0} - A \cdot \left(\frac{2}{\exp(\frac{\Omega}{k_B T}) - 1} + 1 \right) \tag{1.3}$$

where $E_{g,0}$ is the band gap energy of the material at 0 K, A is a temperature-independent constant describing the electron–phonon interaction strength, Ω is the average phonon energy, and k_B is the Boltzmann constant. This relation appears to hold for SiNCs as well, where blue-shift in PL was reported upon temperature decrease.[135–137] Such behaviour is a strong argument in favour of core-emission in SiNCs.

In addition to the shift in PL maximum, an increase in PL lifetimes generally is observed for QDs at lower temperatures.[138,139] For silicon, the increase in decay times

is attributed to population of the triplet state at lower temperatures. Since transitions from the triplet states are parity forbidden, electron–hole recombination rates from that state are slower. Calcott et al.[140,141] expressed the temperature dependence of the singlet-triplet exchange, and thus the radiative recombination rate, Γ_r, as follows:

$$\Gamma_r = \frac{3\Gamma_T + \Gamma_S \exp(-\frac{\Delta}{k_B T})}{3 + \exp(-\frac{\Delta}{k_B T})} \tag{1.4}$$

where Γ_T and Γ_S are the decay rates from the triplet and singlet states, respectively, Δ is the singlet–triplet exchange energy, and $k_B T$ represents the thermal energy. Thus, time-resolved photoluminescence measurements at cryogenic temperatures can be used to analyze the radiative recombination rates in SiNCs. Together with steady-state PL measurements, low temperature studies are powerful tools for the evaluation of the optical response of SiNCs.

1.3.4 The Role of Oxygen in SiNC PL

The nature and effect of oxygen moieties on the optical properties of SiNCs is a heavily debated area of study. Since many of the promising applications of SiNCs in bioimaging, photovoltaics, and sensing arise from the optical properties of SiNCs, the role of oxygen must be elucidated fully. Silicon forms strong, thermodynamically stable bonds with oxygen, which drives the unwanted oxidation of silicon. Numerous reports recorded the oxidation of H-SiNC and even the gradual oxidation of R-SiNCs under ambient conditions. The effect is even more drastic for SiNCs dispersed in alcohols and water.[142,143] Both blue- and red-shift in PL maxima of SiNCs as a result of exposure to oxygen have been reported, seeming to vary depending on the nature of the SiNCs.[2,58,144] Additionally, a decrease in PL intensity and absolute QY of SiNCs as a result of exposure to oxygen has been observed by several researchers,[132] while others reported photoactivation (increase in PL intensity) as a result of oxidation.[145]

The nature of the oxygen surface species affecting the optical response of SiNCs has not been determined definitely. Among the implicated moieties are Si/SiO_2 interfaces, bridging oxygen bonds (Si–O–Si), silicon hydroxyls (Si–OH), back-bonded oxygen (H–Si–O), alkoxy bonds (Si–O–C), and silanones (Si=O).[146] The latter has been observed in bulky molecular systems but is disputed to occur on unstrained silicon surfaces.[147–150] Part of the challenge in identifying the "culprit" is the lack of experimental tools

capable of probing each surface state individually. Several studies utilized Fourier-transform infrared spectroscopy (FTIR) in tandem with PL spectroscopy to investigate the effect of oxidation on the surface of SiNCs.[144,145,151] However, an increase in the signals of various combinations of the above-mentioned functional groups have been observed, with no conclusive correlation between PL change and a specific surface state.

Theoreticians have proposed several models to explain the observed PL maximum shift in SiNCs upon exposure to oxygen. Kanemitsu first proposed surface-mediated emission associated with silicon suboxide defects, where a photon is absorbed by the SiNC core and recombines at the interface between the Si/SiO_2 matrix.[152] Koch and Petrova-Koch expanded on this model, proposing three possible emission pathways: i) fast carrier-radiative recombination in the SiNC core, leading to a blue emission; ii) recombination between a bound electron and a VB hole, leading to a yellow-green emission; and iii) slow recombination between a bound electron and a surface-bound hole, leading to a red emission, summarized in Figure 1.6a.[1,153]

Wolkin et al.[2] suggested a 3-zone model based on crystallite diameter: i) 3–5 nm, zone I, ii) 1.5–3 nm, zone II, and iii) below 1.5 nm, zone III (Figure 1.6b). In zone I, free excitonic recombination occurs, while in zone II radiative recombination occurs between an electron trapped in a surface-state (Si=O) and a free hole. Lastly, in zone III, SiNC emission completely deviates from QC and occurs between two trapped carriers. While this model is straightforward and accounts for some experimental observations, the existence of a Si=O bond (outside of complex molecular systems) has been disputed. Rather, it was shown to be an intermediate bond leading to Si–O–Si. Vasiliev et al.[154] calculated the reduced optical band gap of SiNCs as a result of oxidation, which was attributed to silicon sub-oxides (Si–O–Si and Si–OH) rather than a Si=O bond. However, due to computational challenges, no model currently exists to explain the observed blue-shift in PL max of larger SiNCs. The prevailing theory is the decrease in silicon core as a result of oxidation.[155]

The wealth of theoretical and experimental evidence of change in the PL properties of SiNCs as a result of exposure to oxygen suggests that oxygen does play a key role in SiNC PL. However, it appears that the initial size of the SiNCs dictates in which direction the PL will shift. Both phenomena have not been observed for the same SiNC system so far.

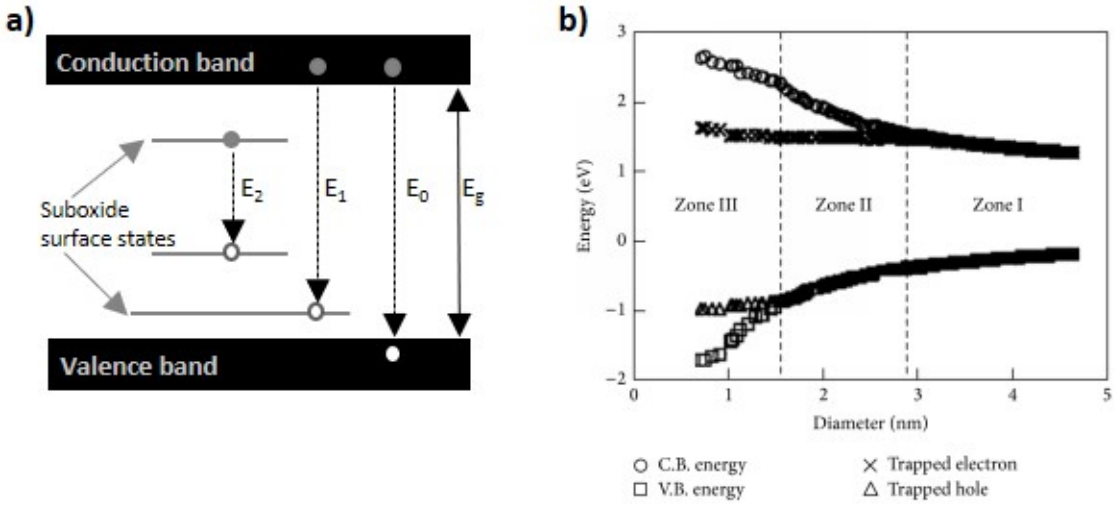

Figure 1.6: *Emission mechanism model for oxidized SiNCs proposed by Koch et al.*[1] *for: (E_0) carrier recombination across the band gap, (E_1) band to surface state recombination, and (E_2) recombination between carriers trapped in surface states (a). Emission mechanism model proposed by Wolkin et al.*[2] *to account for the observed red-shift in silicon PL upon exposure to oxygen (b). Reprinted with permission from Phys. Rev. Lett.* ***1999****, 82, 197–200. Copyright ©2002 American Physical Society.*

1.3.5 Effect of Conjugated Aromatic Ligands on SiNCs PL

The attachment of π-conjugated organic ligands to QDs has been explored as an avenue for QD sensitization or energy transfer for opto-electronic applications. Generally, attachment of a fluorophore to the surface of SiNC can lead to energy transfer from the fluorophore to the SiNC (Figure 1.7a) or the other way around (Figure 1.7b). Through careful energy level matching, the process of exciton insertion or extraction from QDs can be made efficient.[156,157]

Energy transfer to SiNC. In the case of SiNCs, one approach to increasing their QY involves the attachment of fluorescent dyes. Early work by Groenewegen et al. that demonstrated the attachment of 3-vinylthiophene to the Si surface resulted in excited energy transfer from the ligand to the Si conduction band upon photo-excitation with ultrafast pump pulses.[158] While comparison with alkyl passivated SiNCs was not provided, carrier dynamics were monitored directly by femtosecond transient absorption spectroscopy. Similarly, excitation energy transfer was observed from 2- and 4-vinyl pyridine to SiNCs.[159] Since SiNCs are poor light absorbers, attaching π-conjugated

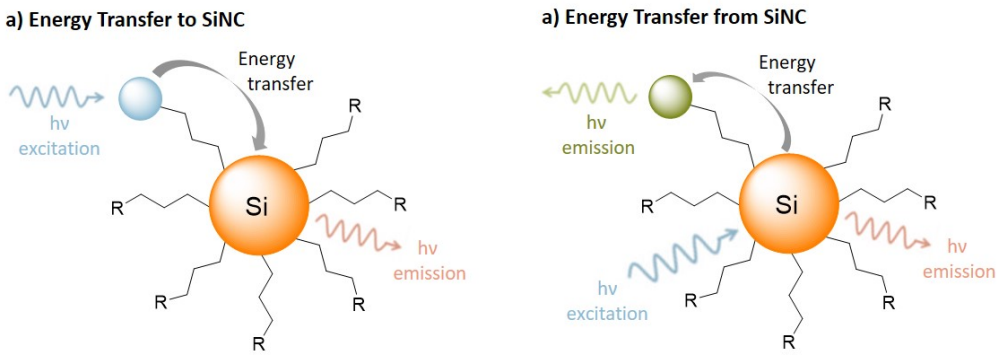

Figure 1.7: *General representation for the mechanism of energy transfer to (a) and from (b) the SiNC to the fluorophore.*

organic ligands that can absorb in the UV region can lead to sensitization of the Si core. The Ceroni and Korgel groups have utilized this approach successfully to make a molecular light-harvesting antenna. Energy transfer from pyrene units to SiNCs resulted in higher QY and longer lifetimes when the chromophore was covalently attached to the SiNC core.[160] In a follow-up study, the effect of chromophore sensitization as a factor of distance from the Si core was investigated.[161] Not surprisingly, the longer the distance between the chromophore and the SiNC, the poorer the energy transfer was. Tetraphenyl porphyrin Zn(II) dyes attached to SiNCs yielded similar light-harvesting capabilities.[162]

Energy transfer from SiNC. Compared to SiNC sensitization studies, less has been reported on energy transfer from the Si core to π-conjugated organic ligands. From studies done on porous Si, it is known that the attachment of aromatic groups to silicon can lead to PL quenching and energy transfer from the Si core to a triplet energy level in the ligand.[163] Kelly and Veinot reported the PL quenching of SiNCs upon grafting of phenylacetylene ligand to the surface.[101] Interaction between SiNCs and carbon allotropes also was reported to result in quenching of the Si PL.[161] However, in one case, attachment of 9-vinylanthracene resulted in dual-emission, coming from the Si core and the anthracene moiety.[164] The varied optical responses observed from the attachment of π-conjugated ligands to the surface of silicon suggest that energy level matching is a key to efficient energy transfer.

1.4 Thesis Outline

The following thesis summarizes the attempts made to gain a fundamental understanding of the origin of SiNC luminescence and the role crystal size and surface chemistry play in affecting the observed optical response. The thesis chapters are organized in the following manner:

- Chapter 2 focuses on the temperature-dependent steady-state and time-resolved PL measurements of SiNCs as a function of size and surface groups. An emission mechanism is proposed to account for the varying optical response for the studied SiNCs.

- Chapter 3 discusses the investigation into the role of oxygen in SiNC PL and attempts to address the disparity that currently exists in the literature regarding the PL maxima shift as a result of oxidation. A key finding of this work suggests that the optical behaviour of SiNCs upon oxidation varies depending on their size.

- Chapter 4 explores the effect that conjugated systems have on the optical response of SiNCs. Through PL spectroscopy and Scanning Tunneling Microscopy, mid-gap states were observed for conjugated systems attached to SiNCs.

- Chapter 5 summarizes the key findings of this thesis and proposes avenues for future investigations.

Chapter 2

On the Role Surface Groups Play in Silicon Nanocrystal Photoluminescence*

2.1 Introduction

Silicon nanocrystals (SiNCs) showcase an array of favourable attributes, such as biocompatibility,[165] rich surface chemistry,[36] tunable colour photo- and electro-luminescence,[117,166] and compatibility within the existing electronics industry. Many far-reaching prototype applications, utilizing SiNCs in the areas of opto-electronics, healthcare, optical sensors, as well as energy conversion and storage, have been reported.[166–170] Most of these applications aim to capitalize on the luminescence of SiNCs, a complex subject that has been debated for many years.

Almost immediately following Canham's report of highly photoluminescent porous silicon,[41] the origin of the intense photoluminescence (PL) was debated widely.[171] The PL mechanism of freestanding SiNCs is similarly complex and controversial, with many different models being proposed to explain the emission spectrum.[146] Several factors appear to play a role in the emission mechanism, including quantum confinement, an incredibly rich and complicated silicon–oxygen (and hydrogen) surface chemistry, and

*Part of this chapter has been published: Sinelnikov, R.; Dasog, M.; Beamish, J.; Meldrum, A.; Veinot, J. G. C. *ACS Photonics* **2017**, *4*, 1920–1929. Reprinted with permission. Copyright 2017 American Chemical Society.

the presence of nonradiative traps. However, the recent preparation of SiNCs with a well-controlled surface chemistry has become possible, leading to quantum efficiencies potentially above 60%[172] along with new light emission and sensing modalities.[168]

Bulk silicon is an indirect band gap semiconductor and, consequently, does not exhibit appreciable PL at ambient pressure and room temperature. When prepared as discrete nanocrystals, however, the relaxation of crystal momentum conservation laws and overlapping of the carrier wave functions leads to an increase in the radiative recombination probability, and room temperature PL is observed routinely.[173] A pure quantum confinement model for SiNCs has been supported by several reports of size-dependent PL.[174–176] However, there are numerous reports of SiNCs exhibiting PL maxima incongruent with theory, suggesting that additional mechanisms are at play.[117,177] Surface-state-related emission in SiNCs has, therefore, been proposed by numerous researchers.[120,121,178] Some of the surface species implicated as influencing the emission wavelength include surface hydroxyl groups (Si-OH), bridging oxygen (Si–O–Si), silicon-oxygen double bonds (Si=O), and silicon oxynitride (SiN_3O) groups, among others.[2,118,146] The many contrasting reports beg the question: Is the PL observed for SiNCs a manifestation of surface states, nanocrystal size, and/or a combination of these effects?

The temperature dependence of the band gap of silicon is well-documented and is described empirically by the Varshni equation;[133] at lower temperatures the band gap increases, leading to a spectral blue-shift of the PL maximum and a lower probability for nonradiative transitions.[179,180] Consistent with this relationship, the optical responses of SiNCs derived from porous silicon,[181] SiNCs embedded in a silica matrix,[176,182] and freestanding SiNCs[93,136,137,183] show similar temperature dependence. However, considering the dramatic influence surface states can have on the SiNC optical response and the established dependence of the surface structure on the preparation method, isolating and understanding surface state effects on SiNC PL is important, though not straightforward. Prior to the incorporation of freestanding SiNCs in practical applications, a more fundamental understanding of the PL emission mechanisms appears necessary.

In this study, the emission behavior of freestanding SiNCs was investigated as a function of temperature, surface chemistry, and size. A series of SiNCs with diameters d = 3 and 5 nm and three different surface functionalities was prepared, and the particles' physical and chemical properties were probed by FTIR, XPS, and TEM.

To gain insight into the PL mechanism, temperature-dependent PL and time-resolved photoluminescence (TRPL) were performed from 37 to 377 K in 20 K increments, demonstrating the dominant influence of surface groups on SiNC emission.

2.2 Materials and Methods

2.2.1 Reagents and Materials

All reagents were used as received, unless otherwise indicated. A methyl isobutyl ketone (MIBK) solution of hydrogen silsesquioxane (HSQ, trade-name FOx-17) was obtained from Dow Corning; the solvent was removed under vacuum, and the resulting white solid was used without further purification. Electronic grade hydrofluoric acid (HF, 49% aqueous solution) was purchased from J. T. Baker. 1-Dodecene (95%), dodecylamine (98%), phosphorus pentachloride (PCl_5, 98%), methanol (reagent grade), ethanol (reagent grade), and toluene (HPLC grade) were obtained from Sigma-Aldrich. HPLC grade acetonitrile was purchased from Caledon Laboratory Chemicals. Toluene and acetonitrile were dried using a Grubbs-type solvent purification system (Innovative Technologies, Inc.) prior to use.

2.2.2 Material Synthesis and Functionalization

Si/SiO_2 Composite Synthesis and SiNC Liberation from Matrix. A detailed account of silicon nanocrystal synthesis can be found elsewhere.[85] Briefly, HSQ was annealed for 1 h at 1100 °C under slightly reducing conditions (5% H_2/ 95% Ar) to produce a Si/SiO_2 composite composed of ∼3-nm silicon nanocrystals embedded in a silica matrix, composite **1**. In order to produce larger nanocrystals (∼5 nm) composite **1** was annealed further for 1 h at 1200 °C to yield composite **2**. Even larger particles (∼8 nm) were obtained by annealing composite **1** for 1 h at 1300 °C to yield composite **3**. Hydride-terminated silicon nanocrystals were liberated from the silica matrix by etching the composite in a 1:1:1 HF/Ethanol/H_2O solution for 1 h, followed by extraction into toluene. (*Caution: Hydrofluoric acid is extremely dangerous and must be handled with great care.*)

Thermal Hydrosilylation. Dodecyl functionalized silicon nanocrystals (R-SiNCs) were synthesized using an established literature procedure for thermal hydrosilyla-

tion.[100] Freshly etched silicon nanocrystals (from composite **1** or **2**), suspended in toluene, were centrifuged twice for 10 min at 3000 rpm. After decanting the supernatant, the particles were dispersed in 1-dodecene (20 mL) and transferred to an oven-dried Schlenk flask, equipped with a Teflon stir bar and filled with Ar. The reaction mixture was degassed three times and then heated for 18 h at 190 °C under an inert atmosphere. On completion of the reaction, the Schlenk flask was transferred to a glovebox for purification by precipitation. The reaction solution was partitioned into equal amounts and transferred to predried 50-mL Teflon centrifuge tubes. Next, a 1:1 solvent:anti-solvent mixture of toluene:acetonitrile was added to the centrifuge tubes for a total volume of ∼40 mL. After centrifugation for 10 min at 7000 rpm, the supernatant was decanted, and the resulting yellow precipitate was dispersed in a minimal amount of toluene. Following an addition of ∼10 mL acetonitrile, the centrifugation was repeated. This step was repeated twice. The resulting precipitate was dispersed in toluene, filtered through 0.45-μm PTFE syringe filter, and the solution stored in a Teflon capped vial until further use.

Photochemical Hydrosilylation. Oxidized dodecyl functionalized silicon nanocrystals (Ox. R-SiNCs) were synthesized following a literature procedure with some modifications.[101] Freshly etched silicon nanocrystals (from composite **1** or **2**), suspended in toluene, were centrifuged twice for 10 min at 3000 rpm. After decanting the supernatant, the particles were dispersed in 1-dodecene (20 mL) and transferred to an oven-dried, argon-filled Schlenk flask equipped with a Teflon stir bar and a quartz insert. Following three cycles of degassing, a 365-nm LED UV light source was placed in the quartz insert, and the reaction flask was covered with aluminum foil. The photochemical reaction was carried out for 48 h under a slow argon flow; the resulting solution was semi-transparent yellow. Purification was carried out by evenly dispensing the reaction solution into 50-mL Teflon centrifuge tubes (∼5 mL) and adding a 1:2 ethanol:methanol mixture, resulting in a cloudy dispersion. Next, the solutions were centrifuged for 20 min at 12000 rpm. After decanting the supernatant and dispersing the particles in a minimal amount of toluene, the centrifugation process was repeated twice more. In the last step, the silicon nanocrystal solution was filtered through a 0.45-μm PTFE syringe filter and stored in a Teflon capped vial until further use.

Chlorination and Amine Functionalization. Dodecylamine functionalized silicon nanocrystals (RN-SiNCs) were synthesized using a slightly modified procedure pre-

viously reported by the group.[117] Starting from larger particles (composite **2** or **3**), freshly etched silicon nanocrystals, suspended in toluene, were centrifuged for 10 min at 3000 rpm. After discarding the supernatant, the particles were redispersed in 15 mL dry toluene and transferred to an oven-dried Schlenk flask, equipped with a Teflon stir bar and filled with Ar. First, the surface of the particles was chlorinated by adding 0.3 g of PCl_5 and heating to 40 °C for 1 h. After removing the solvent and byproducts under reduced pressure, the particles were redissolved in fresh, dry toluene (∼10 mL) and further reacted with 0.2 g dodecylamine for 12 h at 40 °C; the resulting solution was clear yellow. Purification involved multiple washings of the reaction solution with a brine solution using a separatory funnel, followed by solvent and by-product removal under vacuum. The resulting yellow precipitate was dispersed in toluene and filtered through a 0.45-μm PTFE syringe filter, and the solution was stored in a Teflon capped vial until further use.

2.2.3 Material Characterization and Instrumentation

Fourier-transform infrared spectroscopy (FTIR) was performed using a Nicolet Magna 750 IR spectrophotometer.

X-ray photoelectron spectroscopy (XPS) measurements were performed on a Kratos Axis Ultra instrument operating in energy spectrum mode at 210 W. Samples were prepared by drop-casting SiNC dispersions in toluene onto a copper foil substrate. The base pressure and operating chamber pressure were maintained at 10^{-7} Pa. A monochromatic Al Kα source (λ = 8.34 Å) was used to irradiate the samples, and the spectra were obtained with an electron takeoff angle of 90°. CasaXPS software (VAMAS) was used to interpret spectra. All the spectra were calibrated internally to the C 1s emission (284.8 eV). After calibration, the background was subtracted using a Shirley-type background to remove most of the extrinsic structure loss. The high-resolution Si 2p region was fit to Si $2p_{1/2}$ and Si $2p_{3/2}$ components, with spin-orbit splitting fixed at 0.6 eV, and the Si $2p_{1/2}$ / Si $2p_{3/2}$ intensity ratio set to 1/2.

Transmission electron microscopy (TEM) images were obtained using a JEOL-2010 electron microscope equipped with a LaB_6 filament and operated at an accelerating voltage of 200 kV. The TEM samples were prepared by drop-coating SiNC dispersions in toluene onto a lacey carbon coated copper grid with a 300-μm diameter hole. Particle size distribution was calculated by counting at least 200 particles using ImageJ software

(Version 1.49).

Temperature-controlled PL spectroscopy and TRPL measurements were carried out using a CTI cryogenics (controller model 8000 and compressor model 8300) helium closed-cycle refrigerator. First, a solution containing silicon nanocrystals was drop-cast and concentrated to one spot on a 1x1 cm silicon wafer. The wafer was mounted on a copper stage connected to a Cryo-con 32 temperature controller. All measurements were performed under high vacuum (10^{-6} Torr) maintained by a Varian Turbo Dry 70 vacuum pump with a Varian BA2C senTorr gauge controller. An Argon ion laser with a 351-nm emission wavelength was used to excite R-SiNCs and Ox. R-SiNCs. The resulting PL was focused by a double convex 5-cm focal length lens, collected by an optic fiber, passed through a 550-nm long-pass filter to eliminate scattered light from the excitation source, and fed into an Ocean Optics USB2000 spectrometer. The spectral response was calibrated by a black-body radiator (Ocean Optics LS1). For TRPL measurements, the excitation light was modulated by an acousto-optic modulator (response time ∼50 ns) operated at a frequency of 200 Hz with a 50% duty cycle. As before, the PL was fed into an optic fiber, passed through a 550-nm long-pass filter, and was then incident on a Hamamatsu H7422P-50 photomultiplier tube (PMT) interfaced with a Becker-Hickl PMS-400A gated photon counter. The PL data was collected in 1 μs timesteps, and a total of 10000 sweeps were collected for a good signal-to-noise ratio. The responsivity of the PMT falls off rapidly after 850 nm, so any contributions coming from wavelengths much longer than this will not contribute significantly to the measured decay.

For RN-SiNCs, a modelocked, frequency-doubled Ti:sapphire laser (Spectra-Physics Tsunami, 385 nm) operated at 80 MHz with ∼2-ps pulses was used as the excitation source. The resulting PL was focused by a double convex 5-cm focal length lens, collected by an optic fiber, passed through a 400-nm long-pass filter, and fed into an Ocean Optics USB2000 spectrometer. For TRPL, instead of the spectrometer, a Becker-Hickl HPM-100-50 photon counting PMT was used. The arrival times were analyzed by a SPCM multiscaler operated with 50-ps time steps. Since the TRPL results can depend on the excitation power (especially in the high-power, non-linear regime),[184] care was taken to ensure that the excitation power was constant and relatively low (6 mW/cm^2), where the luminescence intensity varied linearly as a function of excitation flux. Absolute quantum yields were measured using a HORIBA K-Sphere Petite integrating sphere (diameter: 3.2 in), equipped with a xenon lamp (185–850 nm) with a

wavelength-selecting monochromator for the excitation.

2.3 Results and Discussion

2.3.1 Size and Surface Characterization of SiNCs

The preparation of the materials used for the present study has been reported previously.[100,101,117] Briefly, SiNCs (diameter ∼3 nm) embedded in a silica-like matrix were formed upon thermal processing of HSQ at 1100 °C under a slightly reducing atmosphere. Subsequent annealing at 1200 and 1300 °C afforded larger particles (i.e., ∼5 and 8 nm diameters, respectively).[85] Following etching in alcoholic hydrofluoric acid, the surfaces of the liberated hydride-terminated SiNCs were functionalized with 1-dodecene using thermal hydrosilylation and photochemical hydrosilylation (Scheme 2.1).[100,101] To prepare N-tethered dodecylamine SiNCs, an alternative functionalization protocol, in which SiNC surfaces were chloride-terminated upon treatment with phosphorus pentachloride (PCl_5), was employed.[117] Using these procedures, three distinct silicon surfaces were obtained: i) alkyl-terminated SiNCs (R-SiNCs; R = monolayer and oligomeric dodecyl) prepared with limited to no surface oxidation; ii) oxidized alkyl-terminated SiNCs (i.e., Ox. R-SiNCs), in which the NC surface was partially oxidized,[92] and iii) alkylamine-terminated nanocrystals (RN-SiNCs) bearing nitrogen-bonded alkyl moieties and oxynitride surface species.

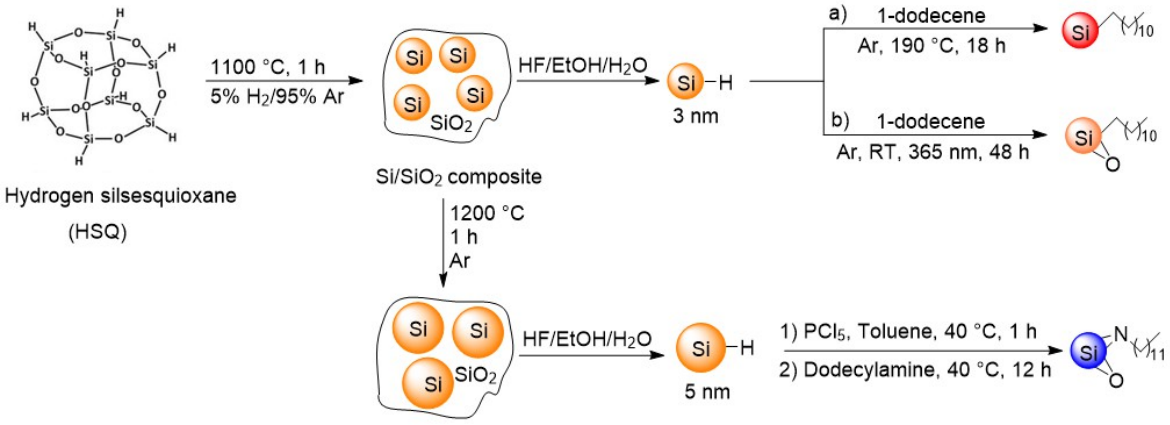

Scheme 2.1: *Synthesis and functionalization of silicon nanocrystals.*

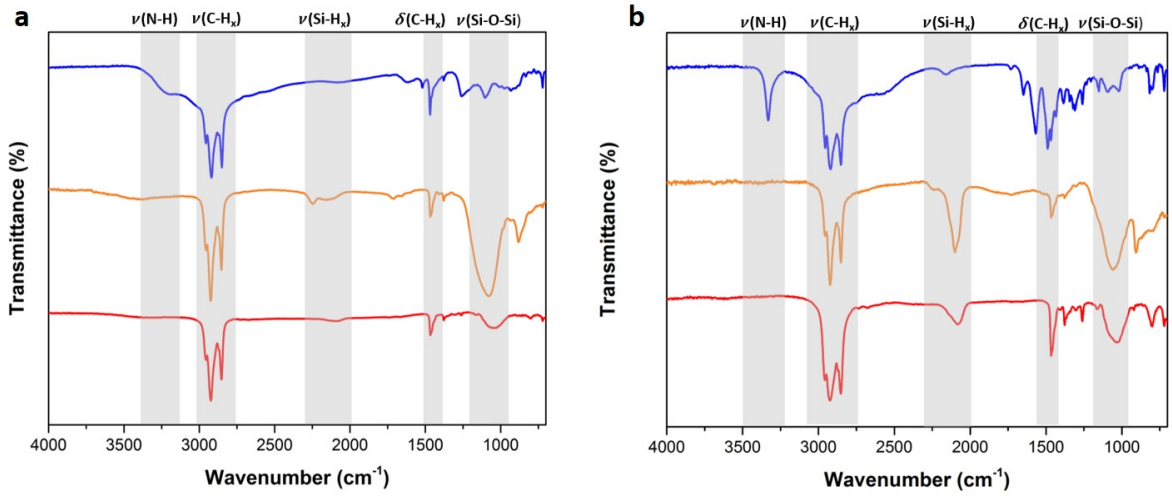

Figure 2.1: *FTIR spectra of 3-nm (a) and 5-nm (b) R-SiNCs (red) Ox. R-SiNCs (orange), and RN-SiNCs (blue).*

The presence of the desired surface groups on SiNCs was confirmed by FTIR. In Figure 2.1, intense vibrations at 2650–2900 cm^{-1} and 1380–1470 cm^{-1}, which are consistent with C–H stretching and bending vibrations of the dodecyl chain, respectively, are observed for all SiNCs. 3- and 5-nm R-SiNCs and RN-SiNCs show lower intensity Si–O–Si (∼1100 cm^{-1}) and Si-H_x (∼2100 cm^{-1}) stretching compared to their Ox. R-SiNCs analogues, suggesting that the surface of the latter particles is less efficiently passivated and more oxidized. In addition, the presence of the N–H stretching (3300–3500 cm^{-1}) and bending (1550–1640 cm^{-1}) signals is consistent with dodecylamine functionalization of SiNCs in the case of RN-SiNCs.

Further evaluation of the SiNCs surfaces and oxidation state(s) was performed using XPS. High resolution spectra of the Si 2p region (Figure 2.2) revealed the presence of an emission at 99.3 eV for 3- and 5-nm R-SiNCs and Ox. R-SiNCs, which was assigned to Si(0). Other components at 100.1, 101.3, 102.4, and 103.4 eV were assigned to ligand passivated silicon surface and sub-oxides.[85] Notably, the Si(IV) component associated with a formal Si–O bond is much stronger in Ox. R-SiNCs (Figure 2.2 c-d) compared to their R-SiNC analogues (Figure 2.2 a-b). In contrast, RN-SiNC spectra only contain Si(II) and Si(III) components, most likely due to the stronger electron withdrawing nature of an oxynitride species.[185]

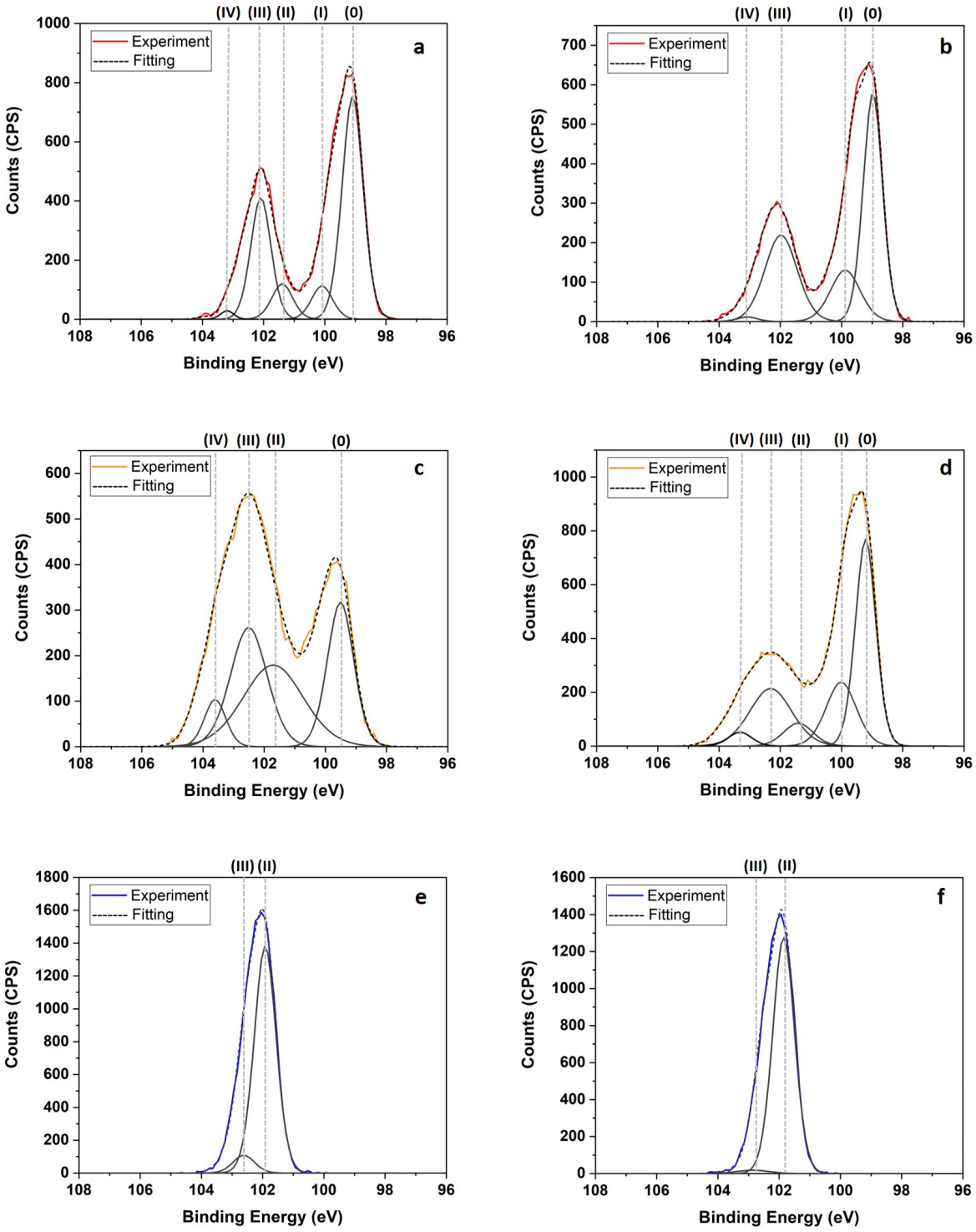

Figure 2.2: *High resolution X-ray photoelectron spectra of Si 2p peak for 3-nm R-SiNCs (a), Ox. R-SiNCs (c), RN-SiNCs (e) and 5-nm R-SiNCs (b), Ox. R-SiNCs (d), and RN-SiNCs (f). Please note, only $2p_{3/2}$ deconvolution components are shown; $2p_{1/2}$ components are omitted for clarity.*

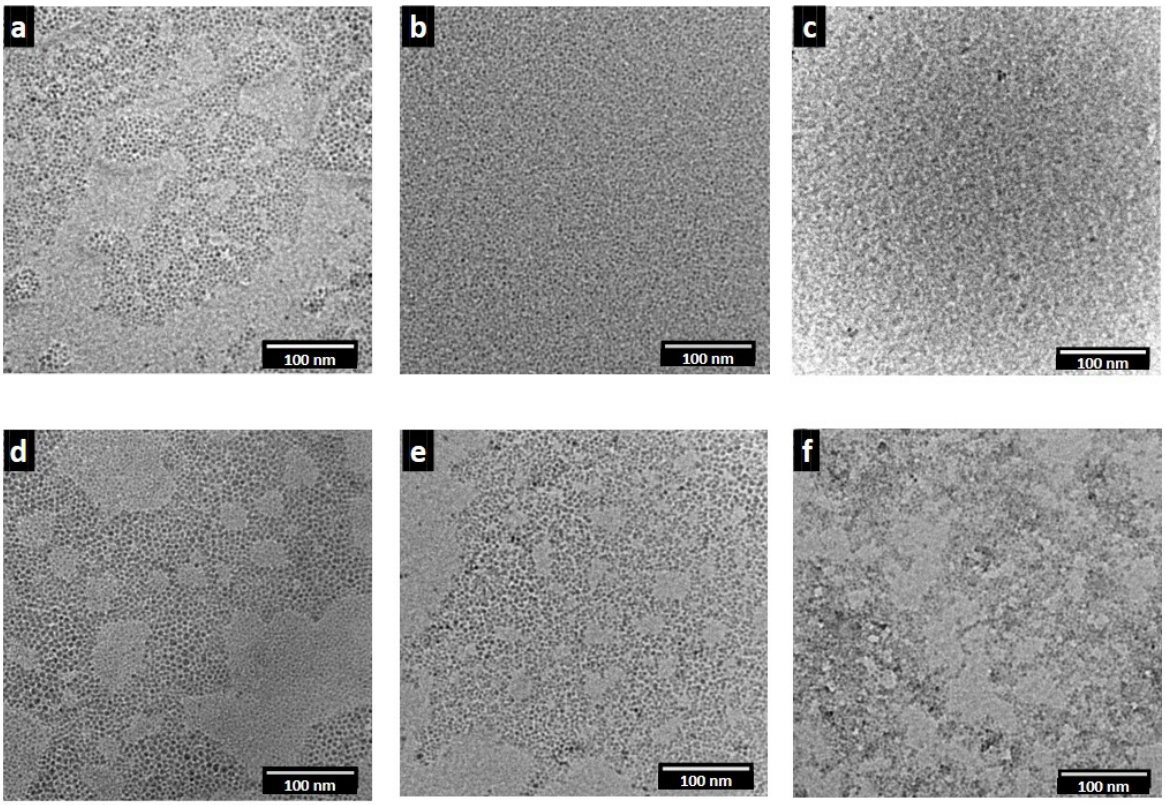

Figure 2.3: *Bright field TEM images for 3-nm R-SiNCs (a), Ox. R-SiNCs (b), RN-SiNCs (c) and 5-nm R-SiNCs (d), Ox. R-SiNCs (e), and RN-SiNCs (f).*

Particle size was confirmed by TEM. Minimal particle aggregation was observed in the TEM micrographs for all six samples, suggesting that effective surface passivation was obtained (Figure 2.3). In addition, size distribution analysis revealed that the particles were statistically equivalent in size for the two sets of particles (3 and 5 nm, Figure 2.4).

The set of NCs provides an opportunity to probe and isolate the roles of various contributing factors affecting SiNC PL. The alkyl-terminated R-SiNC interfaces have been considered innocent in the PL of Si nanomaterials; in this context R-SiNCs are expected to exhibit an intrinsic band gap PL from the SiNC core. The PL response of Ox. R-SiNCs is expected to be influenced by the effects of oxidation, and emission from RN-SiNCs is expected to be affected strongly by the surface amine groups that lead to blue luminescence.[118,121,128] As expected, different PL spectra were observed for the surface functionalities investigated, regardless of NC dimension (Figures 2.3-2.4).

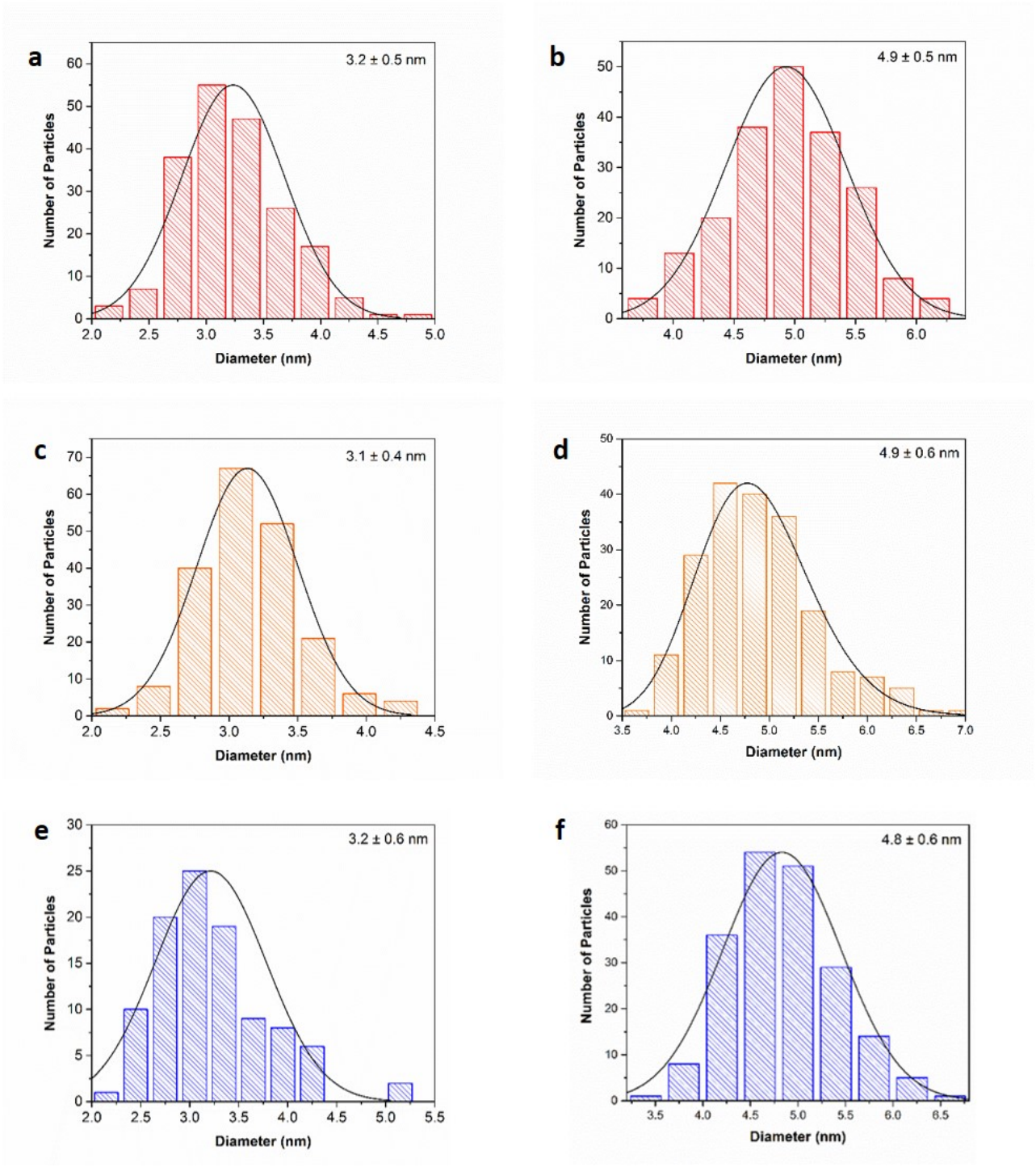

Figure 2.4: *Size-distributions histograms of 3-nm R-SiNCs (a), Ox. R-SiNCs (c), RN-SiNCs (e) and 5-nm R-SiNCs (b), Ox. R-SiNCs (d), and RN-SiNCs (f).*

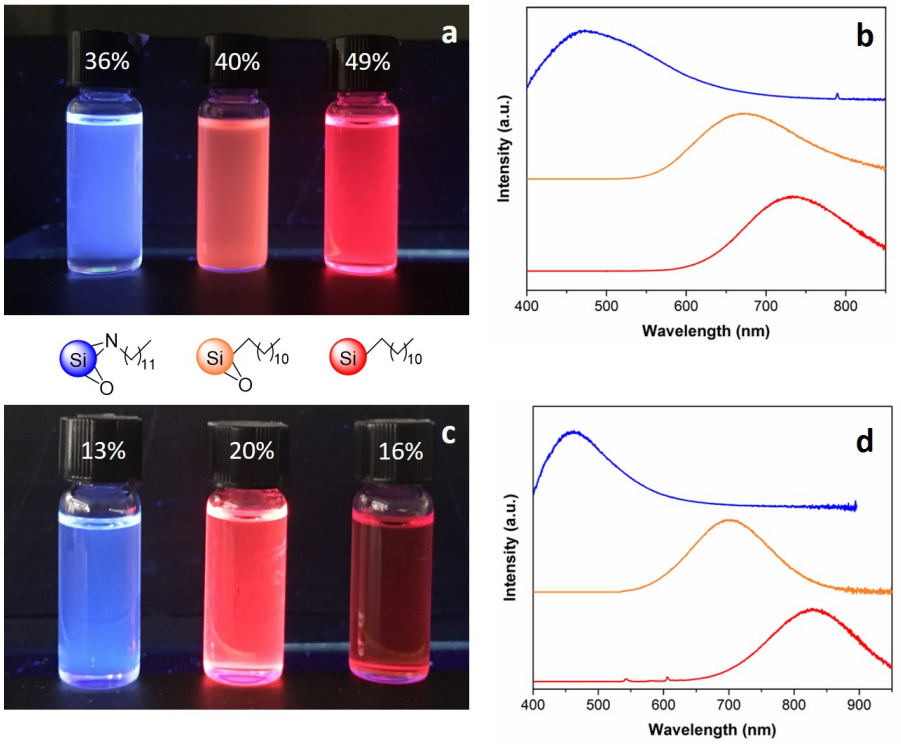

Figure 2.5: *(a) Photograph of 3-nm RN-SiNCs, Ox. R-SiNCs, and R-SiNCs (from left to right) in toluene under benchtop UV illumination. The corresponding QY is shown above each vial. (b) The corresponding room temperature PL spectra upon excitation at 350 nm. (c, d) The same as (a) and (b) for 5-nm SiNCs.*

The PL of R-SiNC, Ox. R-SiNC, and RN-SiNC luminescence appeared red, orange, and blue, respectively (Figure 2.5 a-b). Larger SiNCs showed the same general trend, however, the PL maxima for R-SiNCs and Ox. R-SiNCs were slightly red-shifted for those particles (Figure 2.5 c-d). The quantum yields (QY) for the SiNCs are labeled above the corresponding images in Figure 2.5.

2.3.2 Temperature-dependent Steady-state Photoluminescence of SiNCs

To probe the PL response of the differently functionalized SiNCs further, PL spectroscopy and TRPL measurements were carried out as a function of temperature. The PL spectra of SiNCs with all three surface groups were slightly skewed toward longer wavelengths (Figure 2.6). To determine the peak wavelength, λ_p, the spectra were modeled using a skewed Gaussian function given by:[186]

$$I_{PL} = A \cdot exp\Big[- ln2\Big[ln\Big(1 + \frac{2b(\lambda - \lambda_p)}{\sigma}\Big)\frac{1}{b}\Big]^2\Big] \tag{2.1}$$

where I_{PL} is the emission intensity, σ represents the standard deviation, b is an asymmetry parameter that is positive for positive skewness, and A is a scaling parameter. This model provides an excellent fit to the PL spectra, from which one can extract the peak wavelength, integrated intensity, and degree of skewing in the spectrum. Gaussian, Lorentzian, and lognormal models also were tested but yielded poorer fits, as determined by an analysis of both the errors and residuals. Although one cannot rule out the presence of multiple underlying peaks, in the absence of any reason to assume such multiple peaks, the skewed Gaussian was the model with the fewest free parameters.

The maximum of the PL spectrum shifted to shorter wavelengths (blue-shifted) for the R-SiNCs and Ox. R-SiNCs as the temperature decreased. In comparison, a slight red-shift of the PL maximum for the RN-SiNCs was noted, which yielded a sigmoidal-like temperature dependence (Figures 2.6 a-c and d-f for 3- and 5-nm SiNCs, respectively). The contrasting trends observed for R-SiNCs and RN-SiNCs are consistent with fundamentally different emission mechanisms occurring in the two cases. For R-SiNCs (and perhaps also for Ox. R-SiNCs), the shift in PL maximum is consistent with a temperature-dependent change in the band gap,[133,134] although other factors, such as the singlet–triplet energy gap (also dependent on temperature, as discussed below) could play a role. In contrast, RN-SiNCs do not show a band gap-like temperature dependence of the PL spectrum.

Over-excitation of the SiNCs could be the cause of the observed PL shift, which has been shown to affect PL peak position and intensity.[135,187] Therefore, the PL spectrum and intensity of 5-nm R-SiNCs at 40 K was measured over a range of excitation power

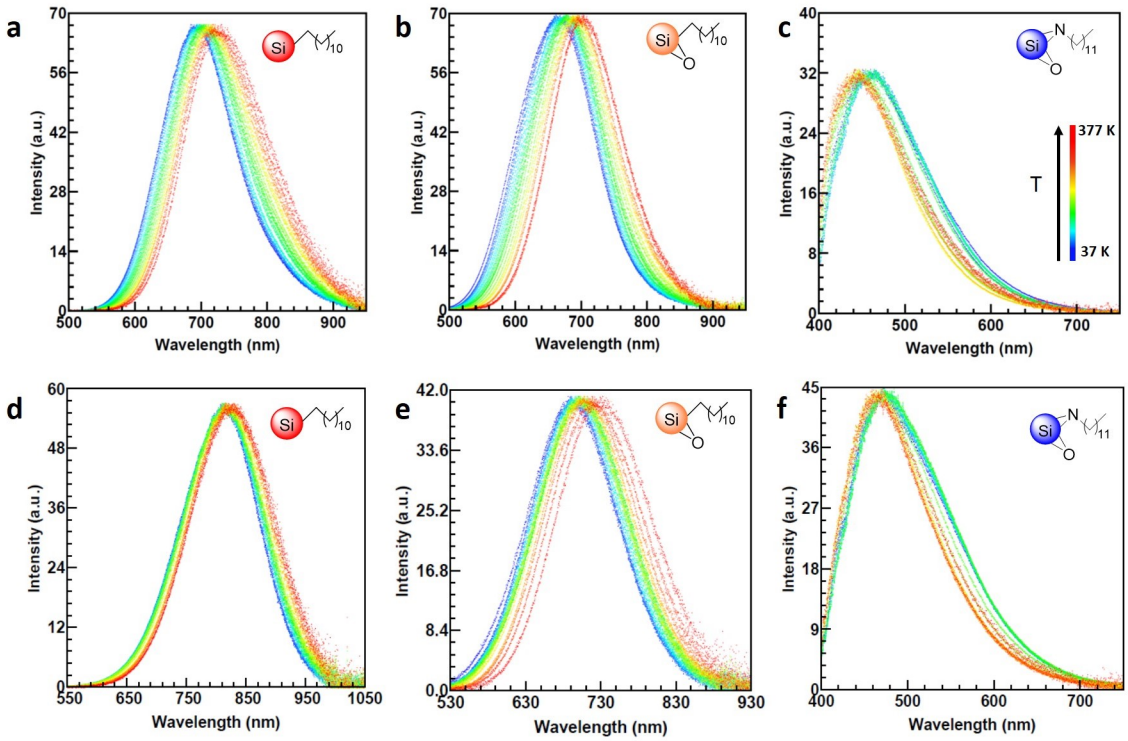

Figure 2.6: *Temperature dependence of the PL spectrum for the 3-nm (a) R-SiNCs, (b) the Ox. R-SiNCs, and (c) the RN-SiNCs, and their 5-nm analogues (d-f), respectively. The data is normalized to make it easier to compare the spectral shapes.*

densities. Figures 2.7 a and b show that the low excitation power density (∼6 mW/cm^2) used in these experiments falls well within the linear regime of the PL intensity vs. excitation power curve before any saturation effects of the PL intensity can be observed. In addition, within the excitation power range measured, very little shift (∼4 nm) in PL maximum was observed.

At low temperatures, the PL maximum corresponded to band gap energies, E_g, of 1.53 and 1.80 eV for the 5- and 3-nm diameter R-SiNCs, respectively. This compares quite well with the first-principles theoretical values given by:[188]

$$E_g = \sqrt{E_{g,Si}^2 + \frac{D}{r^2}} \tag{2.2}$$

where $D = 4.8eV^2 \cdot nm^2$, r is the nanocrystal radius, and $E_{g,Si}$ is the bulk band gap, which yielded 1.46 and 1.87 eV for the two sizes. For Ox. R-SiNCs, the observed peak energies were 1.79 eV (5 nm) and 1.87 eV (3 nm). This relative difference of only 0.08

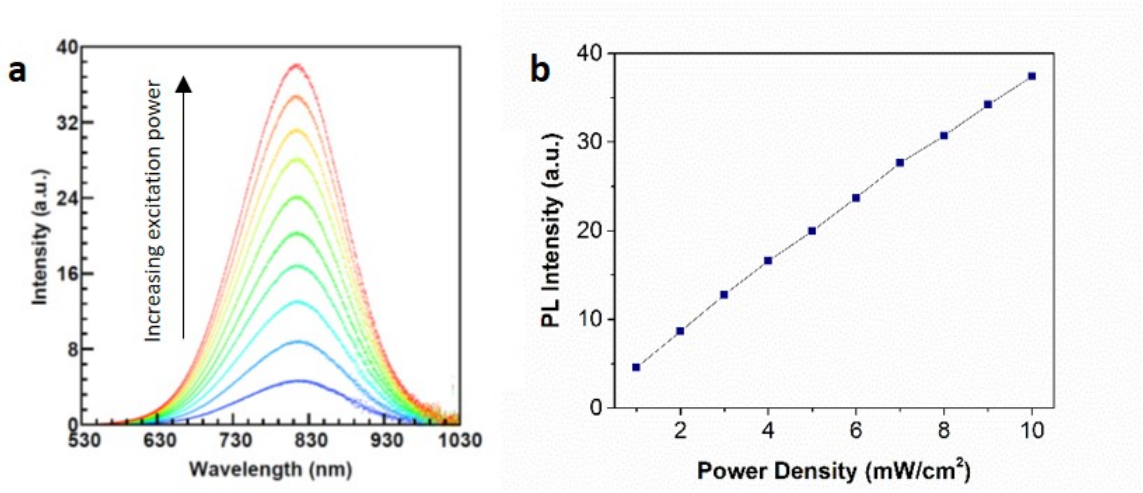

Figure 2.7: *Excitation power density control measurements of 5-nm R-SiNCs at 40 K: (a) PL spectra (b) PL intensity from skew-normal fitting.*

eV is much smaller than for the un-oxidized case (i.e., R-SiNCs) and much smaller than predicted for particles of these sizes. The shift of the PL maximum to higher energies in the oxidized samples and the poor agreement with theory suggest that oxide surface species play a role in the emission mechanism.

RN-SiNCs behaved differently; the PL maximum showed a weaker, sigmoidal temperature dependence, which trended in the opposite sense (i.e., it red-shifted slightly with decreased temperature). Surface-state-related emission arising from charge transfer recently has been shown to be temperature independent in metal–organic complexes,[189,190] and in the case of ZnO nanorods, a weak sigmoidal-like temperature dependence was reported for a surface state emission.[191] Thus, the similar overall behaviour observed for RN-SiNCs could arise from a similar charge transfer to a surface state associated with the nitrogen-based surface termination and, is also expected to display minimal temperature dependence.

The PL intensity of 3- and 5-nm SiNCs also varied as a function of temperature (Figure 2.8 c-d). Consistent with previous reports,[135,176] as the temperature was increased the PL intensity decreased notably across all samples, and nearly complete quenching was observed for 3-nm RN-SiNCs at the highest temperature investigated (377 K). The decrease in PL intensity as the temperature was elevated is attributed typically to the presence of nonradiative decay channels.[48] Thermally activated tunneling of carriers through the surface oxide and increased carrier diffusion from the NC

core to the surface traps have been proposed as nonradiative recombination mechanisms in SiNCs.[134,192] In this context, it is reasonable that the impact of surface states on PL will be influenced by temperature.

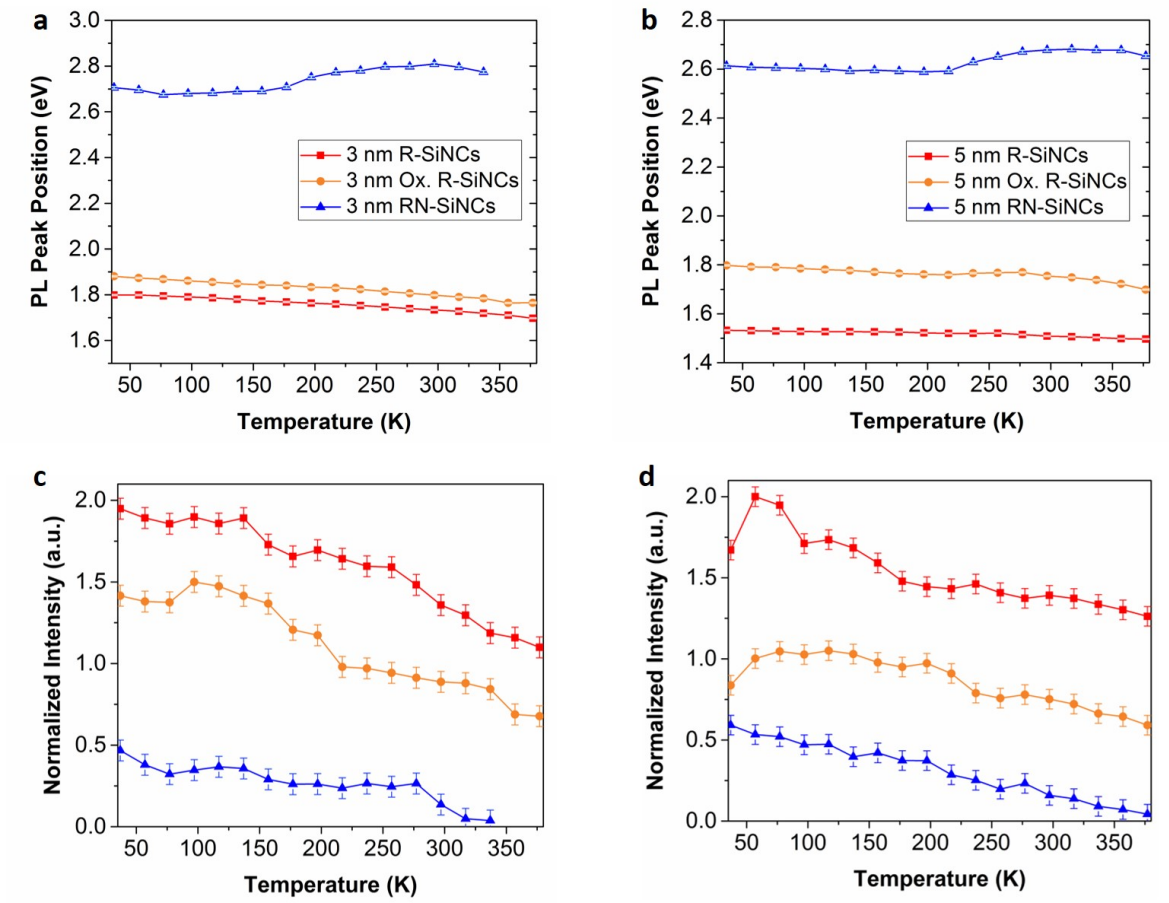

Figure 2.8: *PL peak energy position as a function of temperature for the 3-nm (a) and 5-nm (b) R-SiNCs (red), Ox R-SiNCs (orange), and RN-SiNCs (blue). The uncertainty in the peak positions from the model fit (Eq. 2.1) is smaller than the data points. Integrated intensity as a function of temperature obtained from skew-normal fitting for 3-nm (c) and 5-nm (d) SiNCs. The standard deviations (given as error bars) were obtained by repeating the measurements for two temperatures (60 and 293 K) five times. The data are normalized to the highest intensity and offset for clarity in comparing the trends.*

2.3.3 Temperature-dependent Time-resolved Photoluminescence of SiNCs

To gain further insight into SiNC emission pathways, TRPL measurements were performed at temperatures from 37 to 377 K, in 20 K increments. The overall luminescence decay rate comes from both the radiative and nonradiative decay channels. Although SiNCs most often are assumed to exhibit a stretched exponential decay,[193] in this case, a lognormal distribution of lifetimes provided a better fit to NC decay dynamics,[194,195] and it represents a reasonable approximation to the lognormal size distributions (Figure 2.4). Generally, the decay rate distribution, $\Phi(\Gamma)$, is related to the PL decay curve by:

$$I_t = \int_{\infty}^{0} A \cdot exp\left[-\left(\frac{ln\Gamma - ln\Gamma_0}{W}\right)^2 \right] exp[-\Gamma t] d\Gamma + c \tag{2.3}$$

where the frequency, Γ_0, is the most probable decay rate, c is an offset, W is a parameter related to the width of the frequency distribution on Δ, such that $W = arcsinh[\Delta/(2\Gamma_0)]$, and A is a normalization constant given by:

$$A = \left(\sqrt{\pi}\Gamma_0 W exp\left[\frac{W^2}{4}\right] \right)^{-1} \tag{2.4}$$

Finally, the estimated mean lifetime, μ_τ, is given by:

$$\mu_\tau = \frac{1}{exp\left(ln\Gamma_0 + \frac{\text{arcsin}\, h\left(\frac{\Delta}{2\Gamma_0}\right)^2}{4} \right)} \tag{2.5}$$

Equations 2.3–2.5 were used to model the observed luminescence decays, where the free parameters were Γ_0, Δ, and the offset c.

PL lifetimes were collected at temperatures from 37 to 377 K, in 20 K increments. The R- and Ox. R-SiNCs showed microsecond-scale dynamics upon excitation at 351 nm (Figure 2.9 3 a-b). The temperature-dependent TRPL results show an increasing mean lifetime with decreasing temperature for all samples, with values approaching 1 ms for 3-nm Ox. R-SiNCs (Figure 2.9 c-d). While short lifetimes have been reported previously for heavily oxidized SiNCs,[92] these particles exhibited no nanosecond decay components, most likely due to the lower degree of oxidation.

There is a strong size dependence in the response of the mean lifetimes of the R-

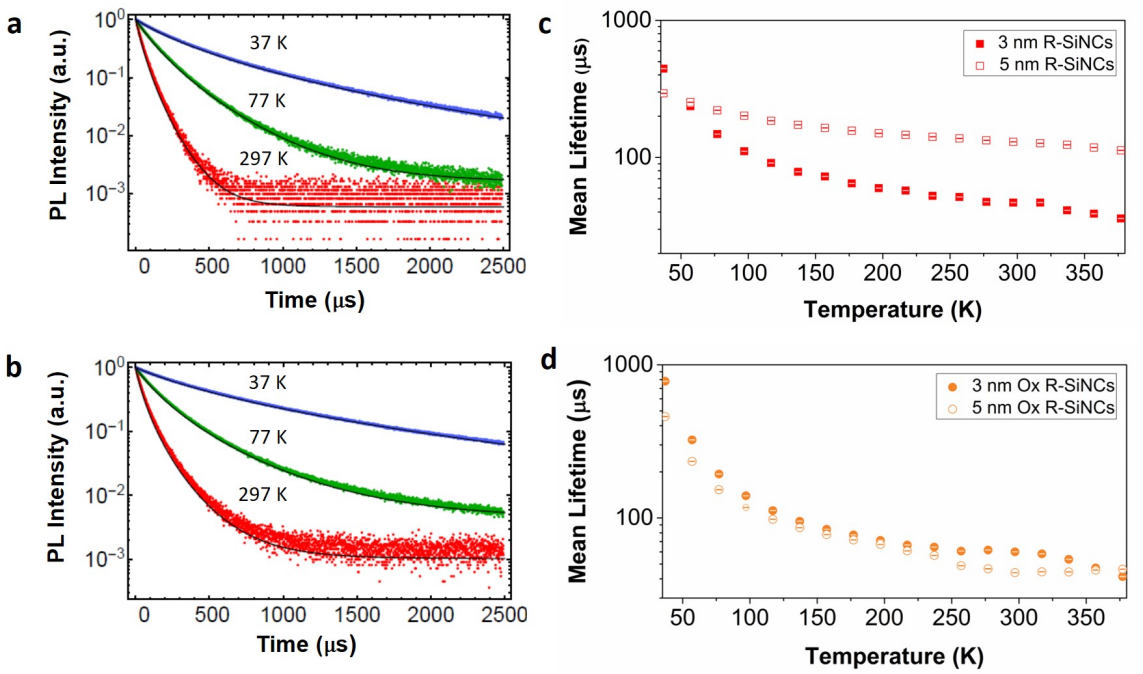

Figure 2.9: *PL decays for 3-nm R-SiNCs (a) and Ox. R-SiNCs (b) at three different temperatures (c) mean lifetime from the lognormal fit as a function of temperature for 3- and 5-nm R-SiNCs and (d) 3- and 5-nm Ox. R-SiNCs.*

SiNCs to temperature. The d = 5-nm particles showed a modest dependence of the mean lifetime with temperature, while the smaller R-SiNCs showed a much more pronounced change. The proportional relationship between PL decay and SiNC diameter has been reported previously[196] and attributed to quantum confinement of electron–hole pairs in real space, which leads to dipole allowed transitions for smaller SiNCs.[7,46] The lifetimes of SiNCs are evaluated usually in terms of the singlet–triplet model proposed by Calcott et al.,[140,141] which accounts for an energy gap ΔS-T between the lower energy excitonic triplet and the higher-energy singlet states. According to this model, at low temperatures the dynamics are dominated by the much slower triplet recombination, thus accounting for the longer lifetimes observed at lower temperatures for R-SiNCs.

The partly oxidized particles, on the other hand, show a different behavior. Not only does the peak PL wavelength shift to higher energy, as previously discussed, but the temperature dependence of the decay rates is also different, especially for the larger NCs. In contrast to the R-SiNCs, the overall temperature dependence appears

essentially similar for both NC sizes. The natural conclusion may be that partial oxidation decreases the effective core diameter, increasing the emission energy, and changing the temperature dependence of the decay rates. However, this explanation is not wholly satisfactory, since the 3-nm Ox. R-SiNCs are not nearly as different from one another as might be expected based on the behavior of the alkyl-terminated NCs. As previously discussed, a proportional relationship between lifetime and particle size exists, thus, if a 3-nm Ox. R-SiNC core is shrinking, a shorter lifetime would be expected compared to 3-nm R-SiNCs. Moreover, if a shrinking Si core is assumed, then the 3-nm Ox. R-SiNCs (being more reactive) should shrink more than their 5-nm counterparts. However, from band gap energy calculations after oxidation, the two sizes emit *closer* in energy, which is opposite to the expected behaviour.

Surface groups exhibit a more dramatic effect on the PL lifetime in the case of the RN-SiNCs (Figure 2.10). For this system, no microsecond component was detected (nanosecond only), and only a very limited temperature dependence of the decay dynamics was found ($\lambda_{ex} = 385$ nm). Several different models were attempted to fit the TRPL data, including a single exponential, stretched exponential, lognormal, and double exponential. According to the latter, the intensity at time t, I_t, decays according to:

$$I(t) = A \cdot e^{(-t/\tau_1)} + B \cdot e^{(-t/\tau_2)} + c \tag{2.6}$$

where A and B are multiplicative factors, τ_1 and τ_2 are the decay times and c is the offset. Equation 2.6 yielded the smallest residuals and errors. For convenience, the two lifetimes are referred to as long and short. The longer lifetime component increased from 3.1 to 3.2 ns (3-nm NCs) and 3.0 to 3.1 ns (5-nm NCs) upon cooling from room temperature to 37 K. The short lifetime is approximately 600 ps and appeared to be temperature independent for both particle sizes. The limited particle size and temperature dependence of the PL lifetimes and the dramatic differences in comparison to the R-SiNCs and Ox. R-SiNCs exhibited by the RN-SiNCs particles provides strong evidence that the oxynitride surface moieties play a dominant and quite different role in the SiNC PL.

Previous studies have shown that high excitation powers can shorten the lifetime dynamics of SiNCs, due especially to Auger processes.[46] At higher optical excitation power, one can generate multiple interacting excitons per nanocrystal, and this is

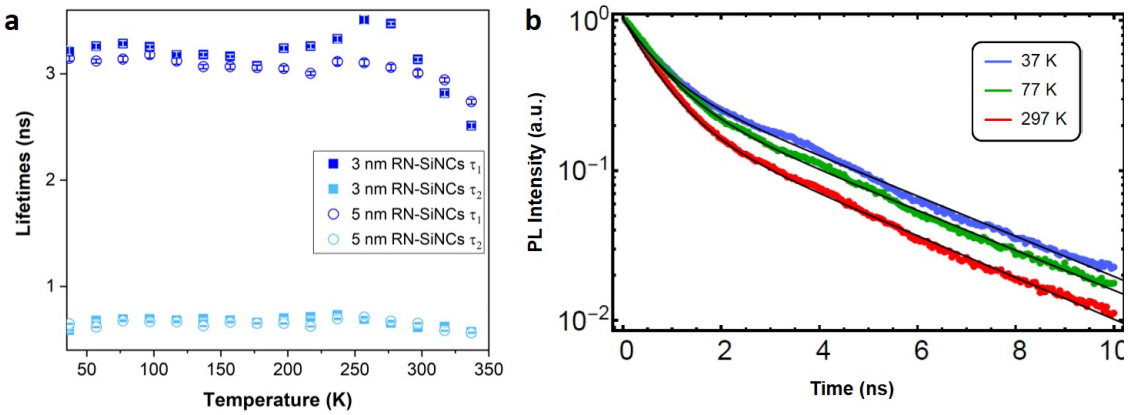

Figure 2.10: *Long (dark blue) and short (light blue) lifetimes for 3-nm (filled squares) and 5-nm (hollow circles) RN-SiNCs (a). Lifetimes for 3-nm RN-SiNCs at selected temperatures (b).*

believed to become more likely at lower temperatures.[187] A control experiment was carried out at 40 K by varying the excitation power density, as shown in Figure 2.11. The changes in the mean lifetimes as a function of excitation power showed no trend and were within the error limits of the measurements. In another study, over-excitation was shown to shorten mainly the fast (nanosecond) component of the PL lifetimes.[184] RN-SiNCs do have nanosecond lifetime dynamics but, here again, no variation in the decay rate was observed as a result of increasing excitation fluence.[121] Thus, the observed trends in the present study are not likely to be caused by over-excitation.

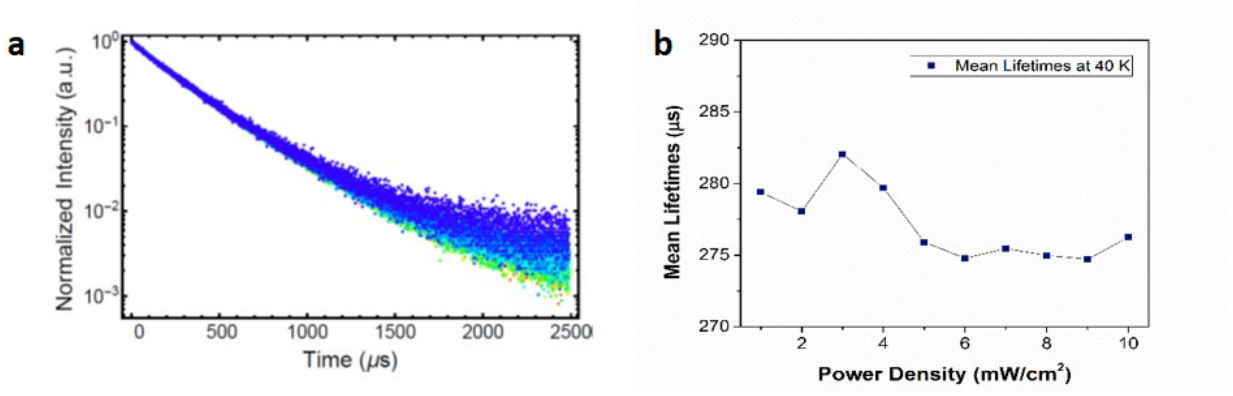

Figure 2.11: *(a) TRPL spectra and (b) the corresponding mean PL lifetimes from lognormal fitting at varying excitation power.*

2.3.4 Proposed Emission Mechanisms for SiNCs

To understand the mechanisms associated with the three different SiNC surfaces investigated here, it is useful to summarize the experimental observations first:

1. The PL emission peak energy decreases as a function of temperature for R-SiNCs and Ox. R-SiNCs but shows a slight, sigmoidal-like increase for RN-SiNCs. This occurs for both 3-and 5-nm NCs.

2. The PL intensity generally decreases as a function of increasing temperature for all the different surface functionalities.

3. The R-SiNCs and Ox. R-SiNCs have a PL lifetime on the order of hundreds of microseconds, which decreases with increasing temperature. In contrast, the RN-SiNCs show only a nanosecond lifetime that is minimally dependent on temperature.

These points and the corresponding spectral evidence provide a basis for resolving the origin of the PL for the three distinct SiNCs presented here. The observed blue-shift in PL maximum and longer lifetimes at lower temperatures for R-SiNCs, along with the lack of evidence for culpable surface groups, indicate that the dominant emission arises from a band gap transition (Figure 2.12). This is consistent with modeling by Li et al.,[197] in which alkyl passivation of SiNCs minimally changes the electronic states of the particles and, as a consequence, has minimal effect on the luminescence. Thus, the R-SiNCs provide a reference point against which the other surface functionalities can be compared directly.

The PL characteristics of the amine-terminated NCs stand out as different from those of the R-SiNCs and Ox. R-SiNCs. The minimal influence of temperature on PL spectra is consistent with a charge-transfer mechanism similar to that noted for Ce^{3+}-activated lanthanide silicon oxynitrides.[198] Similar to the case for the RN-SiNCs, nanosecond-timescale, bi-exponential PL lifetimes were noted for silicon-rich silicon nitride films, which also showed minimal temperature dependence of the PL maxima.[199] The luminescence mechanism was attributed to nitrogen related surface states in SiNCs. Drawing on these observations and another recently proposed mechanism,[121] we suggest that PL from the present RN-SiNCs originates from a rapid charge transfer from the excited state of an SiNC to a high energy silicon oxynitride surface state

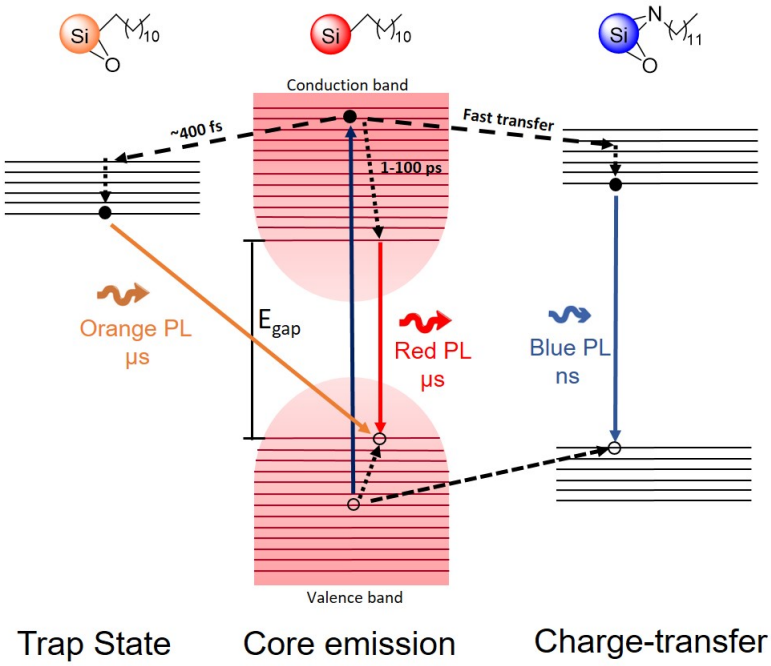

Figure 2.12: *Proposed emission mechanisms for SiNCs. The thermalization rates and electron trapping rates were obtained from ref. 199 and 202, respectively.*

(Figure 2.12, right), which is faster than the thermalization rate of the electron to the lowest level in the conduction band (1–100 ps).[200] Consequently, the exciton recombination occurs entirely at the oxynitride surface state and is isolated from the SiNC core.

The effect of oxide on the surface is more subtle. In this case, the PL emission was only slightly blue-shifted relative to the alkyl-terminated particles, but the temperature dependence was essentially similar (both blue-shifting and increasing in intensity at lower temperature). Moreover, the PL lifetimes of Ox. R-SiNCs remained in the microsecond regime, even increasing slightly relative to the R-SiNCs at low temperature where nonradiative decay mechanisms are minimized. The proposed mechanism (Figure 2.12, left) involves exciton splitting,[201] resulting in an electron being trapped at an oxide surface state (most likely bridging oxygen)[202] and subsequent recombination with a hole in the valence band. Delerue et al. proposed that electron trapping rates are faster than hole trapping rates due to the smaller capture barrier associated with the former.[46] Experimentally, electron trapping rates in silicon oxides were measured to be as short as ∼400 fs.[203] The electron withdrawing nature of the oxygen trap state

and its spatial separation[204] prevent the electron from tunneling back to the bottom of the conduction band, thus, the recombination occurs with the hole at the top of the valance band. The temperature dependence of the Ox. R-SiNC PL maxima is consistent, by and large, with this idea. The luminescent Si-O defect states should be mainly temperature-independent.[205] However, due to band gap broadening at low temperatures, the trapped electron recombines with a free hole in a deeper energy level, leading to the observed small blue-shift at lower temperatures for the Ox. R-SiNCs.

2.4 Conclusion

In summary, the temperature dependence of alkyl, partially oxidized, and alkylamine functionalized SiNCs PL emission was investigated for particles of ∼3 and ∼5 nm in diameter. Alkyl-terminated SiNCs exhibited a behaviour dominated by band-gap transitions consistent with the proposal that alkanes do not interfere with intrinsic core SiNC emission. Similarly, partially oxidized SiNCs displayed temperature-dependent PL emission, with a blue-shift of the PL maximum at lower temperatures. However, the longer lifetimes observed for these particles suggest that oxide moieties do affect the recombination pathways in SiNCs. Lastly, temperature-dependent measurements of blue-emitting alkylamine-functionalized SiNCs provided evidence for surface-state-influenced emission. TRPL measurements revealed limited temperature and size-dependent PL dynamics for RN-SiNCs, further supporting a surface-state emission mechanism. Surface groups evidently have a critical effect on freestanding SiNC luminescence mechanisms, which may be important when considering the preparation of SiNCs for optoelectronic applications.

Chapter 3

The Effect of Oxidation on the Optical Response of Silicon Nanocrystals

3.1 Introduction

Arguably, one of the most fascinating aspects of silicon nanocrystals (SiNCs) is their intricate optical response. To date, room temperature photoluminescence (PL) spanning from the visible to near-infrared has been reported for SiNCs. Numerous studies have shown that SiNC PL can be tuned by varying the nanocrystal size below silicon's Bohr exciton radius (∼4.5 nm), as dictated by quantum confinement (QC).[46,86,90,174] In addition, surface defects, dangling bonds, and surface groups can govern the intensity, colour emission, and excited-state PL lifetimes of SiNCs.[118,177,206,207] As many of the promising applications of SiNCs in bioimaging,[165,208,209] sensing,[168,195] and optoelectronics[210,211] capitalize on their optical response, understanding the factors affecting SiNCs PL is vital.

One factor that appears to play a key role in SiNC emission mechanism is surface oxidation. PL degradation and shift in emission maximum has been known for porous silicon.[2,146,212–214] Similarly, a decrease in absolute quantum yields (AQY) and a PL shift to shorter wavelengths (blue-shift) has been observed for both hydride-terminated and ligand-passivated, free-standing SiNCs.[172,215–217] Generally, a blue-shift in PL maximum has been reported for particles greater than 2 nm in diameter. In contrast, a PL

shift to longer wavelengths (red-shift) upon exposure to ambient conditions has been noted for smaller SiNCs (2–3 nm).[204] Further, SiNC PL enhancement via photoactivation by an oxygen:ethanol mixture has been reported.[145] These conflicting reports regarding the effect of oxidation on the optical response of SiNCs, which may arise due to different preparation methods of the material,[118] impede the elucidation of their emission mechanism.

The exact nature of the surface oxides formed and their effect on the emission mechanism of SiNCs is not understood well. Much effort has been made to identify the oxide species responsible for the observed PL shift in SiNCs upon oxidation.[2,144,154,155,218] Formation of surface silanones (Si=O) has been theorized by several groups as an electron trap state below the conduction band from which recombination occurs, thus accounting for the observed red-shift in small SiNCs.[2,219–221] However, though observed in bulky molecular systems,[147,150] silanone bonds have not been observed experimentally on the surface of silicon nanocrystals. Other suboxides implicated in the observed PL shifts include bridging oxygen bonds (Si–O–Si),[154,222] silanols (Si-OH),[218] and oxygen-backed silicon hydrides (-O_ySi–H_x).[144] Another school of thought suggests that the observed blue-shift in SiNC PL upon surface oxidation is due to silicon core size reduction.[155] As predicted by quantum confinement, smaller SiNCs are expected to emit at shorter wavelengths.[174] In one study, tuning the emission of SiNCs across the visible light spectrum has been achieved by controlled oxidation of H-SiNCs, which led to core shrinkage and formation of a SiO_xH_y shell.[223]

The effect of oxidation seems to vary considerably depending on the initial size of the SiNC. Blue- and red-shift in PL maxima of SiNCs have been reported, however, both phenomena have not been observed for the same SiNC system so far. Thus, the aim of this study is to investigate the role of oxygen in SiNC PL and address the disparity regarding the PL maxima shift as a result of oxidation. H-SiNCs and alkyl-passivated SiNCs were synthesized and their optical response under water vapour and oxygen atmospheres was investigated.

3.2 Materials and Methods

3.2.1 Reagents and Materials

All reagents were used as received, unless otherwise indicated. Electronic grade hydrofluoric acid (HF, 49% aqueous solution) was purchased from J. T. Baker. 1-octene (98%), phosphorus pentachloride (PCl_5, 98%), aluminum oxide (99.5%), methanol (reagent grade), benzene (reagent grade), ethanol (reagent grade), and toluene (HPLC grade) were obtained from Sigma-Aldrich. Toluene was dried using a Grubbs-type solvent purification system (Innovative Technologies, Inc.) prior to use.

3.2.2 Material Synthesis and Functionalization

Si/SiO_2 Composite Synthesis and H-SiNC Liberation. The SiNC synthesis described herein is based on a known method.[85] Briefly, 5.00 g of polymeric HSQ, synthesized following a literature procedure,[224] were placed in a zirconia boat, loaded into a tube furnace, and annealed for 1 h at 1100 °C under slightly reducing conditions (5% H_2/ 95% Ar) to render a Si/SiO_2 composite. The composite was suspended in n-pentane and pulverized using an agate mortar and pestel. The resulting fine powder was suspended in ethanol and transferred to a thick-walled glass flask containing 5 mm borosilicate beads. The solution was shaken for 4 h with a mechanical wrist action shaker. Subsequent Buchner filtration rendered the Si/SiO_2 composite.

Hydride-terminated particles (H-SiNCs) were obtained from the composite by HF etching. (*Caution: Hydrofluoric acid is extremely dangerous and must be handled with great care.*) In a typical reaction, 200 mg of composite were transferred to a Teflon beaker charged with a stir-bar and a 1:1:1 solution of 49% HF:Ethanol:H_2O. The etching time varied depending on the desired particle size (and thus emission colour). For red-emitting SiNCs, a 40 min etch time was employed. To obtain smaller SiNCs, the etch time was extended to 60 min for orange-emitting SiNCs and 90 min for yellow-emitting SiNCs. A colour change from mustard yellow to very pale yellow was observed with increasing etching time. The resulting H-SiNCs were extracted into toluene and further treated as outlined below. It is to be noted that etching time strongly depends on Si/SiO_2 composite. Target SiNCs were tested qualitatively with a hand-held UV flashlight prior to extraction into toluene. The freshly etched H-SiNCs were centrifuged twice for 5 min at 3000 rpm, with redispersion in dry toluene between

cycles.

Next, the H-SiNCs were subjected to further functionalization (vide infra) or dispersed in dry benzene (10 mL) and freeze-dried (lyophilized). Sample freeze-drying was carried out on a Schlenk line, where a suspension of SiNCs in benzene was transferred to an Ar-filled, dry flask. The suspension was subjected first to a quick vacuum, to evacuate the headspace, after which the flask was immersed in a Dewar containing liquid nitrogen under close vacuum. Once the suspension was fully frozen, the flask was opened to vacuum and lifted from the Dewar. The suspension was left to dry overnight on the line, attached to a cold N_2 trap. The resulting H-SiNCs powder was transferred to a N_2-filled glovebox for storage.

Phosphorus Pentachloride Initiated Functionalization of SiNCs. After a second centrifugation round, H-SiNCs in dry toluene (7 mL) were transferred to an oven-dried 50-mL Schlenk flask, equipped with a Teflon stir bar, and filled with Ar. Next, 1-octene (3 mL) was pre-treated by flowing through an oven-dried Pasteur pipette packed with aluminum oxide and transferred to the Schlenk flask. The reaction mixture was subjected to three cycles of freeze-pump-thaw and allowed to warm up to room temperature. 20 mg of PCl_5 were added to the flask and allowed to react for 2 h at room temperature under an Ar atmosphere. Next, 20 mL of methanol were added to the clear solution and stirred for 10 min. The resulting turbid solution was transferred to a 50-mL PTFE centrifuge tube, and 20 mL of ethanol were added to the tube. After centrifugation for 10 min at 10000 rpm, SiNCs precipitated out of solution. The supernatant was decanted, the SiNCs were redispersed in 10 mL of dry toluene, and a 1:1 methanol:ethanol solution mixture was added to the tube. The centrifugation process was repeated twice. After the last cycle, SiNCs were suspended in 2 mL of benzene and filtered through a 0.45-μm PTFE syringe filter into an oven-dried glass vial. Then, SiNCs in benzene were freeze-dried on the Schlenk line for 1 h. The resulting SiNC powder was transported to a N_2 filled glovebox for storage until further use.

3.2.3 Material Characterization and Instrumentation

All sample characterization was performed in the solid state, unless otherwise specified. Fourier-transform infrared spectroscopy (FTIR) was performed using a Nicolet Magna 750 IR spectrophotometer.

X-ray photoelectron spectroscopy (XPS) measurements were performed on a Kratos Axis Ultra instrument operating in energy spectrum mode at 210 W. Samples were prepared on a copper foil substrate. The base pressure and operating chamber pressure were maintained at 10^{-7} Pa. A monochromatic Al Kα source (λ = 8.34 Å) was used to irradiate the samples, and the spectra were obtained with an electron takeoff angle of 90°. CasaXPS software (VAMAS) was used to interpret spectra. All spectra were calibrated internally to the C 1s emission (284.8 eV). After calibration, the background was subtracted using a Shirley-type background to remove most of the extrinsic structure loss. The high-resolution Si 2p region was fit to Si $2p_{1/2}$ and Si $2p_{3/2}$ components, with spin-orbit splitting fixed at 0.6 eV, and the Si $2p_{1/2}$ / Si $2p_{3/2}$ intensity ratio set to 1/2.

Transmission electron microscopy (TEM) images were obtained using a JEOL-2010 electron microscope equipped with a LaB_6 filament and operated at an accelerating voltage of 200 kV. The TEM samples were prepared by drop-casting a dilute solution (∼1 mg/mL) of SiNCs in toluene onto a lacey carbon coated copper grid with a 300-μm diameter hole. Particle size distribution was calculated by counting at least 300 particles using ImageJ software (Version 1.49).

Steady-state and time-resolved PL spectroscopy measurements were performed under a controlled gas environment using an in-house built apparatus (Figure 3.1). SiNCs powder was coated on a 1-cm-diameter quartz wafer using a spatula and loaded into an aluminum sample chamber equipped with a gas inlet and outlet and quartz windows. All samples were loaded inside the glovebox to minimize exposure to oxygen and moisture. A gas manifold was used to control the flow of target gas (Ar or O_2), which flowed directly into the sample chamber or went through a bubbler filled with DI water. The gas flow rate was maintained at 8 L/min. The excitation source, a continuous wave diode laser emitting at 445 nm, was modulated by an Isomet IMDD-T110L-1.5 acousto-optic modulator (AOM) operating at a frequency of 200 Hz with a 50% duty cycle. The PL was collected by an optic fiber, passed through a 500-nm long-pass filter, and collected by an OceanOptics USB2000 spectrometer. The spectral response was calibrated by a black-body radiator (Ocean Optics LS1). For time-resolved PL, the same setup was employed, but the incident light was collected by a Becker-Hickl PMC-100 photon-counting PMT. The PL data was collected in 1-μs timesteps, and a total of 10000 sweeps were collected for a good signal-to-noise ratio.

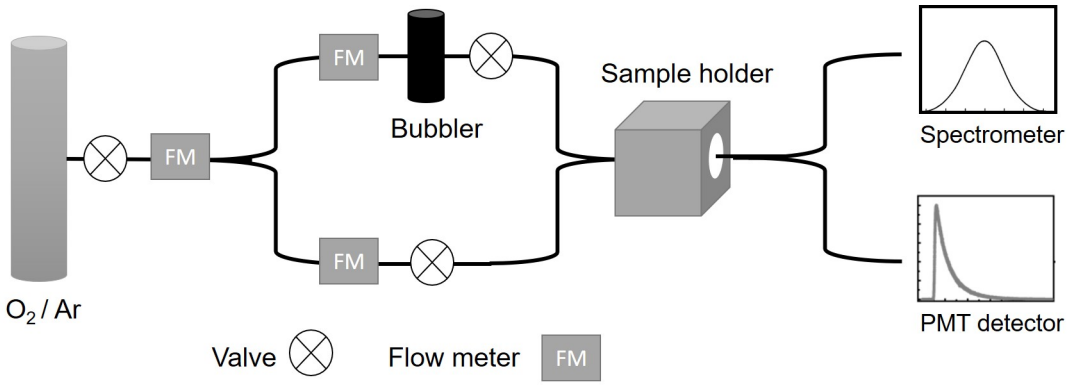

Figure 3.1: *Diagram of the gas manifold used to conduct PL measurements under a controlled gas environment.*

3.3 Results and Discussion

3.3.1 Synthesis and Optical Characterization of H-SiNCs

In order to obtain H-SiNCs with size-dependent colour emission, the HSQ method was utilized with a slight modification.[85] Following the thermal processing of HSQ, H-SiNCs were liberated from the resulting Si/SiO_2 composite by HF etching. By increasing the etching time, H-SiNCs with red (30 min), orange (60 min), and yellow (90 min) emission colour were obtained (Figure 3.2). The resulting SiNC precipitates were lighter yellow in colour the smaller their size. In order to minimize oxidation, the H-SiNCs were freeze-dried and stored in powder form in a N_2-filled glovebox. While TEM imaging of unpassivated SiNC is difficult to carry out due to poor Z-contrast and aggregation of the particles, an attempt to determine the size of the resulting H-SiNCs was made, nonetheless. Figure 3.3 shows TEM images for the yellow- (a), orange- (b), and red-emitting (c) H-SiNCs. Size distribution analysis shows statistically significant difference in H-SiNC sizes, and the particles were determined to be 2.1±0.3 nm (yellow), 2.5±0.3 nm (orange), and 3.0±0.4 nm (red) in diameter (Figure 3.3 d-f), suggesting that the observed colour emission is the result of QC effects.

Following the determination of particle size, PL spectra of the H-SiNCs were taken before and after exposure to a wet Ar atmosphere using the setup outlined in Figure 3.1. A small amount of H-SiNC powder (∼1 mg) was placed on a quartz wafer with a spatula and loaded into the sample chamber inside the glovebox. The samples were excited with a 445-nm diode laser under dry and wet Ar (50% humidity) atmospheres. Due

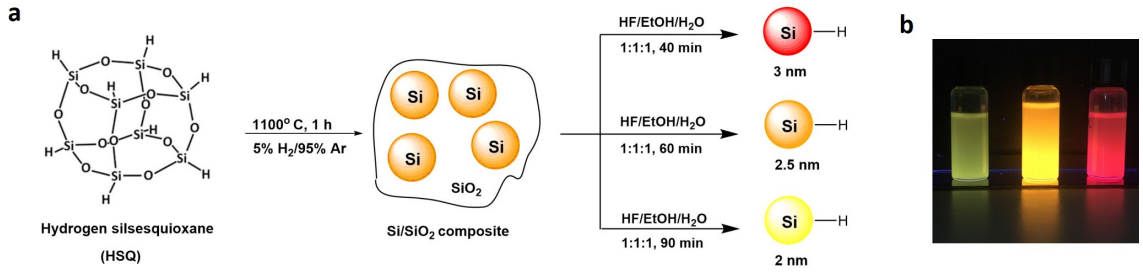

Figure 3.2: *Thermal annealing and H-SiNCs liberation scheme (a). Photograph of corresponding H-SiNCs dispersions in toluene under UV illumination (b).*

to their higher reactivity, the yellow-emitting H-SiNCs were not stable enough for PL measurements since a drastic drop in PL intensity (most likely due to photobleaching) and PL maximum shifting was observed almost immediately. For both the orange- and red-emitting H-SiNCs (Figure 3.4 a,b), an additional peak was observed in the PL spectrum centering around 840 nm. This peak did not change position as a result of exposure to a wet atmosphere and most likely originated from SiNCs that were not fully etched. Since the H-SiNCs were not subjected to any purification or size-exclusion treatment (in order to avoid oxidation), there was no way to eliminate SiNCs still embedded in a thin layer of SiO_2. For clarity, the peaks associated with the IR-emitting species are shaded grey.

Exposure to wet Ar had an opposing effect on the orange- and red-emitting H-SiNCs. While the PL peak associated with the orange-emitting H-SiNCs red-shifted by approximately 40 nm (Figure 3.4 a), the PL peak for the red-emitting H-SiNCs blue-shifted by approximately 40 nm (Figure 3.4 b). Interestingly, time-resolved PL spectroscopy of the same samples showed a different trend, where the final PL lifetime for both samples was similar. From lognormal fitting of the PL decays, the average PL lifetime of the orange-emitting H-SiNCs increased from 18.4 to 36.9 μs following exposure to wet Ar (Figure 3.4 c), and that of the red-emitting H-SiNCs increased from 31.2 to 36.4 μs (Figure 3.4 d). While these preliminary results hint that a surface state might be generated upon exposure of silicon surface to an oxidizing atmosphere, the instability of the unprotected H-SiNCs prevented them from being studied further. More practically, the effect of oxidation on passivated SiNCs is of greater interest due to the their wider applicability.

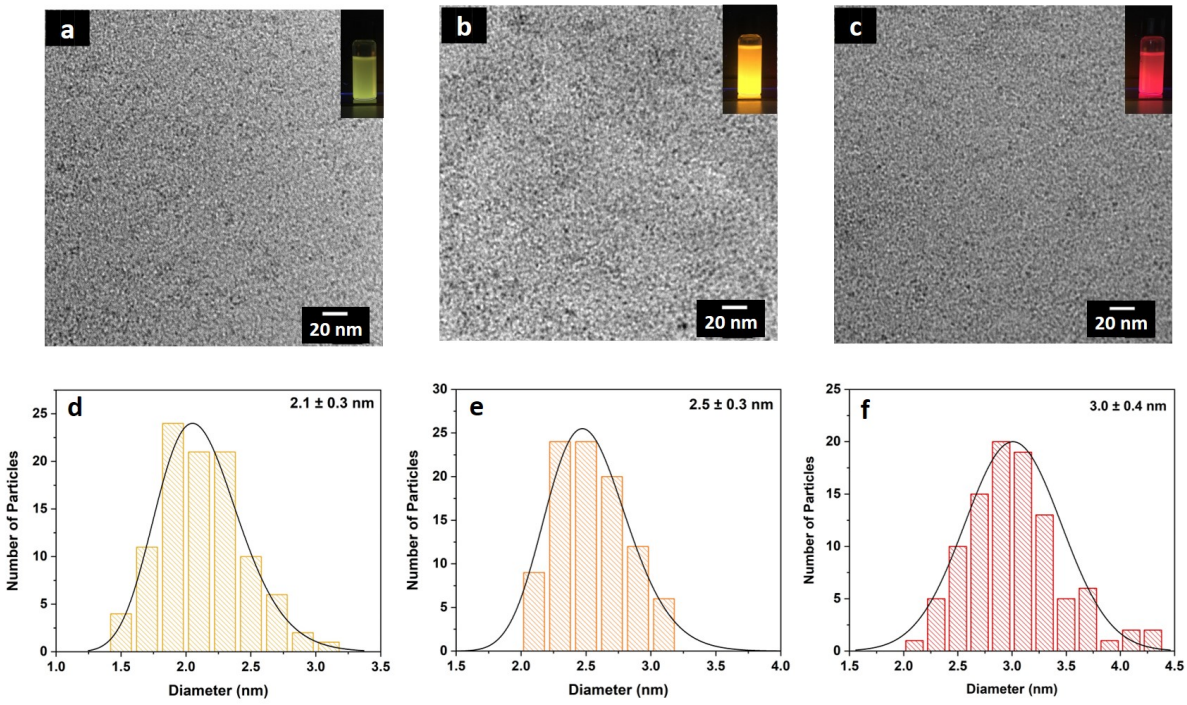

Figure 3.3: *Transmission electron microscopy bright field images for yellow H-SiNCs (a), orange H-SiNCs (b), Red H-SiNCs (c), and their corresponding size distribution histograms (d-f).*

3.3.2 Functionalization and Optical Response of R-SiNCs

Hydrosilylation of SiNC with organic ligands has been an effective route to minimize surface oxidation and PL degradation. However, most hydrosilylation methods involve heat and/or long reaction times.[100,102,106] These conditions are problematic for the functionalization of smaller SiNCs, which readily react with trace water upon heating.[225] Thus, any attempts made to functionalize yellow-emitting H-SiNCs with organic ligands using thermal- or radical-initiated hydrosilylation resulted in orange-emitting particles. Recently, Islam et al.[104] reported a PCl_5-mediated room temperature functionalization of SiNCs with organic ligands. One key feature of the reaction is the dual role of PCl_5 as a radical source and a mild etchant. Thus, when PCl_5 was used to initiate the functionalization of yellow-emitting H-SiNCs with 1-octene, the original emission colour was preserved. This most likely is due to the removal of any suboxide species formed during the reaction by PCl_5. Red-, orange-, and yellow-emitting H-SiNCs were passivated successfully with 1-octene using PCl_5, as outlined in Figure 3.5

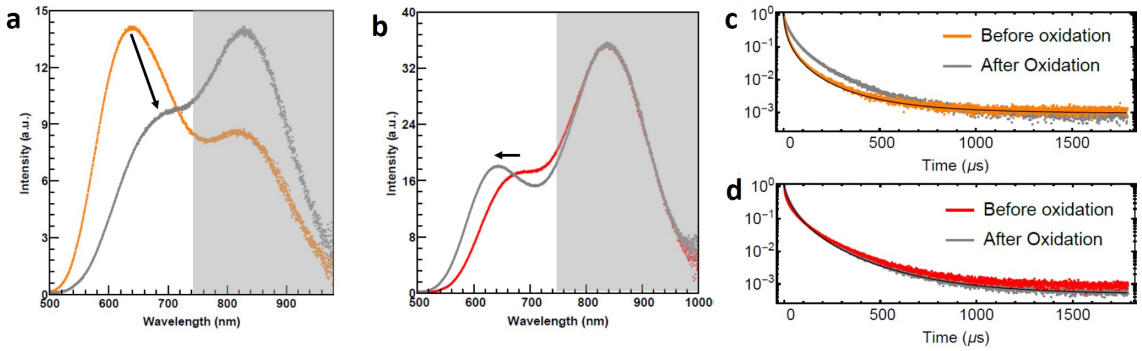

Figure 3.4: *PL of orange (a) and red (b) H-SiNCs before and after exposure to wet Ar and their respective lifetimes (c-d). The greyed-out area is added for clarity.*

a. The octyl passivated SiNCs (R-SiNCs) were readily dispersible in organic solvents and showed visible PL emission under UV excitation (Figure 3.5 b,c). The R-SiNCs were freeze-dried and stored in the glovebox in order to minimize oxidation as much as possible.

Figure 3.5: *PCl_5-mediated hydrosilylation of SiNCs with 1-octene (a), dispersions of R-SiNCs in toluene under ambient (b) and UV light (c).*

TEM images of the yellow-, orange-, and red-emitting R-SiNCs are shown in Figure 3.6. The R-SiNCs were determined to be 2.1±0.3 nm (yellow), 2.4±0.5 nm (orange), and 3.1±0.5 nm (red) in diameter, which is comparable to the H-SiNCs diameters reported in Figure 3.3, indicating that the blue-shift in PL emission observed with decrease in particle size is consistent with QC theory.

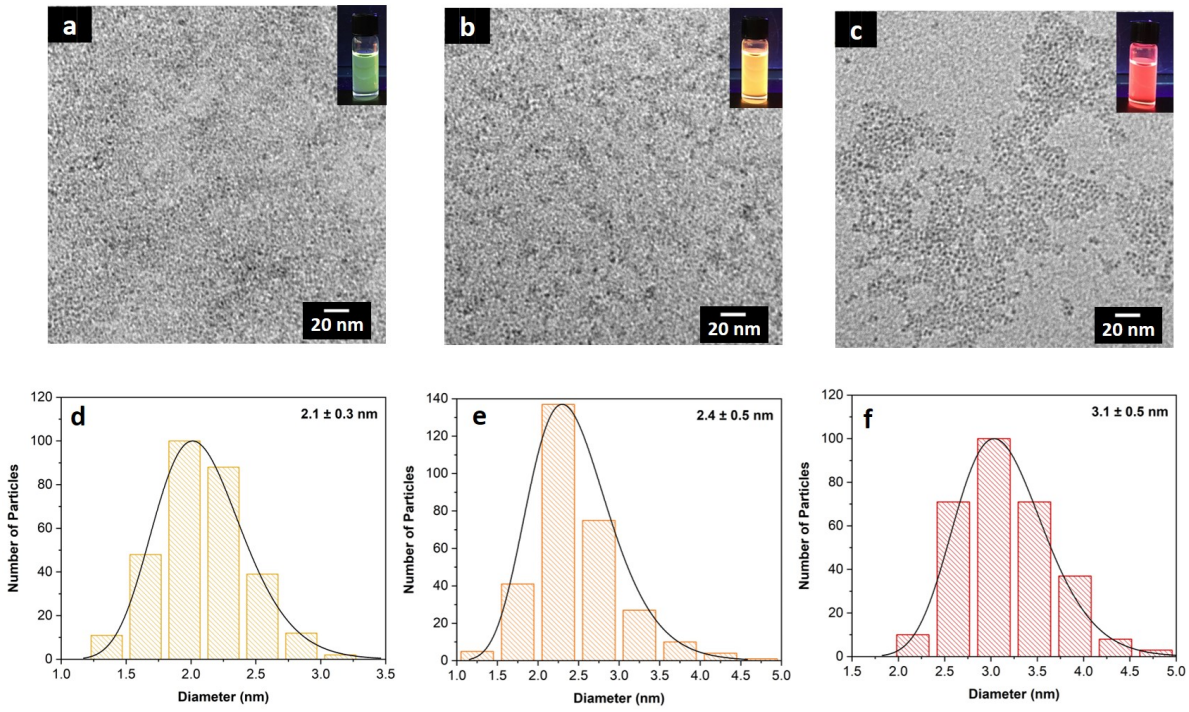

Figure 3.6: *Transmission electron microscopy bright field images for yellow- (a), orange- (b), and red-emitting R-SiNCs (c).*

The optical response of the synthesized R-SiNCs was investigated under three conditions: exposure to wet Ar, dry O_2, and wet O_2. The different atmospheres were controlled by a gas manifold and a liquid bubbler filled with DI water, as outlined in Figure 3.1. PL spectra were collected at 10 s intervals under continuous excitation by a 445-nm light source. All samples were irradiated under a dry Ar atmosphere prior to the introduction of the different atmosphere in order to stabilize the PL response. As previously observed,[132] minimal change in PL maximum ($\Delta = 5$ nm) was recorded upon sample excitation under a dry Ar atmosphere. However, the PL intensity did decrease under continuous excitation, most likely due to photobleaching.[195] Once the PL response stabilized, such that a minimal change in PL maximum and intensity was observed, the in-situ PL measurements under various chemical environments commenced.

The PL evolution of the yellow-, orange-, and red-emitting R-SiNCs upon exposure to wet Ar (50% humidity) is depicted in Figure 3.7. The IR emission at 840 nm seen in the H-SiNC PL spectra (Figure 3.4) is no longer observed for the passivated R-SiNCs,

confirming the elimination of these emissive species during the purification process. From skew-normal fitting of the PL data,[186] upon exposure to wet Ar, a 26-nm red-shift in PL maxima of the yellow-emitting R-SiNCs was observed (Figure 3.7 a). In addition, the PL intensity of the yellow-emitting R-SiNCs decreased by ∼80%. The red-emitting R-SiNCs, on the other-hand, showed a 7-nm blue-shift upon exposure to wet Ar and a ∼19% increase in PL intensity (Figure 3.7 c). A more complicated optical response was recorded for the orange-emitting R-SiNCs (Figure 3.7 b). Initially, a small blue-shift (4 nm) and a decrease in PL intensity (∼12%) was observed, followed by a red-shift of 6 nm and recovery of the PL intensity (∼10%).

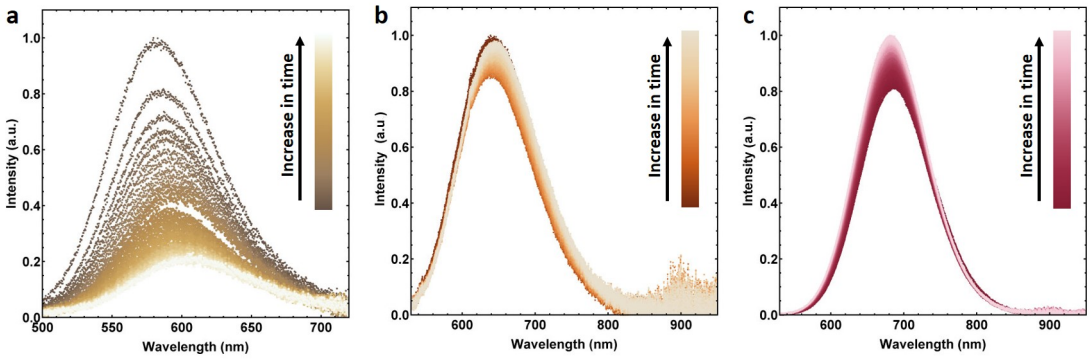

Figure 3.7: *PL spectra as a function of exposure time to wet Ar (50% humidity) atmosphere for yellow- (a), orange- (b), and red-emitting R-SiNCs (c).*

In the case of a dry O_2 atmosphere, an appreciable decrease in PL intensity was observed for all samples (Figure 3.8). Both yellow- and red-emitting R-SiNCs displayed a ∼55% decrease in intensity from their initial value, while the PL of the orange-emitting R-SiNCs decreased by ∼46%. PL quenching of SiNCs in porous silicon as a result of exposure to O_2 has been observed previously.[212,214] The photodegradation was attributed to the generation of singlet oxygen species, which react with the silicon surface to form non-radiative defects.[226,227] The presence of Si–H bonds on the surface of R-SiNCs, as evidenced by FTIR analysis (vide infra), provides a convenient platform for the singlet oxygen to react with. The trends in PL peak emission were consistent with those observed for a wet Ar atmosphere. The yellow-emitting R-SiNCs shifted to longer wavelengths, and the red-emitting particles shifted to shorter wavelengths. In the case of orange-emitting R-SiNCs, a 23-nm red-shift was recorded.

Lastly, the combined effect of water vapour and oxygen on the optical response

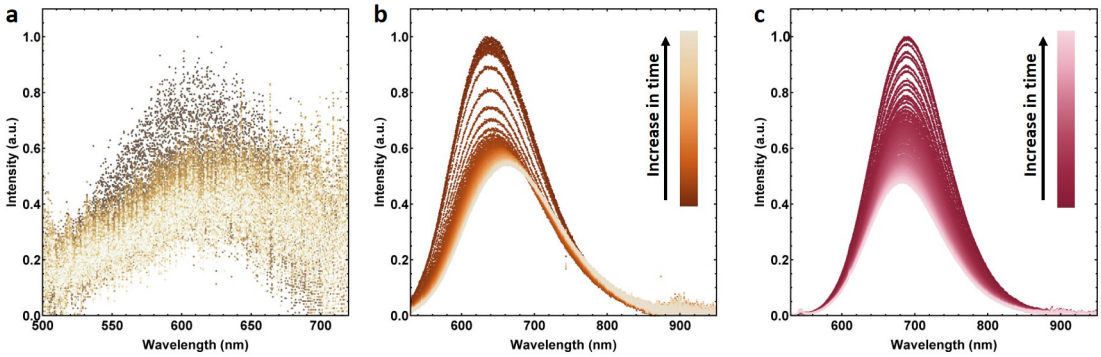

Figure 3.8: *PL spectra as a function of exposure time to a dry O_2 atmosphere for yellow- (a), orange- (b), and red-emitting R-SiNCs (c).*

of the R-SiNCs was probed using a wet O_2 atmosphere (50% humidity) and shown in Figure 3.9. Not surprisingly, a more pronounced change in PL maximum was observed under these conditions due to the combined effect of water and oxygen. The yellow-emitting R-SiNCs red-shifted by 27 nm, while the orange-emitting R-SiNCs red-shifted by 40 nm. On the other hand, consistent with the previous conditions (wet Ar and dry O_2), the red-emitting R-SiNCs blue-shifted by 33 nm. More interestingly, photoactivation was observed in the case of the yellow- and orange-emitting R-SiNCs. Upon exposure to wet O_2, the PL intensity of the yellow-emitting R-SiNCs increased by ∼30%. While an initial decrease in intensity was observed for the orange-emitting R-SiNCs, a subsequent increase is seen clearly in Figure 3.9. In a similar study, photoactivation of SiNCs was observed under blue-light irradiation and in the presence of an ethanol:O_2 mixture.[145] The increase in PL intensity was attributed to irreversible surface oxidation, which passivated dangling bonds.

In addition to PL spectroscopy, the excited state PL lifetimes of the R-SiNCs were collected before and after exposure to wet Ar, dry O_2, and wet O_2. The decay traces were fit using a log-normal lifetime distribution,[194] and the extracted mean excited-state lifetimes are summarized in Table 3.1. As predicted by theory,[196] the initial excited state lifetimes of the R-SiNCs increased with particle size. In addition, upon exposure to the various gaseous environments, similar trends to those observed in the PL spectra of the R-SiNCs emerge. The excited state lifetimes of the yellow- and orange-emitting R-SiNCs increased following exposure to water and oxygen, while those of the red-emitting R-SiNCs decreased. The PL lifetime data is not definitive

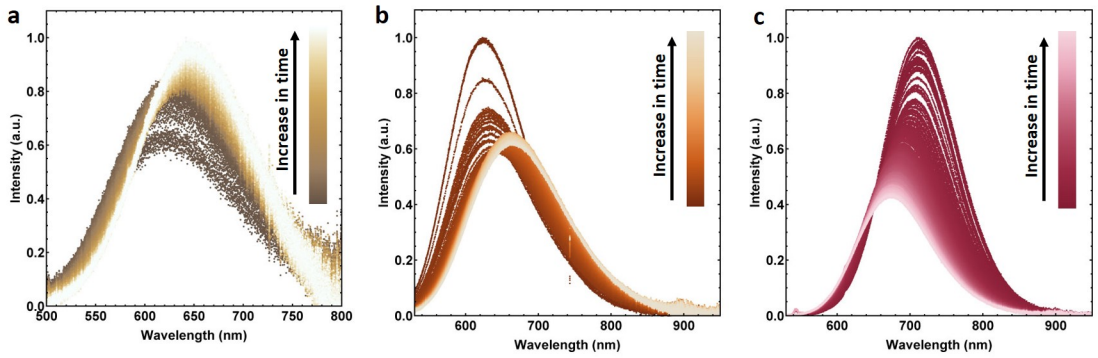

Figure 3.9: *PL spectra as a function of exposure time to a wet O_2 atmosphere for yellow- (a), orange- (b), and red-emitting R-SiNCs (c).*

enough to draw any conclusions regarding the underlying emission mechanisms associated with the oxidation of the particles. However, even though the final values for all three samples are different, they are trending towards a similar average lifetime value, suggesting an underlying common surface state.

Table 3.1: *Mean PL Lifetimes of R-SiNCs Under Various Conditions*

	Yellow R-SiNCs		Orange R-SiNCs		Red R-SiNCs	
	τ_{initial} (μs)	τ_{final} (μs)	τ_{initial} (μs)	τ_{final} (μs)	τ_{initial} (μs)	τ_{final} (μs)
Wet Ar	10.3 ± 0.1	19.3 ± 0.1	14.6 ± 0.1	16.0 ± 0.1	39.9 ± 0.1	30.3 ± 0.1
Dry O_2	16.4 ± 0.1	27.3 ± 0.2	27.0 ± 0.1	39.0 ± 0.2	40.3 ± 0.1	34.4 ± 0.1
Wet O_2	16.9 ± 0.1	44.3 ± 0.1	25.3 ± 0.1	54.0 ± 0.2	49.2 ± 0.1	40.6 ± 0.1

3.3.3 R-SiNCs Surface Characterization

From the in-situ PL measurements carried out, it became apparent that while water and oxygen have an effect on the PL of R-SiNCs, the full extent of their effect on the optical response could not be evaluated within the parameters of the experiment. Thus, the PL spectra of the yellow-, orange-, and red-emitting R-SiNCs was collected immediately after synthesis under an inert atmosphere and after three month exposure to ambient air. Though the air composition and humidity differed from the in-situ experimental setup, it presented a more realistic representation of conditions to which R-SiNCs are to be exposed in future applications. The resulting PL spectra are depicted

in Figure 3.10. As has been the trend so far, the yellow- and orange-emitting R-SiNCs red-shifted, while the red-emitting R-SiNCs blue-shifted. Remarkably, all three samples converged to the same emission wavelength, around 660 nm, suggesting that a common surface state may be forming upon oxidation.

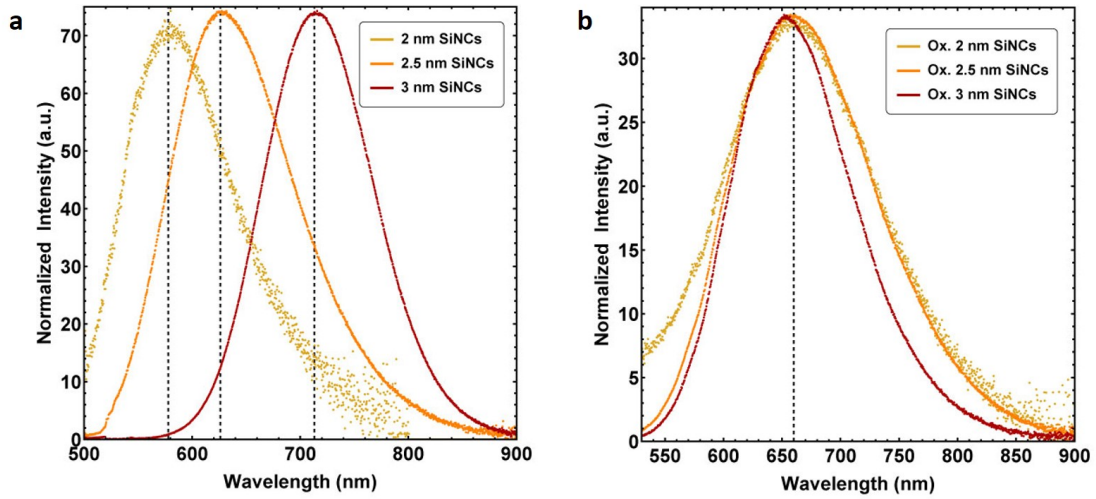

Figure 3.10: *PL spectra as a function of yellow-, orange-, and red-emitting R-SiNCs before (a) and after (b) exposure to ambient air.*

In order to gain more insight into the surface of the R-SiNCs following oxidation under ambient conditions, FTIR analysis of the R-SiNCs was performed. FTIR spectra of the as synthesized R-SiNCs are shown in Figure 3.11 a. All three samples displayed intense vibrations in the 2650–2900 cm^{-1} region, attributed to C–H stretching of the octyl ligand. In addition, C–H bending vibrations were observed at 1380–1470 cm^{-1}. The presence of Si–H_x bending and scissoring vibrations at 2100 and 900 cm^{-1}, respectively, suggests that the silicon surface was not passivated fully. While incomplete surface coverage is undesirable under normal circumstances, the remaining Si–H bonds provided a convenient platform for the oxidation of R-SiNCs. Lastly, while efforts were made to minimize surface oxidation, Si–O–Si and -O_ySi–H_x stretching features at 1100 and 2250 cm^{-1}, respectively, were observed, suggesting some surface oxidation was present in the original samples.

Following exposure to ambient conditions, several changes in the FTIR spectra were observed (Figure 3.11 b). The vibrations associated with C–H stretching and bending (2650–2900 and 1380–1470 cm^{-1}, respectively) were still present, while a significant decrease in the intensity of the Si–H_x stretching vibration was observed. In addition,

the Si–O–Si mode at 1100 cm^{-1} increased in comparison to the initial FTIR spectra. All three samples displayed new features associated with oxygen backed silicon hydride ($-O_ySi–H_x$) stretching and scissoring at 2250 and 880 cm^{-1}, respectively.[151] Recently, Chen et al.[144] reported that the shift in PL maxima observed in SiNCs was related directly to the $-OSiH_x$ species. Another feature that appears in the 3200–3700 cm^{-1} range for the red- and yellow-emitting R-SiNCs is of note. This vibration most commonly is assigned to OH stretching, although SiO–H stretching cannot be ruled out fully.[151]

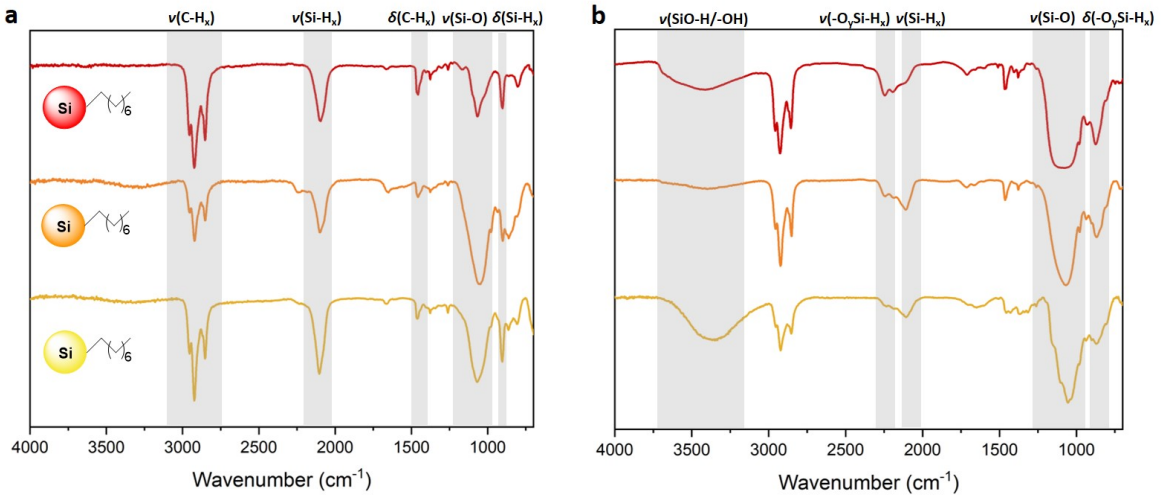

Figure 3.11: *FTIR spectra of red-, orange-, and yellow-emitting R-SiNCs before (a) and after (b) oxidation.*

High-resolution X-ray photoelectron spectra of the Si 2p region provided further insight into the surface of the R-SiNCs before and after exposure to ambient atmosphere (Figure 3.12). Initially, all three samples showed minimal oxidation at the sensitivity of the method, as evidenced by the dominant Si(0) peak at 99.4 eV in the Si 2p spectra (Figure 3.12 a,c,e). Additional peaks, formally assigned to Si(II) and Si(III), are the result of surface ligands and suboxides,[85] which is in agreement with the FTIR spectra. However, the Si(0) peak decreased by 94%, 74%, and 77% for the yellow-, orange-, red-emitting R-SiNCs, respectively following exposure to air (Figure 3.12 b, d, f). Additional components appear in the 101 to 106 eV region, associated with silicon suboxides and SiO_2, confirming the increased oxidation of the silicon in all three R-SiNC samples.

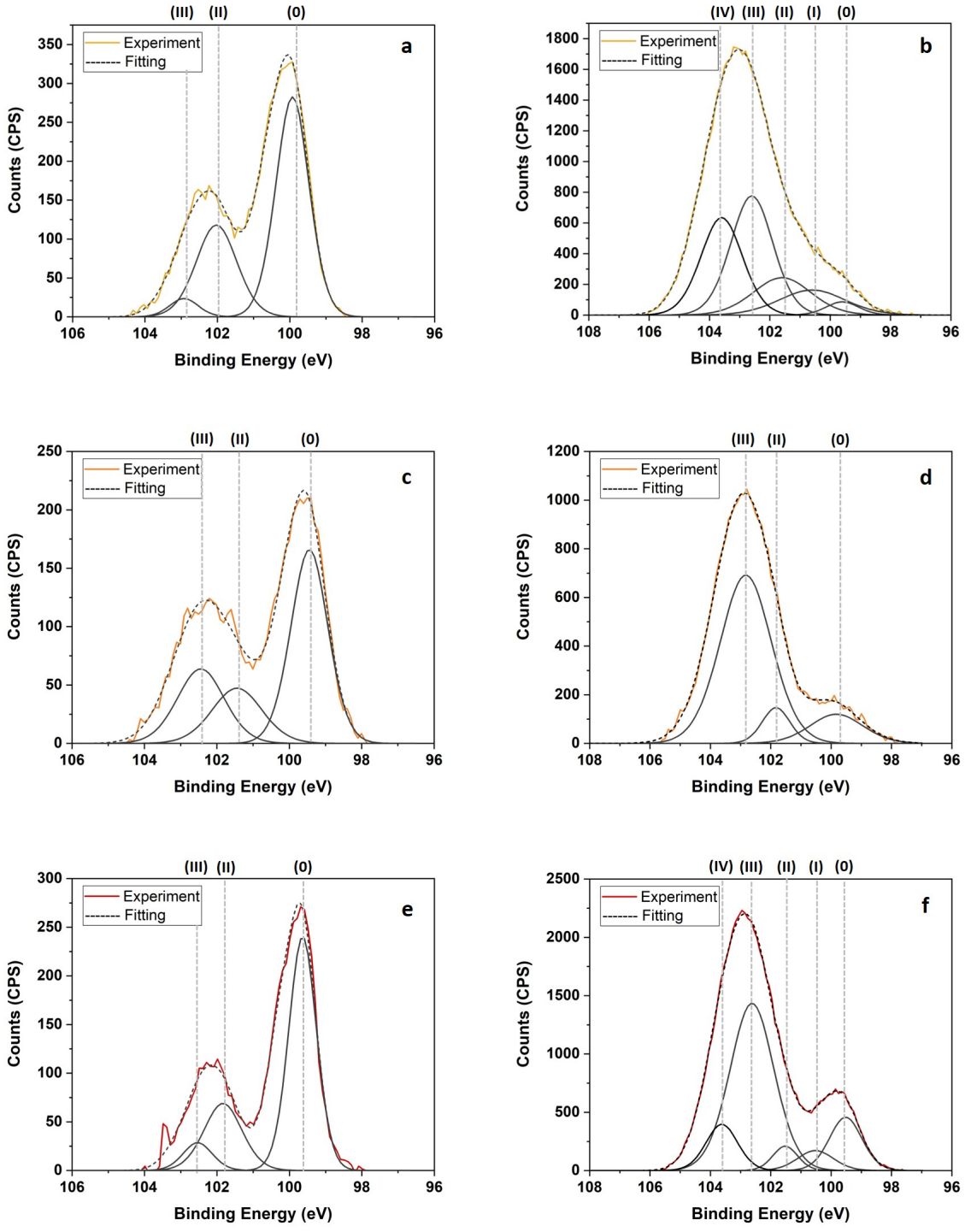

Figure 3.12: *High resolution X-ray photoelectron spectra of Si 2p region for yellow-, orange-, and red-emitting R-SiNCs before (a,c,e) and after oxidation (b,d,f). Please note, only $2p_{3/2}$ deconvolution components are shown; $2p_{1/2}$ components are omitted for clarity.*

The presence of the same suboxides, as confirmed by FTIR and XPS analyses for all three R-SiNC sizes, form a compelling argument for an oxide surface-state-related emission in oxidized R-SiNCs. A consistent trend in PL shift has been observed for the R-SiNCs under all conditions investigated that are known to promote surface oxidation.[132] SiNCs larger than 2.5 nm in diameter showed blue-shift, while those smaller that 2.5 nm displayed red-shift upon oxidation. More importantly, the oxidized R-SiNCs luminescence appeared to centre around 1.9 eV (∼650 nm). A review of the literature reveals numerous examples of SiNC oxidation in air leading to emission in the same range.[72,92,117,144,217,228,229] One convincing theory invokes shrinkage of the silicon core upon oxidation, which will lead to blue-shifting of the PL.[155,230] The oxidation is proposed to be a self-limiting process due to the increased interface curvature between the SiNC and the forming of native oxide. As a result, the SiNCs do not fully convert to SiO_2. If this argument is to be followed, then the smaller, more reactive SiNCs also are expected to shrink in size and blue-shift. However, the opposite is observed. Moreover, upon oxidation, the excited-state lifetimes of the smaller SiNCs became longer; this contradicts the proportional relationship between PL lifetimes and SiNC size.[196]

Drawing from the experimental evidence in the present and previously published work,[92,231] an oxide-related surface-state emission mechanism is proposed, whereby an electron is trapped at an oxide surface state and recombines with a free hole in the conduction band. A similar mechanism was proposed by Wolkin et al. for SiNCs 1.5–3 nm in diameter.[2] However, the proposed mechanism is extended to SiNCs greater than 3 nm, where the oxide-based surface state occurs at a higher energy than the bottom of the conduction band in the silicon core.[200] Thus, the position of the oxide surface state with respect to the SiNC conduction band depends on the crystal size. While the nature of the oxide surface state cannot be determined conclusively from the presented data, the increase in bridging oxygen in the FTIR, as well as oxygen-backed silicon hydride, suggest that these species might be involved in the observed PL shifts. Resonant coupling between the vibration mode of bridging oxygen and the electronic states of SiNCs has been reported previously.[232] In addition, theoretical calculations by Vasiliev et al.[154] and Luppi et al.[202] suggest that bridging oxygen can play a role in SiNC PL.

3.4 Conclusion

In the present study, the effect of oxidation on the optical response of hydride and alkyl-passivated SiNCs was investigated. In-situ PL spectroscopy under three oxidizing atmospheres, wet Ar, dry O_2, and wet O_2, revealed the effect of oxidation on the optical response of SiNCs is size-dependent. Larger nanocrystals (d>2.5 nm) blue-shifted upon exposure to water vapour and oxygen atmosphere, while smaller nanocrystals (d<2.5 nm) red-shifted under the same conditions. Interestingly, all three SiNC samples under investigation converged to the same emission maximum after prolonged exposure to ambient atmosphere, which suggests that an oxygen-related surface state affects the emission mechanism of SiNCs. Understanding the long-term effect of oxygen on the optical response of SiNCs is of fundamental importance and a key to the successful incorporation of SiNCs in optoelectronic applications.

Chapter 4

Interfacing Silicon Nanocrystals with Conjugated Surface Groups*

4.1 Introduction

Quantum dots (QD) are often touted as promising alternatives to organic dyes for optoelectronic and medical imaging applications. Photophysical properties of import include: brightness, high quantum yields and molar absorption coefficients, narrow full-width-at-half-maximum (FWHM) emission, and minimal blinking and photobleaching behaviour.[209,233] Traditional Cd-based QDs display most of the listed photophysical requirements,[234–236] however, their application is hindered due to potential toxicity concerns and regional restrictions.[237] In addition, for bioimaging applications, the emission lifetimes of direct band gap QDs are within the timescale of cell autofluorescence (i.e., pico to nanosecond scale).[238] SiNCs, on the other hand, display microsecond lifetimes, which is suitable for time-gated imaging. In addition, SiNCs have low cytotoxicity.[239] However, unlike conventional direct band gap QDs, SiNCs suffer from broad FWHM,[240] low molar absorption coefficients,[241] blinking,[242] and relatively low QYs.[117]

One strategy for enhancing the optical properties of QDs involves coupling with organic chromophores, leading to energy transfer.[157,243] Zhou et al.[244] demonstrated band gap tuning of SiNCs by functionalization with conjugated surface groups through an alkyne, whereby a 70-nm red-shift was observed. A first-principles study by Wang et

*Part of this chapter has been published: Angı, A.; Sinelnikov, R.; Meldrum, A.; Veinot, J. G. C.; Balberg, I.; Azulay, D.; Millo, O.; Rieger, B. *Nanoscale* **2016**, *8*, 7849–7853. Reproduced by permission of The Royal Society of Chemistry.

al.[245] proposed that interfacing surface groups with SiNCs through conjugated bonds changes the electronic structure and optical properties of SiNCs. PL enhancement and increased absorption in the visible range was observed by the Swihart[246] and Ceroni groups[160,161] when SiNCs were interfaced with conjugated aromatic groups. Le and Jeong proposed that a strong electronic interaction between SiNCs and conjugated capping molecules through the covalent bond is a possible mechanism for a more direct band gap character of SiNCs.[247] More recently, sensitization of SiNC PL using pyrene- and perylene-capping and their application in bioimaging was demonstrated.[248]

In this Chapter, a series of studies on the effects of interfacing conjugated surface groups with SiNCs is presented. First, the influence of fluorophore distance from the SiNC core on the latter's optical response was investigated through PL spectroscopy studies of a series of SiNCs passivated with naphthenyl groups with varying chain length. Next, the effect of aryl aldehyde fluorophores with varying degrees of conjugation on the absorption and emission properties of SiNCs was evaluated. Lastly, the impact of conjugated surface groups on the optoelectronic properties of SiNCs was studied via optical and scanning tunneling spectroscopies.

4.2 Materials and Methods

4.2.1 Reagents and Materials

All reagents were used as received, unless otherwise indicated. Electronic grade hydrofluoric acid (HF, 49% aqueous solution) was purchased from J. T. Baker. Xenon difluoride (XeF_2, 99.5%) 2-naphthaldehyde (98%), 9-anthracenecarboxaldehyde (98%), and 1-pyrenecarboxaldehyde (99%) were purchased from Alfa Aesar. Allyl bromide (99%), 4-bromo-1-butene (97%), 5-bromo-1-pentene (95%), 2-vinylnaphthalene (98%), 1-dodecene (95%), 2-naphthylmagnesium bromide (0.5 M in THF), ($Ni(dppe)Cl_2$) [1,2-bis(diphenylphosphino)ethane]-dichloronickel(II), phenyllithium (1.8 M in dibutyl ether), n-hexyllithium (2.3 M in hexane), n-butyllithium (2.5 M in hexane), 1,2-dichlorobenzene (99%), aluminum oxide (99.5%), methanol (reagent grade), benzene (reagent grade), ethanol (reagent grade), hexanes (reagent grade), and toluene (HPLC grade) were obtained from Sigma-Aldrich. Acetonitrile (HPLC grade) and tetrahydrofuran (THF, inhibitor-free, HPLC grade) were obtained from Caledon Laboratory Chemicals. Acetonitrile, toluene and THF were dried using a Grubbs-type solvent

purification system (Innovative Technologies, Inc.) prior to use.

4.2.2 Material Synthesis and Functionalization

General Procedure for Naphthenyl Derivatives Synthesis using Kumada Cross-Coupling. Naphthalene ligands with vinyl alkenes were prepared using a literature procedure.[249] In a typical reaction, $Ni(dppe)Cl_2$ (8 mg, 0.015 mmol) and alkenyl halide (3 mmol, 1.5 eq.) were dissolved in 20 mL dry toluene and degassed. The reaction flask was cooled to −78 °C using an acetone/dry-ice bath, 2-naphthylmagnesium bromide (8 mL, 4 mmol, 2 eq.) was added to the reaction mixture drop-wise, and the reaction was brought slowly to room temperature. The solution was stirred at room temperature for 20 h. Work-up was carried out by first quenching the reaction with dilute hydrochloric acid. Next, the organic layer and the ether extracts from the aqueous layer were combined, dried over magnesium sulfate, and concentrated in vacuo. The crude product was purified by column chromatography with a 9:1 hexanes:toluene eluent mixture.

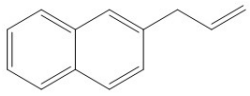

2-allylnaphthalene. Synthesized according to outlined procedure (vide supra) from allyl bromide (0.25 mL). Clear yellow liquid was isolated by column chromatography.

^{1}H NMR ($CDCl_3$, 500 MHz) δ(ppm) = 7.84–7.79 (m, 3H), 7.66 (s, 1H), 7.48–7.46 (m, 3H), 6.01 (m, 1H), 5.10 (m, 2H), 3.58 (d, 2H).

EI-MS. Calculated $[M]^+$ for $C_{13}H_{12}$ 168.09, detected 168.09.

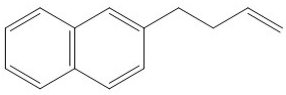

2-(3-Butenyl)naphthalene. Synthesized according to outlined procedure (vide supra) from 4-bromo-1-butene (0.3 mL). Clear yellow liquid was isolated by column chromatography.

^{1}H NMR ($CDCl_3$, 500 MHz) δ(ppm) = 7.85–7.77 (m, 3H), 7.66 (s, 1H), 7.48–7.46 (m, 3H), 5.92 (m, 1H), 5.08 (m, 2H), 2.91 (t, 2H), 2.51 (q, 2H).

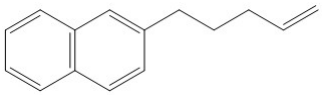

EI-MS. Calculated $[M]^+$ for $C_{14}H_{14}$ 182.11, detected 182.11.

2-(4-pentenyl)naphthalene. Synthesized according to outlined procedure (vide supra) from 5-bromo-1-pentene (0.35 mL). Yellow solid was isolated by column chromatography.

^{1}H NMR ($CDCl_3$, 500 MHz) δ(ppm) = 8.01–7.79 (m, 3H), 7.66 (s, 1H), 7.55–7.46 (m, 3H), 5.87 (m, 1H), 5.06 (m, 2H), 2.83 (t, 2H), 2.15 (q, 2H), 1.87 (quin, 2H).

EI-MS. Calculated $[M]^+$ for $C_{15}H_{16}$ 196.13, detected 196.12.

SiNC/SiO_2 Composite Synthesis and SiNC Liberation from Matrix. As was outlined in Section 3.2.2, Si/SiO_2 composite was synthesized and processed following a literature procedure.[85] In a typical reaction, 200 mg of composite were etched for 40 min in a 1:1:1 49% HF:Ethanol:H_2O solution. (*Caution: Hydrofluoric acid is extremely dangerous and must be handled with great care.*) The resulting H-SiNCs were extracted with toluene and centrifuged at 3000 rpm for 10 min.

Thermal Hydrosilylation of H-SiNCs with Naphthenyl Derivatives. H-SiNCs were functionalized with the naphthenyl derivatives following an established literature procedure for thermal hydrosilylation.[100] Freshly etched H-SiNCs were dispersed in 1,2-dichlorobenzene (10 mL) and transferred to an oven-dried Schlenk flask containing 0.2 g of naphthenyl ligand and a Teflon stir bar. The flask was equipped with a water-cooled condenser and charged with Ar. The reaction mixture was degassed three times and then heated for 18 h at 160 °C under an inert atmosphere. Upon reaction completion, the solution was dispensed evenly into 50-mL PTFE centrifuge tubes and filled with a 1:2 methanol:hexanes mixture. The precipitate was isolated by centrifugation at 12000 rpm for 15 min. The supernatant was decanted, the particles were redispersed in a minimum amount of toluene and, subsequently, precipitated by addition of the 1:2 methanol:hexanes mixture again. The centrifugation and decanting procedure was repeated twice. The resulting precipitate was dispersed in toluene, filtered through a 0.45-μm PTFE syringe filter, and the solution was stored in a Teflon capped vial until further use.

Xenon Difluoride Mediated Functionalization of H-SiNCs with Aldehydes. H-SiNCs were passivated with alkyl and aryl aldehydes using a slightly modified procedure previously reported by the group.[103] Briefly, freshly etched H-SiNCs were dispersed in 10 mL of benzene, transferred to an oven-dried Schlenk flask, freeze-dried for 12 h, and transferred to a N_2-filled glovebox. H-SiNCs were dispersed in 3 mL of toluene and transferred to a Teflon reaction tube equipped with a magnetic stir bar. Lauric aldehyde (1.5 mL) was pre-treated by flowing through a Pasteur pipette packed with aluminum oxide and added to the reaction tube. An aryl aldehyde of choice (5 mg) was dissolved in toluene (1 mL) for ease of transfer and added to the reaction mixture. Finally, 3–5 mg of xenon difluoride (XeF_2) crystals were added to the vigorously stirred reaction mixture. The reaction was allowed to stir for 5 min, during which time gas evolution and a change in solution transparency was observed. Next, ∼30 mL of acetonitrile were added to the transparent solution as an antisolvent. The SiNCs were precipitated out of solution by a 15 min centrifugation at 7000 rpm and redispersed in a minimal amount of toluene. The redispersion–antisolvent addition–isolation cycle was repeated twice more. The resulting precipitate was dispersed in toluene, filtered through a 0.45-μm PTFE syringe filter, and stored in the glovebox until further use.

Synthesis of Phenylacetylide. Phenylacetylene (1.53 g, 15 mmol, 1 eq.) was dissolved in 9 ml THF, and n-butyllithium (4.8 ml, 2.5 M in hexanes, 12 mmol, 0.8 eq.) was added to the reaction flask dropwise over 30 min at −78 °C. Upon addition completion, the reaction mixture was stirred for an additional 15 min and brought to room temperature. The product was obtained as a clear yellow/orange liquid. The solution was degassed and stored in a Schlenk flask until further use.

Functionalization of SiNCs with Organolithium Reagents. Freshly etched H-SiNCs were dispersed in 2 mL of an organolithium reagent that was first diluted with toluene to render 0.1 M solutions. The dispersion was transferred to an Ar-filled Schlenk flask, degassed, and stirred overnight. The reaction was terminated by precipitating functionalized SiNCs in 5 ml 1:1 ethanol:methanol mixture acidified with conc. HCl (0.2 ml). The obtained SiNCs were centrifuged at 9000 rpm for 10 min, and the precipitate was redispersed in a minimum amount of toluene. The precipitation-centrifugation-redispersion step was performed twice more. Finally, functionalized SiNCs were dispersed in toluene and filtered through a 0.45-μm PTFE syringe filter.

4.2.3 Material Characterization and Instrumentation

Fourier-transform infrared spectroscopy (FTIR) was performed using a Nicolet Magna 750 IR spectrophotometer. UV–vis absorption spectra were collected using a Hewlett-Packard 8453 UV–vis spectrophotometer. PL spectra were acquired using a Varian Cary Eclipse Fluorescence Spectrometer. Solution NMR spectra were recorded on a Agilent/Varian 500 MHz spectrometer operating at the resonance frequency of 499.8 MHz for ^{1}H nuclei.

Steady-state and time-resolved PL spectra for SiNCs, discussed in Section 4.3.3, were measured with a 445 nm excitation from a continuous wave diode laser, which was modulated by an Isomet IMDD-T110L-1.5 acousto-optic modulator (AOM) operating at a frequency of 200 Hz with a 50% duty cycle. The PL was collected by an optic fiber, passed through a 500-nm long-pass filter, and collected by an OceanOptics USB2000 spectrometer. The spectral response was calibrated by a black-body radiator (Ocean Optics LS1). For time-resolved PL, the same setup was employed, but the incident light was collected by a Becker-Hickl PMC-100 photon-counting PMT. The PL data was collected in 1-μs timesteps, and a total of 10000 sweeps were collected for a good signal-to-noise ratio.

High resolution TEM (HRTEM) imaging was performed on a JEOL-2200FS TEM instrument with an accelerating voltage of 200 kV. Samples were prepared by drop-casting a dilute solution ($\sim$1 mg/mL) of SiNCs in toluene onto a holey carbon grid. Particle analysis was performed using ImageJ software (Version 1.49).

Scanning tunneling microscopy (STM) measurements were carried out by the Millo group from the Hebrew University of Jerusalem. SiNCs were spin-cast from a toluene solution onto atomically flat flame-annealed Au(111) substrates. All measurements were performed at room temperature using Pt-Ir tips. Tunneling current-voltage (I-V) characteristics were acquired after positioning the STM tip above individual NCs, realizing a double barrier tunnel junction (DBTJ) configuration[250] and momentarily disabling the feedback loop. In general, care was taken to retract the tip as far as possible from the NC so that the applied tip-substrate voltage would fall mainly on the tip–NC junction rather than on the NC–substrate junction whose properties (capacitance and tunneling resistance) are determined by the layer of organic capping ligands that cannot be modified during the STM measurement. This protocol reduces the voltage division induced broadening effects, thus the measured gaps and level separations,

in general, correspond better to the real SC gaps, however, a broadening on the order of 10% is expected.[250–253] The dI/dV-V tunneling spectra, proportional to the local tunneling density of states (DOS), were derived numerically from the measured I-V curves. The topographic images were acquired with a set sample-bias, V_s, of 2.2 V and a set current, I_s, of 0.2 nA. This bias value ensured tunneling to states well above the conduction band edge, where the DOS is rather large, thus, the measured SiNC height corresponds well to the real height. The tunneling spectra (on the NCs) were measured with a lower set bias, of $V_s \cong 1.2$–1.5 V, and $I_s \cong 0.1$–0.3 nA. These V_s values still ensure tunneling above the band edge (before disconnecting the feedback loop), while being sensitive to the details of the DOS around the band edge. The I_s was reduced as much as possible to the lowest value that still allowed acquisition of smooth tunneling spectra in order to retract the tip as much as possible from the NC (thus reducing the voltage division factor).

4.3 Results and Discussion

4.3.1 Effect of Fluorophore Proximity to Silicon Surface on SiNC PL

In order to probe the effect, if any, of the distance between a fluorophore and a SiNC core has on the latter's optical properties, a series of naphthalene derivatives with varying alkenyl chain lengths were tested. With the exception of the commercially available vinyl naphthalene, all other naphthenyl derivatives were synthesized via Kumada cross-coupling.[249] 2-Napthylmagnesium bromide was reacted with vinyl halides in the presence of Ni(dppe)Cl_2 catalyst to yield 2-allylnaphthalene (AN), 2-(3-Butenyl)naphthalene (BN), and 2-(4-pentenyl)naphthalene (PN), as outlined in Scheme 4.1. The products were confirmed by electron ionization mass spectrometry (EI-MS) and ^{1}H NMR spectroscopy.

Next, thermal hydrosilylation of SiNCs with synthesized naphthenyl derivatives and vinyl naphthalene (VN) was carried out at 160 °C, as outlined in Scheme 4.2a. The resulting vinyl naphthalene- (VN-SiNCs), 2-allylnaphthalene- (AN-SiNCs), 2-(3-Butenyl)naphthalene- (BN-SiNCs), and 2-(4-pentenyl)naphthalene- (PN-SiNCs) functionalized SiNCs readily disperesed in toluene, affording transparent yellow solutions.

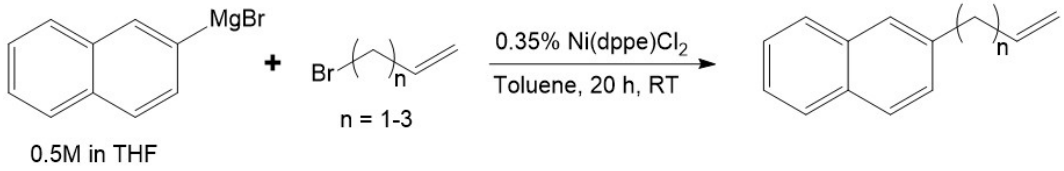

Scheme 4.1: *Kumada cross-coupling of 2-naphthylmagnesium bromide and alkenyl halides.*

Dodecyl functionalized SiNCs (Dod-SiNCs) were prepared in neat 1-dodecene as a reference material (Scheme 4.2b). Passivation of SiNCs was evaluated by FTIR (Figure 4.1). The dod-SiNC sample displayed intense vibrations in the 2650–2900 cm^{-1} region, attributed to C–H stretching of the dodecyl ligand. In addition, C–H bending vibrations were observed at 1380–1470 cm^{-1}. The small Si–O–Si stretching feature at 1100 cm^{-1} suggest that the dod-SiNCs were protected well from oxidation. In contrast, SiNCs functionalized with naphthenyl derivatives showed intense vibrations in the same region, suggesting that the bulkier ligands did not passivate the silicon surface as well. The presence of Si–H_x bending vibrations at 2100 cm^{-1} further support this claim. Nonetheless, surface passivation by naphthenyl derivatives was achieved, as confirmed by the presence of aromatic C–H and alkyl C–H stretches at 3130–3070 and 2650–2900 cm^{-1}, respectively.

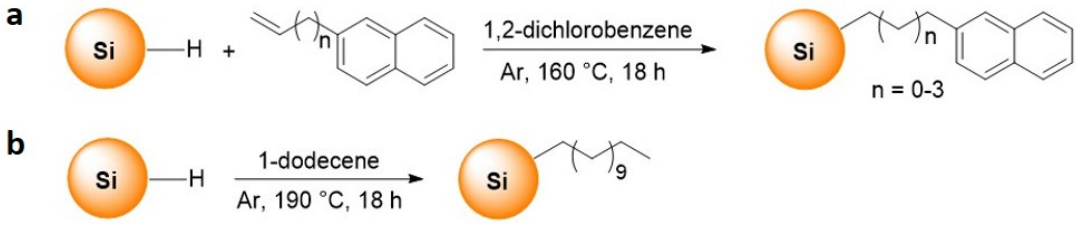

Scheme 4.2: *Thermal hydrosilylation of SiNCs with naphthenyl derivatives (a) and 1-dodecene (b).*

Next, the effect of the fluorophore distance from the SiNC core was investigated by PL spectroscopy. Using dod-SiNCs as a reference material, it became apparent that the effect of attaching naphthalene at an increasing distance from the silicon surface was negligible as all samples had a similar PL emission maximum. However, in the case where naphthalene was closest to the surface (VA-SiNCs), dual emission (blue and orange PL) was detected (Figure 4.1b). Such a phenomenon has been reported

previously by Wang et al. for 9-ethylanthracene functionalized SiNCs.[164] Since the only effect of note occurred when the fluorophore was closest to the surface, a different approach for interfacing SiNCs with fluorophores was explored.

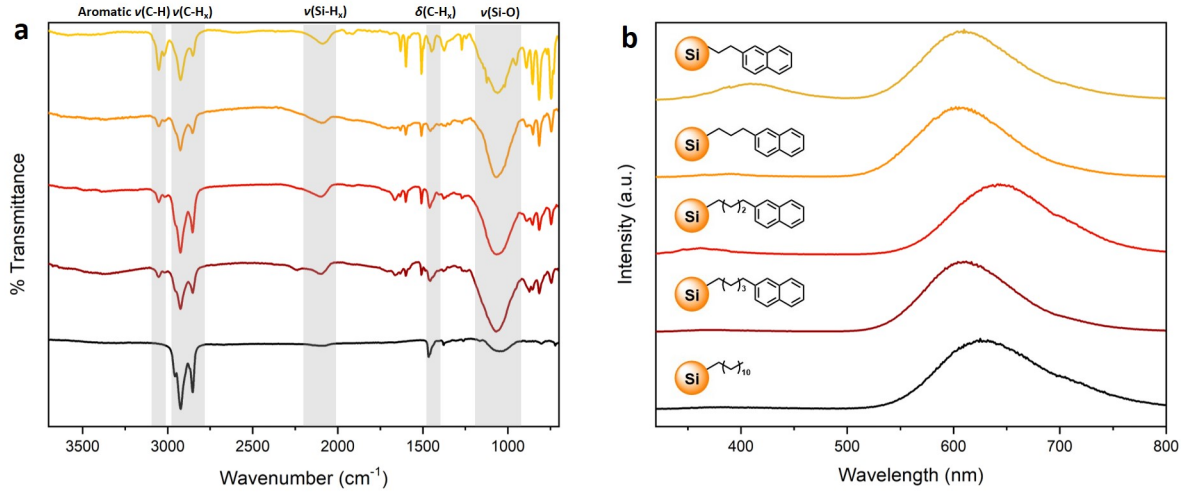

Figure 4.1: *FTIR spectra of VN-SiNCs (yellow), AN-SiNCs (orange), BN-SiNCs (red), PN-SiNCs (dark red), and dod-SiNCs (black) (a), and their corresponding PL spectra under 300 nm excitation (b).*

4.3.2 Functionalization of SiNCs with Aryl Aldehydes

Efficient energy transfer from pyrene moieties to SiNCs was demonstrated recently by the Ceroni group, whereby the SiNCs' PL was enhanced by tethering a fluorophore to their surface.[160,161] Based on this observation and the insight gained from the previous study regarding the proximity of the fluorophore to the SiNC surface, SiNCs were passivated with the following aryl aldehydes: 2-naphthaldehyde, 9-anthracenecarboxaldehyde, and 1-pyrenecarboxaldehyde. A new functionalization method recently developed in the group was utilized for the hydrosilylation of H-SiNCs with the carbonyl centre (C=O) on the aldehyde to form Si–O–C linkages,[103] thereby increasing the proximity of the fluorophore to the silicon surface. Due to the bulky nature of some of the fluorophores used, the SiNCs were passivated with a mixed surface of fluorophore and lauraldehyde (LA). The reaction was carried out in a N_2-filled glovebox using XeF_2, as outlined in Scheme 4.3.

SiNCs passivated with only lauraldehyde (SiNC-LA), lauraldehyde and 2-naphth-

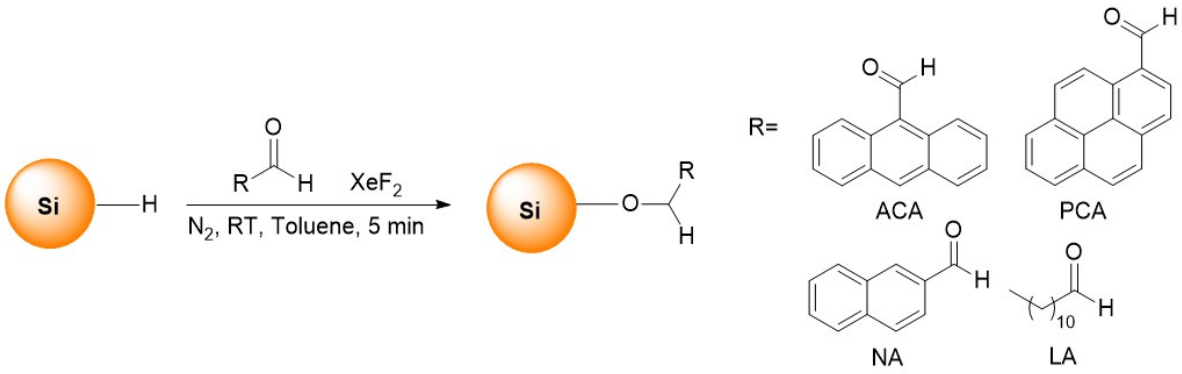

Scheme 4.3: *Functionalization of H-SiNCs with aryl and alkyl aldehydes in the presence of XeF_2.*

aldehyde (SiNC-NA), lauraldehyde and 9-anthracenecarboxaldehyde (SiNC-ACA), and lauraldehyde and 1-pyrenecarboxaldehyde (SiNC-PCA) were evaluated first by FTIR. The spectra for both the passivated SiNCs and their ligands are shown in Figure 4.2a. As expected, C–H bending and stretching vibrations associated with LA were observed for all SiNC samples in the 1380–1470 and 2650–2900 cm^{-1} regions, respectively. The presence of a small vibration at 1740 cm^{-1} for all SiNC samples associated with aldehyde carbonyl suggests that some free ligand was still present in the solution. Si-alkoxy groups were identified in the 1100–960 cm^{-1} region for the same samples. However, the attachment of the fluorophores to the SiNC surface was not confirmed by FTIR as the aromatic C–H stretching vibrations observed for the free ligands at 3040 cm^{-1} were not detected for the passivated SiNCs. Since the SiNCs were functionalized with both aryl and alkyl aldehydes, it is likely that the bulkier aryl groups were attached in smaller quantities to the silicon surface compared to their alkyl analogues, leading to a weaker vibration in FTIR.

UV-Vis spectroscopy provided further insight regarding the attachment of fluorophores to the SiNC surface (Figure 4.2b). The featureless SiNC-LA spectrum, which is commonly observed for alkyl passivated SiNCs,[86] served as a reference for the influence of the fluorophores. In contrast, structured absorption spectra were observed for both SiNC-ACA and SiNC-PCA. While the free ACA and PCA ligands absorb between 320–450 nm and 320–410 nm, respectively, when they were attached to the SiNC surface, a blue-shift in absorption was observed for both. This can be reasoned by the breaking of the carbonyl bond in PCA and ACA and the formation of an alkoxy

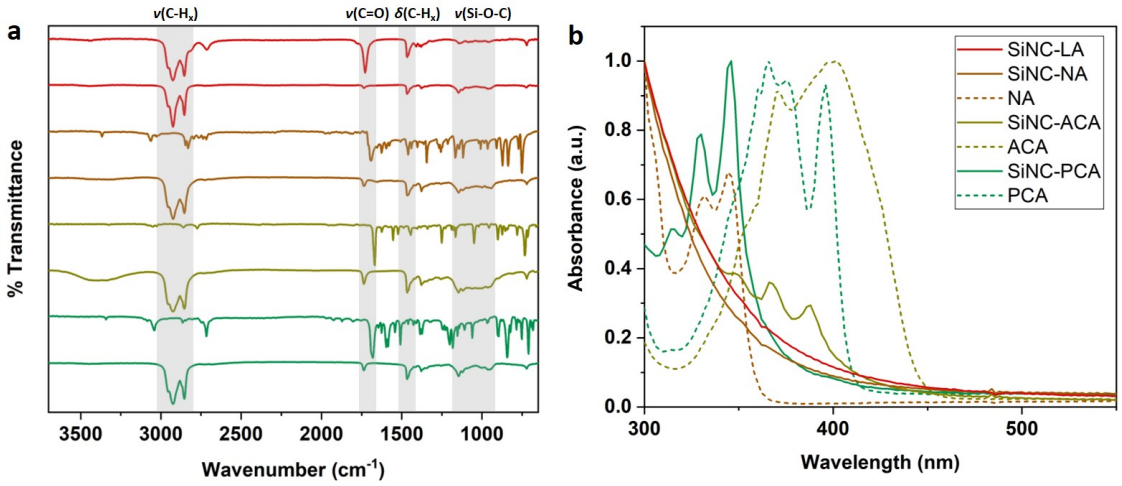

Figure 4.2: *FTIR spectra of LA ligand and SiNC-LA (red), NA ligand and SiNC-NA (brown), ACA ligand and SiNC-ACA (yellow), PCA ligand and SiNC-PCA (green) (a), and their corresponding UV-Vis spectra (b).*

bond with SiNCs since stronger electron withdrawing anchoring groups are known to red-shift the absorption of pyrene moieties.[254,255] No features were observed in the absorption spectrum of SiNC-NA, which can be due to the overlap in the absorbance of SiNCs and NA individually.

Following the confirmation of a successful attachment of the fluorophores to the SiNC surface, their optical response was evaluated by PL spectroscopy. Figure 4.3 depicts the PL spectra of the passivated SiNCs and free ligands. Note that due to the excitation wavelength dependent emission of free ligands, different excitations were employed, while the SiNC systems were probed under the same conditions. Upon a 300-nm excitation, SiNC-LA emitted at 640 nm, whereas dual emission was observed for SiNC-NA. The red component of the emission appeared in the same region as for SiNC-LA, but the blue component was slightly blue-shifted in comparison to the free ligand (Figure 4.3b) and higher in intensity. Interestingly, almost no PL was observed in the red region for SiNC-ACA and SiNC-PCA, while a significant blue-shift in the PL associated with the ACA and PCA ligands was observed. Analogous to the case in UV-Vis, such a shift in PL emission maximum can be explained by a change in the derivatization of the anthracene and pyrene moieties upon functionalization with SiNCs. Less electron-withdrawing groups on the fluorophores blue-shift the PL.[255] Moreover, the emission of the bonded ligands appeared more structured compared to

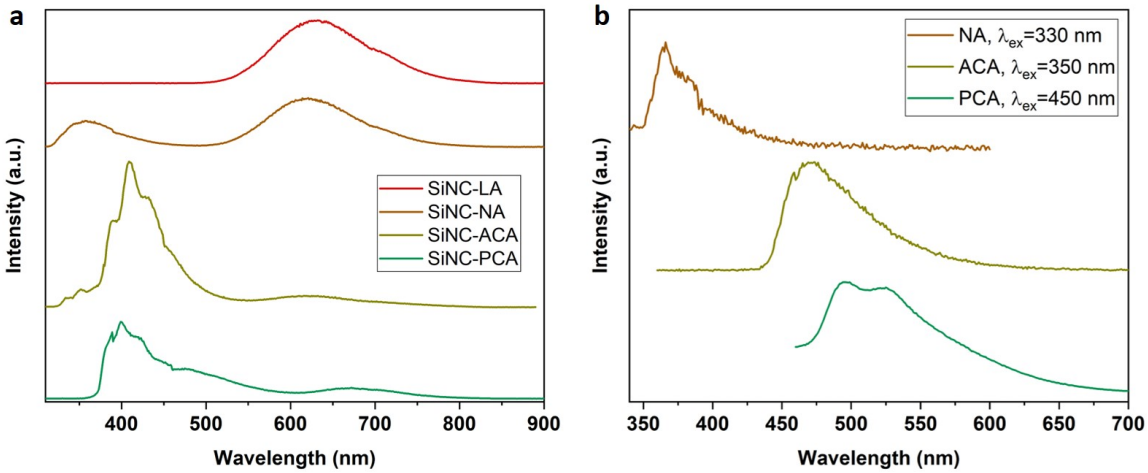

Figure 4.3: *PL spectra of SiNC-LA (red), SiNC-NA (brown), SiNC-ACA (yellow), SiNC-PCA (green) under 300 nm excitation (a), and the PL spectra of the free ligands in toluene: NA, ACA and PCA (b).*

that of the free ligands, further confirming the tethering of ACA and PCA moieties to the SiNC surface and a subsequent decrease in range of motion. Upon excitation of the SiNC at longer wavelengths than the emission maximum of the ligands, no PL was observed. The reduction in SiNC core emission intensity and enhancement in ligand PL suggest that the SiNC are sensitizing the ligand, which is in contrast to previous reports.[160,161] Thus, the chosen group of fluorophores was not suitable for tuning the optical response of SiNCs, and a different strategy was required.

4.3.3 Tuning SiNC Luminescence through In-Gap States

Several studies have demonstrated that aryl alkynes can influence the PL of SiNCs. Red-shift in the PL of SiNCs functionalized with phenylacetylene was noted by some,[105,112] while PL quenching was observed by others.[110] In a collaborative effort with the Rieger and Millo groups, a detailed investigation of this phenomenon was carried out. In order to gain insight into the effect of conjugated surface groups on SiNC PL, SiNCs were passivated with alkyl (hexane, Hex-SiNCs), aryl (phenyl, Phen-SiNCs), and aryl alkyne (phenylacetylene, PhenAc-SiNCs) using an established method for SiNC functionalization with organolithium reagents,[112] as outlined in Scheme 4.4. The optical and optoelectronic properties of the resulting SiNCs were evaluated using PL spectroscopy and scanning tunneling microscopy/spectroscopy (STM/STS).

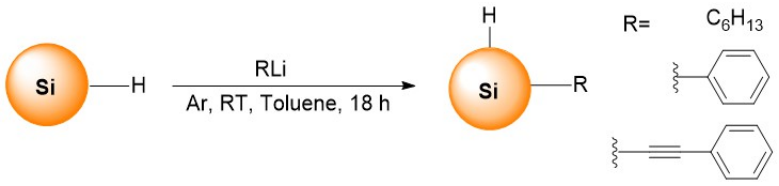

Scheme 4.4: *Functionalization of H-SiNCs with RLi ligands.*

Under 445 nm excitation, Hex-SiNCs and Phen-SiNCs had a similar PL emission at 695 and 700 nm, respectively, as determined by skew-normal fitting,[186] while that of PhenAc-SiNCs was red-shifted by $\sim$ 45 nm (Figure 4.4a). In contrast, time-resolved PL spectroscopy revealed no significant difference: all three samples had microsecond lifetimes. From log-normal fitting[194] of PL decays, the average lifetimes of Hex-SiNCs, Phen-SiNCs and PhenAc-SiNCs were found to be 88.9±0.1, 79.8±0.2, and 99.8±0.2 μs, respectively. No short lifetime component was detected for any of the SiNCs, which eliminates surface defects as the possible culprits for the observed PL shift. In addition, high-resolution TEM of the SiNCs confirmed that all three samples were 3 nm in diameter (Figure 4.5), thus excluding the possibility of size modification of the SiNCs upon functionalization with phenylacetylene. According to QC, a reduction in particle size leads to wider band gap (blue-shift), which was not observed.

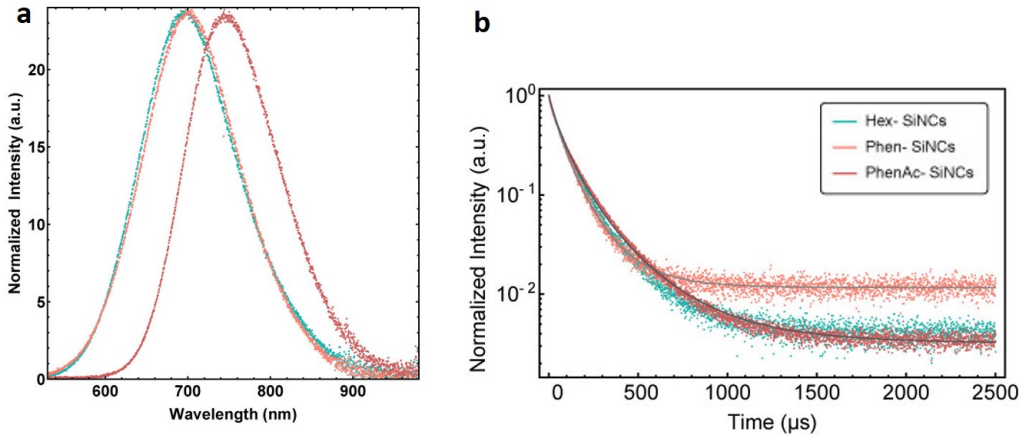

Figure 4.4: *PL spectra of Hex-SiNCs, Phen-SiNCs and PhenAc-SiNCs under 445 nm illumination (a) and their time-resolved PL decays (b).*

In order to gain further insight and eliminate potential ensemble effects, STS/STM measurements were carried out next. Tunneling spectra measured on isolated SiNCs are shown for all three different SiNCs together with the corresponding STM topography

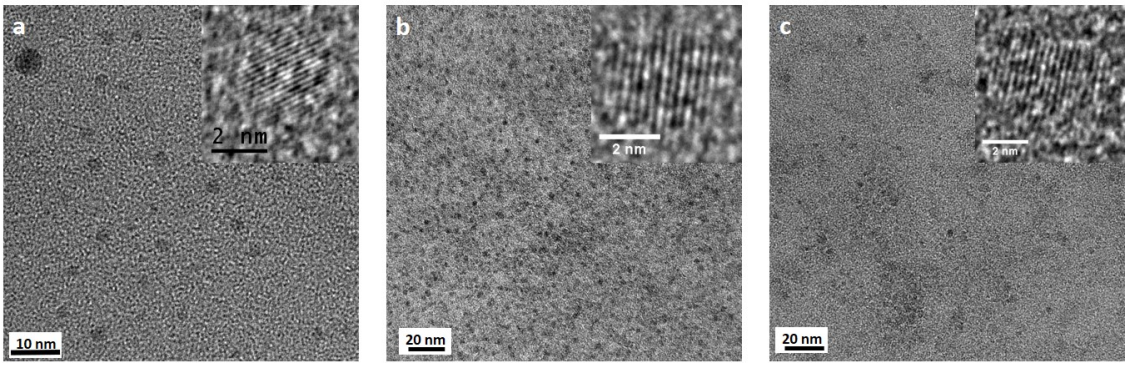

Figure 4.5: *HRTEM images of Hex-SiNCs (a), Phen-SiNCs (b), and PhenAc-SiNCs(c). Lattice fringes of a single SiNC are shown in the insets.*

images and cross-sections in the insets (Figure 4.6). Band gaps were deduced directly from the STS data from the energy difference between the valence band (VB) and conduction band (CB) edges. For each band, the edge was defined as the mid-value between the position of the first peak (or shoulder) and the onset of detectable DOS.[256] This method afforded band gaps of Hex-SiNCs and Phen-SiNC of 2.1±0.1 eV. Note that the band gap values obtained by STS are larger than the exciton band gaps determined by PL maxima (695 nm = 1.78 eV.) The reason for that is three-fold. First, the electronhole Coulomb interaction that is incorporated in the optical (excitonic) gap does not play a role in the fundamental single-particle gap measured by STS.[250,257] Second, the tunneling spectra were measured in the double-barrier tunnel junction configuration, therefore, the apparent gap was broadened due to the effect of voltage division between the two tunnel barriers involved, the tip–SiNC and the SiNC–substrate junctions.[250] Third, the polarization energy associated with electron tunneling through the SiNC also contributed to the widening of the measured gap.[252]

In the case of PhenAc-SiNCs, the band gap was still in the 2.1±0.1 eV range, despite the red-shifted PL. However, an in-gap state close to the CB-edge of the SiNCs was observed clearly in their tunneling spectra (Figure 4.6c). This observation was very robust and was detected in every measurement acquired for these NCs. The separation of the in-gap state from the CB-edge varied between 140 meV (red and green curves in Figure 4.6c) and 190 meV (blue curve), where most spectra showed an ∼160 meV separation. These values are in the range of, yet somewhat larger than, the PL red-shift (±130 meV). The slight enlargement may be due to the aforementioned voltage division effect. The observed in-gap state combined with the surface-group-independent band

gap (as determined by STS) suggest that the red-shift in PL maximum for PhenAc-SiNCs is due to a recombination from the in-gap state. Direct covalent bonding of a π-conjugated molecule to a silicon atom can reduce its HOMO–LUMO gap efficiently because of the $\sigma^* - \pi^*$ conjugation between the Si core and the bonded conjugated molecule.[258] The formation of states near band edges theoretically was expected to be the reason for the narrowing of the band gap.[245]

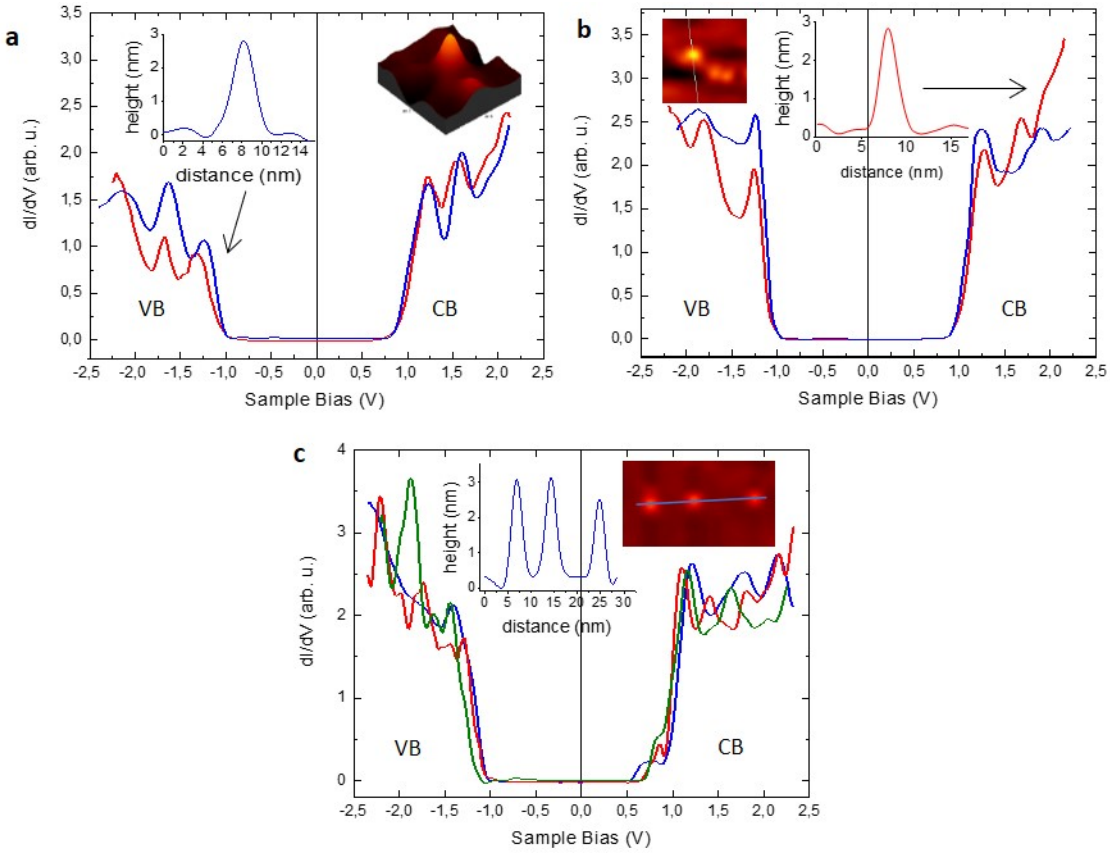

Figure 4.6: *Tunneling spectra measured on Hex-SiNCs (a), Phen-SiNCs (b), and PhenAc-SiNCs (c). The insets show some of the NCs and the corresponding cross-section on which the spectra were acquired. The extracted band gaps of the Si-NCs are all around 2.1 eV, except for the green curve in (c) which was measured on the smaller, rightmost, NC.*

4.4 Conclusion

The series of studies presented in this Chapter underscore the profound influence that a conjugated surface group can have on the optical response of SiNCs. Fluorophore proximity to the SiNC surface was shown to be significant in order to observe an appreciable interaction between the two. Upon conjugation of SiNCs with fluorophores at close proximity, blue-shifts in the absorption and emission spectra of the resulting materials were observed in comparison to the original fluorophore. Further evidence of the effect that conjugated surface groups have on the optoelectronic properties of SiNCs was demonstrated by STS/STM measurements, which revealed an in-gap state close to the CB edge of SiNCs functionalized with a conjugated system. Together, these studies demonstrate the feasibility of tuning the optical properties of SiNCs through surface chemistry.

Chapter 5

Conclusions and Future Directions

5.1 Conclusions

The research work presented in this thesis outlines the efforts made to gain further insight into the optical response of SiNCs and the factors that affect their PL. Contributions made to the collective fundamental understanding of the intricate interplay between size and surface of SiNCs pave the way towards the realization of SiNCs' potential in luminescence-based applications. Key findings and possible future directions are summarized here.

In Chapter 2, an investigation of the optical properties of SiNCs as a function of size and surface chemistry was carried out. Temperature-dependent steady-state and time-resolved PL measurements were performed to gain further insight into the origin of PL in SiNCs. Alkyl passivated SiNCs were found to display temperature-dependent PL profiles, consistent with band gap emission, while the presence of nitrogen containing groups on the surface of silicon led to a temperature-independent, surface-state-related emission. Oxidized alkyl passivated SiNCs presented a more complicated PL profile: temperature-dependent emission was observed, however, at shorter emission wavelengths compared to their nonoxidized counterparts. A general mechanism was proposed to explain all three phenomena, suggesting that surface groups play a crucial role in SiNC optical response.

Chapter 3 expanded the investigation into the effect of surface oxidation on the optical response of SiNCs. Alkyl passivated SiNCs with three distinct sizes were subjected to wet Ar, dry O_2, and wet O_2 atmospheres, and their optical response was probed

by in-situ luminescence spectroscopy. The existing disparity regarding the PL maxima shifts upon surface oxidation was resolved through size-dependent rationalization. SiNCs greater than 2.5 nm displayed blue-shift in PL maximum upon oxidation, while smaller particles displayed red-shift under the same conditions. An oxide-related surface state was invoked as the cause for the orange PL observed for all SiNCs, regardless of initial size. The degradation in colour purity of SiNCs, even upon functionalization with surface groups, emphasized the susceptibility of SiNCs to surface oxidation and the need for better protection.

Chapter 4 explored different strategies for the improvement and tuning of SiNC optical response through functionalization with conjugated surface groups. Proximity to the silicon surface and the degree of surface group conjugation were found to play a role in the extent of influence on the optical response. Dual emission and absorption in the visible light range was obtained by modification of the silicon surface with polycyclic aromatic groups. In addition, optical and scanning tunneling spectroscopy studies of SiNCs passivated with conjugated surface groups revealed changes in the optical and electronic structures of SiNCs. Upon functionalization with an alkynyl(aryl) molecule, an in-gap state near the conduction band of SiNC was observed, effectively minimizing the band gap. The series of studies presented in this chapter showcase how conjugated surface groups afford an alternative route to the control of SiNC electronic structure and optical properties.

The overall message of the work presented in this thesis can be summarized as follows: when it comes to SiNC PL, both size and surface matter.

5.2 Future Directions

An overarching theme of the present thesis is the importance of surface chemistry and its drastic effects on the optical response of SiNCs. In particular, water and oxygen were shown to affect the emission colour of SiNCs drastically. One strategy to mitigate this problem is to functionalize SiNCs with hydrophobic surface groups, such as perfluoroalkyls. This approach has been proven successful for large SiNCs[259] and can be extended now to smaller SiNCs using PCl_5-mediated hydrosilylation,[104] thus realizing stable, core-emission from SiNCs across the visible spectrum with high QYs; these can be utilized in light-emitting diode (LED) applications. QD-based LED

displays have been commercialized already, and QDs show great promise for general illumination applications.[260–262] By combining red-, green-, and blue-emitting SiNCs in one device, one can envision white-light emission from a single material source. In addition, core-emission from green-emitting SiNCs, whose existence is debated,[91] can be evaluated using temperature-dependent PL studies, as has been demonstrated in this thesis.

The exact nature of the surface oxide species leading to SiNC PL shifts remains an open-ended question that needs to be addressed. Solid-state NMR provides a promising platform to probe the surface chemistry of SiNCs and has been used successfully to probe H-SiNCs of various sizes using ^{29}Si NMR in our group. Additionally, multidimensional NMR spectroscopy was utilized recently to probe ligand-passivated SiNCs.[263] A natural next step is to extend the study to passivated SiNCs with oxygen and nitrogen containing groups using both ^{29}Si and ^{17}O solid-state NMR,[264–266] thus allowing the elucidation of the exact oxide species affecting SiNC PL. Beyond the fundamental importance of such a study, establishing a library of surface groups and their effect on the optical response of SiNCs will allow one to tailor the photophysics of SiNCs for target applications.

Despite the fundamental questions yet to be answered with regard to the optical response of SiNCs, the latter are perfect candidates for luminescence-based sensing applications.[168] Changes in the optical response of SiNCs upon exposure to nitroaromatics, commonly the basis for explosives, has been demonstrated.[195,267] However, these materials lack specificity. Conjugation of SiNCs with β-cyclodextrin can render ratiometric sensors with high specificity, thanks to the cyclodextrin unit. These units have been attached successfully to Cd-based QDs,[268,269] organic dyes,[270] and porous silicon.[271] However, as previously highlighted, SiNCs offer the benefit of low toxicity, photostability, and tailorable surface chemistry. Thus, a ratiometric sensor based on a SiNC–cyclodextrin bioconjugate is a natural next step.

Realizing stimulated emission in SiNCs for LASER applications and developing SiNC-base waveguide amplifiers has been a longstanding goal of the silicon photonics community.[38,272] One promising approach to stimulate emission involves doping with rare-earth elements, such as Er^{3+}.[273] Sensitization of Er^{3+} by bulk silicon, SiNCs embedded in silica matrix, or silicon-rich nitride films has been demonstrated to generate strong emission at 1.54 μm wavelength.[274–277] Since the absorption cross-section of SiNCs is orders of magnitude larger than that of erbium, sensitization by SiNC

offers an avenue to increase the efficiency of the intra-4f-shell transition in erbium (1.54 μm).[278] However, very few reports exist on free-standing erbium-doped SiNCs for waveguide applications.[279,280] Thus, with the expertise developed in our research group with regard to surface passivation of SiNCs and the insight gained from this thesis work regarding the importance of sensitizer proximity for efficient energy transfer, direct attachment of Er^{3+} complexes is proposed. First, the optimal ratio of SiNC to Er^{3+} dopant must be established, followed by pump-probe measurements to test for population inversion and optical gain, a first sign for possible stimulated emission.[272]

Bibliography

[1] Koch, F.; Petrova-Koch, V. *J. Non-Cryst. Solids* **1996**, *198-200*, 840–846.

[2] Wolkin, M. V.; Jorne, J.; Fauchet, P. M.; Allan, G.; Delerue, C. *Phys. Rev. Lett.* **1999**, *82*, 197–200.

[3] Feynman, R. P. *Engineering and Science* **1960**, *23*, 22–36.

[4] Efros, A.; L. Efros, A. *Sov. Phys. Semicond.* **1982**, *16*, 772–775.

[5] Ekimov, A. I.; Efros, A. L.; Onushchenko, A. A. *Solid State Commun.* **1985**, *56*, 921–924.

[6] Brus, L. E. *J. Chem. Phys.* **1983**, *79*, 5566–5571.

[7] Takagahara, T.; Takeda, K. *Phys. Rev. B* **1992**, *46*, 15578–15581.

[8] Yoffe, A. D. *Adv. Phys.* **1993**, *42*, 173–262.

[9] Alivisatos, A. P. *J. Phys. Chem.* **1996**, *100*, 13226–13239.

[10] Rabouw, F. T.; Donega, C. d. M. *Top Curr Chem (Z)* **2016**, *374*, 58.

[11] Rossetti, R.; Nakahara, S.; Brus, L. E. *J. Chem. Phys.* **1983**, *79*, 1086–1088.

[12] Rossetti, R.; Ellison, J. L.; Gibson, J. M.; Brus, L. E. *J. Chem. Phys.* **1984**, *80*, 4464–4469.

[13] Hirai, T.; Sato, H.; Komasawa, I. *Ind. Eng. Chem. Res.* **1994**, *33*, 3262–3266.

[14] Wichiansee, W.; Nordin, M. N.; Green, M.; Curry, R. J. *J. Mater. Chem.* **2011**, *21*, 7331–7336.

[15] Murray, C. B.; Norris, D. J.; Bawendi, M. G. *J. Am. Chem. Soc.* **1993**, *115*, 8706–8715.

[16] Peng, Z. A.; Peng, X. *J. Am. Chem. Soc.* **2001**, *123*, 183–184.

[17] Micic, O. I.; Curtis, C. J.; Jones, K. M.; Sprague, J. R.; Nozik, A. J. *J. Phys. Chem.* **1994**, *98*, 4966–4969.

[18] Frank, A. C.; Stowasser, F.; Sussek, H.; Pritzkow, H.; Miskys, C. R.; Ambacher, O.; Giersig, M.; Fischer, R. A. *J. Am. Chem. Soc.* **1998**, *120*, 3512–3513.

[19] Olshavsky, M. A.; Goldstein, A. N.; Alivisatos, A. P. *J. Am. Chem. Soc.* **1990**, *112*, 9438–9439.

[20] Xu, Y.; Al-Salim, N.; Bumby, C. W.; Tilley, R. D. *J. Am. Chem. Soc.* **2009**, *131*, 15990–15991.

[21] Moreels, I.; Lambert, K.; Smeets, D.; De Muynck, D.; Nollet, T.; Martins, J. C.; Vanhaecke, F.; Vantomme, A.; Delerue, C.; Allan, G.; Hens, Z. *ACS Nano* **2009**, *3*, 3023–3030.

[22] Bae, W. K.; Joo, J.; Padilha, L. A.; Won, J.; Lee, D. C.; Lin, Q.; Koh, W.-k.; Luo, H.; Klimov, V. I.; Pietryga, J. M. *J. Am. Chem. Soc.* **2012**, *134*, 20160–20168.

[23] Murphy, J. E.; Beard, M. C.; Norman, A. G.; Ahrenkiel, S. P.; Johnson, J. C.; Yu, P.; Mićić, O. I.; Ellingson, R. J.; Nozik, A. J. *J. Am. Chem. Soc.* **2006**, *128*, 3241–3247.

[24] Veinot, J. G. C. *Chem. Commun.* **2006**, *0*, 4160–4168.

[25] Dashiell, M. W.; Denker, U.; Müller, C.; Costantini, G.; Manzano, C.; Kern, K.; Schmidt, O. G. *Appl. Phys. Lett.* **2002**, *80*, 1279–1281.

[26] Stella, A.; Nisoli, M.; De Silvestri, S.; Svelto, O.; Lanzani, G.; Cheyssac, P.; Kofman, R. *Phys. Rev. B* **1996**, *53*, 15497–15500.

[27] Hines, M. A.; Guyot-Sionnest, P. *J. Phys. Chem.* **1996**, *100*, 468–471.

[28] Benaissa, M.; Gonsalves, K. E.; Rangarajan, S. P. *Appl. Phys. Lett.* **1997**, *71*, 3685–3687.

[29] Guo, Q.; Hillhouse, H. W.; Agrawal, R. *J. Am. Chem. Soc.* **2009**, *131*, 11672–11673.

[30] Panthani, M. G.; Akhavan, V.; Goodfellow, B.; Schmidtke, J. P.; Dunn, L.; Dodabalapur, A.; Barbara, P. F.; Korgel, B. A. *J. Am. Chem. Soc.* **2008**, *130*, 16770–16777.

[31] Protesescu, L.; Yakunin, S.; Bodnarchuk, M. I.; Krieg, F.; Caputo, R.; Hendon, C. H.; Yang, R. X.; Walsh, A.; Kovalenko, M. V. *Nano Lett.* **2015**, *15*, 3692–3696.

[32] Ying Lim, S.; Shen, W.; Gao, Z. *Chem. Soc. Rev.* **2015**, *44*, 362–381.

[33] Wang, Y.; Herron, N. *J. Phys. Chem.* **1991**, *95*, 525–532.

[34] Alivisatos, A. P. *Science* **1996**, *271*, 933–937.

[35] Dohnalová, K.; Gregorkiewicz, T.; Kůsová, K. *J. Phys.: Condens. Matter* **2014**, *26*, 173201.

[36] Buriak, J. M. *Chem. Rev.* **2002**, *102*, 1271–1308.

[37] Chelikowsky, J. R.; Cohen, M. L. *Phys. Rev. B* **1974**, *10*, 5095–5107.

[38] Pavesi, D. J. L. a. L. *Silicon Photonics*; Topics in Applied Physics; Springer, Berlin, Heidelberg, 2004; pp 1–50.

[39] Furukawa, S.; Miyasato, T. *Phys. Rev. B* **1988**, *38*, 5726–5729.

[40] Furukawa, S.; Miyasato, T. *Jpn. J. Appl. Phys.* **1988**, *27*, L2207.

[41] Canham, L. T. *Appl. Phys. Lett.* **1990**, *57*, 1046–1048.

[42] Takagi, H.; Ogawa, H.; Yamazaki, Y.; Ishizaki, A.; Nakagiri, T. *Appl. Phys. Lett.* **1990**, *56*, 2379–2380.

[43] Hybertsen, M. S. *Phys. Rev. Lett.* **1994**, *72*, 1514–1517.

[44] Kovalev, D.; Heckler, H.; Ben-Chorin, M.; Polisski, G.; Schwartzkopff, M.; Koch, F. *Phys. Rev. Lett.* **1998**, *81*, 2803–2806.

[45] Daldosso, N.; Pavesi, L. *Laser & Photon. Rev.* **2009**, *3*, 508–534.

[46] Delerue, C.; Allan, G.; Lannoo, M. *Phys. Rev. B* **1993**, *48*, 11024–11036.

[47] Xie, Y. H.; Wilson, W. L.; Ross, F. M.; Mucha, J. A.; Fitzgerald, E. A.; Macaulay, J. M.; Harris, T. D. *J. Appl. Phys.* **1992**, *71*, 2403–2407.

[48] Cullis, A. G.; Canham, L. T.; Calcott, P. D. J. *J. Appl. Phys.* **1997**, *82*, 909–965.

[49] Mastronardi, M. L.; Maier-Flaig, F.; Faulkner, D.; Henderson, E. J.; Kübel, C.; Lemmer, U.; Ozin, G. A. *Nano Lett.* **2012**, *12*, 337–342.

[50] Delley, B.; Steigmeier, E. F. *Phys. Rev. B* **1993**, *47*, 1397–1400.

[51] Kůsová, K.; Hapala, P.; Valenta, J.; Jelínek, P.; Cibulka, O.; Ondič, L.; Pelant, I. *Adv. Mater. Interfaces* **2014**, *1*, 1300042–1300051.

[52] Kůsová, K.; Pelant, I.; Valenta, J. *Light Sci. Appl.* **2015**, *4*, e336.

[53] Poddubny, A. N.; Dohnalová, K. *Phys. Rev. B* **2014**, *90*, 245439–245446.

[54] Werwa, E.; Seraphin, A. A.; Chiu, L. A.; Zhou, C.; Kolenbrander, K. D. *Appl. Phys. Lett.* **1994**, *64*, 1821–1823.

[55] Patrone, L.; Nelson, D.; Safarov, V. I.; Sentis, M.; Marine, W.; Giorgio, S. *J. Appl. Phys.* **2000**, *87*, 3829–3837.

[56] Shimizu-Iwayama, T.; Fujita, K.; Nakao, S.; Saitoh, K.; Fujita, T.; Itoh, N. *J. Appl. Phys.* **1994**, *75*, 7779–7783.

[57] Mutti, P.; Ghislotti, G.; Bertoni, S.; Bonoldi, L.; Cerofolini, G. F.; Meda, L.; Grilli, E.; Guzzi, M. *Appl. Phys. Lett.* **1995**, *66*, 851–853.

[58] Min, K. S.; Shcheglov, K. V.; Yang, C. M.; Atwater, H. A.; Brongersma, M. L.; Polman, A. *Appl. Phys. Lett.* **1996**, *69*, 2033–2035.

[59] Bley, R. A.; Kauzlarich, S. M.; Davis, J. E.; Lee, H. W. H. *Chem. Mater.* **1996**, *8*, 1881–1888.

[60] Nayfeh, M. H.; Barry, N.; Therrien, J.; Akcakir, O.; Gratton, E.; Belomoin, G. *Appl. Phys. Lett.* **2001**, *78*, 1131–1133.

[61] Belomoin, G.; Therrien, J.; Smith, A.; Rao, S.; Twesten, R.; Chaieb, S.; Nayfeh, M. H.; Wagner, L.; Mitas, L. *Appl. Phys. Lett.* **2002**, *80*, 841–843.

[62] Heintz, A. S.; Fink, M. J.; Mitchell, B. S. *Adv. Mater.* **2007**, *19*, 3984–3988.

[63] Ehbrecht, M.; Ferkel, H.; Huisken, F.; Holz, L.; Polivanov, Y. N.; Smirnov, V. V.; Stelmakh, O. M.; Schmidt, R. *J. Appl. Phys.* **1995**, *78*, 5302–5306.

[64] Ehbrecht, M.; Huisken, F. *Phys. Rev. B* **1999**, *59*, 2975–2985.

[65] Li, X.; He, Y.; Talukdar, S. S.; Swihart, M. T. *Langmuir* **2003**, *19*, 8490–8496.

[66] Li, X.; He, Y.; Swihart, M. T. *Langmuir* **2004**, *20*, 4720–4727.

[67] Mangolini, L.; Thimsen, E.; Kortshagen, U. *Nano Lett.* **2005**, *5*, 655–659.

[68] Pi, X. D.; Liptak, R. W.; Campbell, S. A.; Kortshagen, U. *Appl. Phys. Lett.* **2007**, *91*, 083112.

[69] Tamir, S.; Berger, S. *Appl. Surf. Sci.* **1995**, *86*, 514–520.

[70] Tamura, H.; Rückschloss, M.; Wirschem, T.; Vepřek, S. *Thin Solid Films* **1995**, *255*, 92–95.

[71] Iacona, F.; Franzò, G.; Spinella, C. *J. Appl. Phys.* **2000**, *87*, 1295–1303.

[72] Pi, X. D.; Liptak, R. W.; Nowak, J. D.; Wells, N. P.; Carter, C. B.; Campbell, S. A.; Kortshagen, U. *Nanotechnology* **2008**, *19*, 245603.

[73] Heath, J. R. *Science* **1992**, *258*, 1131–1133.

[74] Bley, R. A.; Kauzlarich, S. M. *J. Am. Chem. Soc.* **1996**, *118*, 12461–12462.

[75] Baldwin, R. K.; Pettigrew, K. A.; Ratai, E.; Augustine, M. P.; Kauzlarich, S. M. *Chem. Commun.* **2002**, *0*, 1822–1823.

[76] Tilley, R. D.; Warner, J. H.; Yamamoto, K.; Matsui, I.; Fujimori, H. *Chem. Commun.* **2005**, *0*, 1833–1835.

[77] Warner, J. H.; Hoshino, A.; Yamamoto, K.; Tilley, R. D. *Angew. Chem. Int. Ed.* **2005**, *44*, 4550–4554.

[78] He, Y.; Zhong, Y.; Peng, F.; Wei, X.; Su, Y.; Lu, Y.; Su, S.; Gu, W.; Liao, L.; Lee, S.-T. *J. Am. Chem. Soc.* **2011**, *133*, 14192–14195.

[79] Zhong, Y.; Sun, X.; Wang, S.; Peng, F.; Bao, F.; Su, Y.; Li, Y.; Lee, S.-T.; He, Y. *ACS Nano* **2015**, *9*, 5958–5967.

[80] Liu, S.-m.; Sato, S.; Kimura, K. *Langmuir* **2005**, *21*, 6324–6329.

[81] Sun, W.; Qian, C.; Chen, K. K.; Ozin, G. A. *ChemNanoMat* **2016**, *2*, 847–855.

[82] Pauthe, M.; Bernstein, E.; Dumas, J.; Saviot, L.; Pradel, A.; Ribes, M. *J. Mater. Chem.* **1999**, *9*, 187–191.

[83] Sorarù, G. D.; Modena, S.; Bettotti, P.; Das, G.; Mariotto, G.; Pavesi, L. *Appl. Phys. Lett.* **2003**, *83*, 749–751.

[84] Henderson, E. J.; Kelly, J. A.; Veinot, J. G. C. *Chem. Mater.* **2009**, *21*, 5426–5434.

[85] Hessel, C. M.; Henderson, E. J.; Veinot, J. G. C. *Chem. Mater.* **2006**, *18*, 6139–6146.

[86] Hessel, C. M.; Reid, D.; Panthani, M. G.; Rasch, M. R.; Goodfellow, B. W.; Wei, J.; Fujii, H.; Akhavan, V.; Korgel, B. A. *Chem. Mater.* **2012**, *24*, 393–401.

[87] Niquet, Y. M.; Delerue, C.; Allan, G.; Lannoo, M. *Phys. Rev. B* **2000**, *62*, 5109–5116.

[88] Wang, L. W.; Zunger, A. *J. Phys. Chem.* **1994**, *98*, 2158–2165.

[89] Garrido, B.; López, M.; González, O.; Pérez-Rodriguez, A.; Morante, J. R.; Bonafos, C. *Appl. Phys. Lett.* **2000**, *77*, 3143–3145.

[90] Barbagiovanni, E. G.; Lockwood, D. J.; Simpson, P. J.; Goncharova, L. V. *Appl. Phys. Rev.* **2014**, *1*, 011302–011349.

[91] Wen, X.; Zhang, P.; Feng, Y.; Shrestha, S.; Coniber, G.; Huang, S.; Smith, T. A.; Anthony, R. J.; Kortshagen, U. R.; Yu, P. *Sci. Rep-UK* **2015**, 12469.

[92] Yang, Z.; De los Reyes, G. B.; Titova, L. V.; Sychugov, I.; Dasog, M.; Linnros, J.; Hegmann, F. A.; Veinot, J. G. C. *ACS Photonics* **2015**, *2*, 595–605.

[93] Brown, S. L.; Miller, J. B.; Anthony, R. J.; Kortshagen, U. R.; Kryjevski, A.; Hobbie, E. K. *ACS Nano* **2017**, *11*, 1597–1603.

[94] Yu, Y.; Fan, G.; Fermi, A.; Mazzaro, R.; Morandi, V.; Ceroni, P.; Smilgies, D.-M.; Korgel, B. A. *J. Phys. Chem. C* **2017**, *121*, 23240–23248.

[95] Zhou, Z.; Brus, L.; Friesner, R. *Nano Lett.* **2003**, *3*, 163–167.

[96] Fojtik, A.; Henglein, A. *Chem. Phys. Lett.* **1994**, *221*, 363–367.

[97] Anthony, R. J.; Rowe, D. J.; Stein, M.; Yang, J.; Kortshagen, U. *Adv. Funct. Mater.* **2011**, *21*, 4042–4046.

[98] Reboredo, F. A.; Galli, G. *J. Phys. Chem. B* **2005**, *109*, 1072–1078.

[99] Li, Q. S.; Zhang, R. Q.; Niehaus, T. A.; Frauenheim, T.; Lee, S. T. *J. Chem. Theory Comput.* **2007**, *3*, 1518–1526.

[100] Yang, Z.; Iqbal, M.; Dobbie, A. R.; Veinot, J. G. C. *J. Am. Chem. Soc.* **2013**, *135*, 17595–17601.

[101] Kelly, J. A.; Veinot, J. G. C. *ACS Nano* **2010**, *4*, 4645–4656.

[102] Purkait, T. K.; Iqbal, M.; Wahl, M. H.; Gottschling, K.; Gonzalez, C. M.; Islam, M. A.; Veinot, J. G. C. *J. Am. Chem. Soc.* **2014**, *136*, 17914–17917.

[103] Mobarok, M. H.; Purkait, T. K.; Islam, M. A.; Miskolzie, M.; Veinot, J. G. C. *Angew. Chem. Int. Ed.* **2017**, *56*, 6073–6077.

[104] Islam, M. A.; Mobarok, M. H.; Sinelnikov, R.; Purkait, T. K.; Veinot, J. G. C. *Langmuir* **2017**, *33*, 8766–8773.

[105] Höhlein, I. M. D.; Kehrle, J.; Helbich, T.; Yang, Z.; Veinot, J. G. C.; Rieger, B. *Chem. Eur. J.* **2014**, *20*, 4212–4216.

[106] Yang, Z.; Gonzalez, C. M.; Purkait, T. K.; Iqbal, M.; Meldrum, A.; Veinot, J. G. C. *Langmuir* **2015**, *31*, 10540–10548.

[107] Helbich, T.; Kloberg, M. J.; Sinelnikov, R.; Lyuleeva, A.; Veinot, J. G. C.; Rieger, B. *Nanoscale* **2017**, *9*, 7739–7744.

[108] Mastronardi, M. L.; Henderson, E. J.; Puzzo, D. P.; Ozin, G. A. *Adv. Mater.* **2012**, *24*, 5890–5898.

[109] Yang, Z.; Wahl, M. H.; Veinot, J. G. *Can. J. Chem.* **2014**, *92*, 951–957.

[110] Kelly, J. A.; Shukaliak, A. M.; Fleischauer, M. D.; Veinot, J. G. C. *J. Am. Chem. Soc.* **2011**, *133*, 9564–9571.

[111] Yu, Y.; Hessel, C. M.; Bogart, T. D.; Panthani, M. G.; Rasch, M. R.; Korgel, B. A. *Langmuir* **2013**, *29*, 1533–1540.

[112] Höhlein, I. M. D.; Angı, A.; Sinelnikov, R.; Veinot, J. G. C.; Rieger, B. *Chem. Eur. J.* **2015**, *21*, 2755–2758.

[113] Angı, A.; Loch, M.; Sinelnikov, R.; Veinot, J. G. C.; Becherer, M.; Lugli, P.; Rieger, B. *Nanoscale* **2018**,

[114] Yang, C.-S.; Bley, R. A.; Kauzlarich, S. M.; Lee, H. W. H.; Delgado, G. R. *J. Am. Chem. Soc.* **1999**, *121*, 5191–5195.

[115] Baldwin, R. K.; Pettigrew, K. A.; Garno, J. C.; Power, P. P.; Liu, G.-y.; Kauzlarich, S. M. *J. Am. Chem. Soc.* **2002**, *124*, 1150–1151.

[116] Pettigrew, K. A.; Liu, Q.; Power, P. P.; Kauzlarich, S. M. *Chem. Mater.* **2003**, *15*, 4005–4011.

[117] Dasog, M.; De los Reyes, G. B.; Titova, L. V.; Hegmann, F. A.; Veinot, J. G. C. *ACS Nano* **2014**, *8*, 9636–9648.

[118] Dasog, M.; Yang, Z.; Regli, S.; Atkins, T. M.; Faramus, A.; Singh, M. P.; Muthuswamy, E.; Kauzlarich, S. M.; Tilley, R. D.; Veinot, J. G. C. *ACS Nano* **2013**, *7*, 2676–2685.

[119] Li, Q.; He, Y.; Chang, J.; Wang, L.; Chen, H.; Tan, Y.-W.; Wang, H.; Shao, Z. *J. Am. Chem. Soc.* **2013**, *135*, 14924–14927.

[120] Wang, L.; Li, Q.; Wang, H.-Y.; Huang, J.-C.; Zhang, R.; Chen, Q.-D.; Xu, H.-L.; Han, W.; Shao, Z.-Z.; Sun, H.-B. *Light Sci. Appl.* **2015**, *4*, e245.

[121] Reyes, G. B. D. l.; Dasog, M.; Na, M.; Titova, L. V.; Veinot, J. G. C.; Hegmann, F. A. *Phys. Chem. Chem. Phys.* **2015**, *17*, 30125–30133.

[122] Shirahata, N.; Furumi, S.; Sakka, Y. *J. Cryst. Growth* **2009**, *311*, 634–637.

[123] Zou, J.; Baldwin, R. K.; Pettigrew, K. A.; Kauzlarich, S. M. *Nano Lett.* **2004**, *4*, 1181–1186.

[124] Purkait, T. K.; Iqbal, M.; Islam, M. A.; Mobarok, M. H.; Gonzalez, C. M.; Hadidi, L.; Veinot, J. G. C. *J. Am. Chem. Soc.* **2016**, *138*, 7114–7120.

[125] Rogozhina, E. V.; Eckhoff, D. A.; Gratton, E.; Braun, P. V. *J. Mater. Chem.* **2006**, *16*, 1421–1430.

[126] Mayeri, D.; Phillips, B. L.; Augustine, M. P.; Kauzlarich, S. M. *Chem. Mater.* **2001**, *13*, 765–770.

[127] Lee, S.; Cho, W. J.; Chin, C. S.; Han, I. K.; Choi, W. J.; Park, Y. J.; Song, J. D.; Lee, J. I. *Jpn. J. Appl. Phys.* **2004**, *43*, L784.

[128] Dasog, M.; Bader, K.; Veinot, J. G. C. *Chem. Mater.* **2015**, *27*, 1153–1156.

[129] P. Bell, J.; E. Cloud, J.; Cheng, J.; Ngo, C.; Kodambaka, S.; Sellinger, A.; Williams, S. K. R.; Yang, Y. *RSC Adv.* **2014**, *4*, 51105–51110.

[130] Ma, Y.; Chen, X.; Pi, X.; Yang, D. *J. Phys. Chem. C* **2011**, *115*, 12822–12825.

[131] Li, Q.; Luo, T.-Y.; Zhou, M.; Abroshan, H.; Huang, J.; Kim, H. J.; Rosi, N. L.; Shao, Z.; Jin, R. *ACS Nano* **2016**, *10*, 8385–8393.

[132] Mastronardi, M. L.; Chen, K. K.; Liao, K.; Casillas, G.; Ozin, G. A. *J. Phys. Chem. C* **2015**, *119*, 826–834.

[133] Varshni, Y. P. *Physica* **1967**, *34*, 149–154.

[134] Vial, J. C.; Bsiesy, A.; Gaspard, F.; Hérino, R.; Ligeon, M.; Muller, F.; Romestain, R.; Macfarlane, R. M. *Phys. Rev. B* **1992**, *45*, 14171–14176.

[135] Hartel, A. M.; Gutsch, S.; Hiller, D.; Zacharias, M. *Phys. Rev. B* **2012**, *85*, 165306.

[136] Maier-Flaig, F.; Henderson, E. J.; Valouch, S.; Klinkhammer, S.; Kübel, C.; Ozin, G. A.; Lemmer, U. *Chem. Phys.* **2012**, *405*, 175–180.

[137] Van Sickle, A. R.; Miller, J. B.; Moore, C.; Anthony, R. J.; Kortshagen, U. R.; Hobbie, E. K. *ACS Appl. Mater. Interfaces* **2013**, *5*, 4233–4238.

[138] Valerini, D.; Cretí, A.; Lomascolo, M.; Manna, L.; Cingolani, R.; Anni, M. *Phys. Rev. B* **2005**, *71*, 235409.

[139] Gaponenko, M. S.; Lutich, A. A.; Tolstik, N. A.; Onushchenko, A. A.; Malyarevich, A. M.; Petrov, E. P.; Yumashev, K. V. *Phys. Rev. B* **2010**, *82*, 125320.

[140] Calcott, P. D. J.; Nash, K. J.; Canham, L. T.; Kane, M. J.; Brumhead, D. *J. Phys.: Condens. Matter* **1993**, *5*, L91.

[141] Calcott, P. D. J.; Nash, K. J.; Canham, L. T.; Kane, M. J.; Brumhead, D. *J. Lumin.* **1993**, *57*, 257–269.

[142] DeBenedetti, W. J. I.; Chiu, S.-K.; Radlinger, C. M.; Ellison, R. J.; Manhat, B. A.; Zhang, J. Z.; Shi, J.; Goforth, A. M. *J. Phys. Chem. C* **2015**, *119*, 9595–9608.

[143] Prtljaga, N.; D'Amato, E.; Pitanti, A.; Guider, R.; Froner, E.; Larcheri, S.; Marina Scarpa,; Pavesi, L. *Nanotechnology* **2011**, *22*, 215704.

[144] Chen, C.-L.; Zeng, J.; Bao, N.; Dai, H.; Gu, H.-Y. *RSC Adv.* **2017**, *7*, 44655–44658.

[145] Lockwood, R.; Yang, Z.; Sammynaiken, R.; Veinot, J. G. C.; Meldrum, A. *Chem. Mater.* **2014**, *26*, 5467–5474.

[146] Rodríguez, J. A.; Vásquez-Agustín, M. A.; Morales-Sánchez, A.; Aceves-Mijares, M. *J. Nanomater.* **2014**, *2014*, 1–17.

[147] Xiong, Y.; Yao, S.; Driess, M. *J. Am. Chem. Soc.* **2009**, *131*, 7562–7563.

[148] Xiong, Y.; Yao, S.; Driess, M. *Angew. Chem. Int. Ed.* **2010**, *49*, 6642–6645.

[149] Muraoka, T.; Abe, K.; Haga, Y.; Nakamura, T.; Ueno, K. *J. Am. Chem. Soc.* **2011**, *133*, 15365–15367.

[150] Filippou, A. C.; Baars, B.; Chernov, O.; Lebedev, Y. N.; Schnakenburg, G. *Angew. Chem. Int. Ed.* **2014**, *53*, 565–570.

[151] Mawhinney, D. B.; Glass, J. A.; Yates, J. T. *J. Phys. Chem. B* **1997**, *101*, 1202–1206.

[152] Kanemitsu, Y. *Phys. Rev. B* **1996**, *53*, 13515–13520.

[153] Koch, F.; Petrova-Koch, V.; Muschik, T. *J. Lumin.* **1993**, *57*, 271–281.

[154] Vasiliev, I.; Chelikowsky, J. R.; Martin, R. M. *Phys. Rev. B* **2002**, *65*, 121302.

[155] Biteen, J. S.; Lewis, N. S.; Atwater, H. A.; Polman, A. *Appl. Phys. Lett.* **2004**, *84*, 5389–5391.

[156] Watson, D. F.; Meyer, G. J. *Annu. Rev. Phys. Chem.* **2004**, *56*, 119–156.

[157] Medintz, I. L.; Mattoussi, H. *Phys. Chem. Chem. Phys.* **2008**, *11*, 17–45.

[158] Groenewegen, V.; Kuntermann, V.; Haarer, D.; Kunz, M.; Kryschi, C. *J. Phys. Chem. C* **2010**, *114*, 11693–11698.

[159] Sommer, A.; Cimpean, C.; Kunz, M.; Oelsner, C.; Kupka, H. J.; Kryschi, C. *J. Phys. Chem. C* **2011**, *115*, 22781–22788.

[160] Locritani, M.; Yu, Y.; Bergamini, G.; Baroncini, M.; Molloy, J. K.; Korgel, B. A.; Ceroni, P. *J. Phys. Chem. Lett.* **2014**, *5*, 3325–3329.

[161] Mazzaro, R.; Locritani, M.; Molloy, J. K.; Montalti, M.; Yu, Y.; Korgel, B. A.; Bergamini, G.; Morandi, V.; Ceroni, P. *Chem. Mater.* **2015**, *27*, 4390–4397.

[162] Fermi, A.; Locritani, M.; Carlo, G. D.; Pizzotti, M.; Caramori, S.; Yu, Y.; Korgel, B. A.; Bergamini, G.; Ceroni, P. *Faraday Discuss.* **2015**, *185*, 481–495.

[163] Song, J. H.; Sailor, M. J. *J. Am. Chem. Soc.* **1997**, *119*, 7381–7385.

[164] Wang, G.; Ji, J.; Xu, X. *J. Mater. Chem. C* **2014**, *2*, 1977–1981.

[165] McVey, B. F. P.; Tilley, R. D. *Acc. Chem. Res.* **2014**, *47*, 3045–3051.

[166] Maier-Flaig, F.; Rinck, J.; Stephan, M.; Bocksrocker, T.; Bruns, M.; Kübel, C.; Powell, A. K.; Ozin, G. A.; Lemmer, U. *Nano Lett.* **2013**, *13*, 475–480.

[167] Choi, J.; Wang, N. S.; Reipa, V. *Bioconjugate Chem.* **2008**, *19*, 680–685.

[168] Gonzalez, C. M.; Veinot, J. G. C. *J. Mater. Chem. C* **2016**, *4*, 4836–4846.

[169] Conibeer, G.; Green, M.; Corkish, R.; Cho, Y.; Cho, E.-C.; Jiang, C.-W.; Fangsuwannarak, T.; Pink, E.; Huang, Y.; Puzzer, T.; Trupke, T.; Richards, B.; Shalav, A.; Lin, K.-l. *Thin Solid Films* **2006**, *511*, 654–662.

[170] Chou, S.-L.; Wang, J.-Z.; Choucair, M.; Liu, H.-K.; Stride, J. A.; Dou, S.-X. *Electrochem. Commun.* **2010**, *12*, 303–306.

[171] Canham, L. T. *phys. stat. sol. (b)* **1995**, *190*, 9–14.

[172] Jurbergs, D.; Rogojina, E.; Mangolini, L.; Kortshagen, U. *Appl. Phys. Lett.* **2006**, *88*, 233116.

[173] Ueda, K.; Tayagaki, T.; Fukuda, M.; Fujii, M.; Kanemitsu, Y. *Phys. Rev. B* **2012**, *86*, 155316.

[174] Ledoux, G.; Gong, J.; Huisken, F.; Guillois, O.; Reynaud, C. *Appl. Phys. Lett.* **2002**, *80*, 4834–4836.

[175] Wilson, W. L.; Szajowski, P. F.; Brus, L. E. *Science* **1993**, *262*, 1242–1244.

[176] Rinnert, H.; Jambois, O.; Vergnat, M. *J. Appl. Phys.* **2009**, *106*, 023501.

[177] Angı, A.; Sinelnikov, R.; Meldrum, A.; Veinot, J. G. C.; Balberg, I.; Azulay, D.; Millo, O.; Rieger, B. *Nanoscale* **2016**, *8*, 7849–7853.

[178] Allan, G.; Delerue, C.; Lannoo, M. *Phys. Rev. Lett.* **1996**, *76*, 2961–2964.

[179] Bludau, W.; Onton, A.; Heinke, W. *J. Appl. Phys.* **1974**, *45*, 1846–1848.

[180] Alex, V.; Finkbeiner, S.; Weber, J. *J. Appl. Phys.* **1996**, *79*, 6943–6946.

[181] Mitra, S.; Švrček, V.; Macias-Montero, M.; Velusamy, T.; Mariotti, D. *Sci. Rep-UK* **2016**, *6*, srep27727.

[182] Wen, X.; Dao, L. V.; Hannaford, P. *J. Phys. D: Appl. Phys.* **2007**, *40*, 3573.

[183] Sykora, M.; Mangolini, L.; Schaller, R. D.; Kortshagen, U.; Jurbergs, D.; Klimov, V. I. *Phys. Rev. Lett.* **2008**, *100*, 067401.

[184] Hartel, A. M.; Gutsch, S.; Hiller, D.; Zacharias, M. *Phys. Rev. B* **2013**, *87*, 035428.

[185] Okada, K.; Kameshima, Y.; Yasumori, A. *J. Am. Ceram. Soc.* **1998**, *81*, 1970–1972.

[186] Rusch, P. F.; Lelieur, J. P. *Anal. Chem.* **1973**, *45*, 1541–1543.

[187] Kovalev, D.; Diener, J.; Heckler, H.; Polisski, G.; Künzner, N.; Koch, F. *Phys. Rev. B* **2000**, *61*, 4485–4487.

[188] Belyakov, V. A.; Burdov, V. A.; Lockwood, R.; Meldrum, A. *Adv. Opt. Tech. 2008*, 1–32.

[189] Sakuda, E.; Ando, Y.; Ito, A.; Kitamura, N. *Inorg. Chem.* **2011**, *50*, 1603–1613.

[190] Suzuki, T.; Ohishi, Y. *Appl. Phys. Lett.* **2006**, *88*, 191912.

[191] van Dijken, A.; Meulenkamp, E. A.; Vanmaekelbergh, D.; Meijerink, A. *J. Phys. Chem. B* **2000**, *104*, 1715–1723.

[192] Pavesi, L. *J. Appl. Phys.* **1996**, *80*, 216–225.

[193] Linnros, J.; Lalic, N.; Galeckas, A.; Grivickas, V. *J. Appl. Phys.* **1999**, *86*, 6128–6134.

[194] van Driel, A. F.; Nikolaev, I. S.; Vergeer, P.; Lodahl, P.; Vanmaekelbergh, D.; Vos, W. L. *Phys. Rev. B* **2007**, *75*, 035329.

[195] Nguyen, A.; Gonzalez, C. M.; Sinelnikov, R.; Newman, W.; Sun, S.; Lockwood, R.; Veinot, J. G. C.; Meldrum, A. *Nanotechnology* **2016**, *27*, 105501.

[196] Garcia, C.; Garrido, B.; Pellegrino, P.; Ferre, R.; Moreno, J. A.; Morante, J. R.; Pavesi, L.; Cazzanelli, M. *Appl. Phys. Lett.* **2003**, *82*, 1595–1597.

[197] Li, Q. S.; Zhang, R. Q.; Lee, S. T.; Niehaus, T. A.; Frauenheim, T. *J. Chem. Phys.* **2008**, *128*, 244714.

[198] Dierre, B.; Xie, R.-J.; Hirosaki, N.; Sekiguchi, T. *J. Mater. Res.* **2007**, *22*, 1933–1941.

[199] Dal Negro, L.; Yi, J. H.; Michel, J.; Kimerling, L. C.; Chang, T.-W. F.; Sukhovatkin, V.; Sargent, E. H. *Appl. Phys. Lett.* **2006**, *88*, 233109–233102.

[200] Boer, W. D. A. M. d.; Timmerman, D.; Dohnalová, K.; Yassievich, I. N.; Zhang, H.; Buma, W. J.; Gregorkiewicz, T. *Nat. Nano* **2010**, *5*, 878–884.

[201] Gowrishankar, V.; Scully, S. R.; McGehee, M. D.; Wang, Q.; Branz, H. M. *Appl. Phys. Lett.* **2006**, *89*, 252102–252105.

[202] Luppi, E.; Iori, F.; Magri, R.; Pulci, O.; Ossicini, S.; Degoli, E.; Olevano, V. *Phys. Rev. B* **2007**, *75*, 033303–033307.

[203] Trojánek, F.; Neudert, K.; Malý, P.; Dohnalová, K.; Pelant, I. *J. Appl. Phys.* **2006**, *99*, 116108–116111.

[204] Dohnalová, K.; Kůsová, K.; Pelant, I. *Appl. Phys. Lett.* **2009**, *94*, 211903–211906.

[205] Burfeindt, B.; Hannappel, T.; Storck, W.; Willig, F. *J. Phys. Chem.* **1996**, *100*, 16463–16465.

[206] von Bardeleben, H. J.; Stievenard, D.; Grosman, A.; Ortega, C.; Siejka, J. *Phys. Rev. B* **1993**, *47*, 10899–10902.

[207] Ondič, L.; Kůsová, K.; Ziegler, M.; Fekete, L.; Gärtnerová, V.; Cháb, V.; Holý, V.; Cibulka, O.; Herynková, K.; Gallart, M.; Gilliot, P.; Hönerlage, B.; Pelant, I. *Nanoscale* **2014**, *6*, 3837–3845.

[208] Fucikova, A.; Valenta, J.; Pelant, I.; Kalbacova, M. H.; Broz, A.; Rezek, B.; Kromka, A.; Bakaeva, Z. *RSC Adv.* **2014**, *4*, 10334–10342.

[209] Cheng, X.; Lowe, S. B.; Reece, P. J.; Gooding, J. J. *Chem. Soc. Rev.* **2014**, *43*, 2680–2700.

[210] Cheng, K.-Y.; Anthony, R.; Kortshagen, U. R.; Holmes, R. J. *Nano Lett.* **2010**, *10*, 1154–1157.

[211] Mastronardi, M. L.; Henderson, E. J.; Puzzo, D. P.; Chang, Y.; Wang, Z. B.; Helander, M. G.; Jeong, J.; Kherani, N. P.; Lu, Z.; Ozin, G. A. *Small* **2012**, *8*, 3647–3654.

[212] Tischler, M. A.; Collins, R. T.; Stathis, J. H.; Tsang, J. C. *Appl. Phys. Lett.* **1992**, *60*, 639–641.

[213] Prokes, S. M. *Appl. Phys. Lett.* **1993**, *62*, 3244–3246.

[214] Harper, J.; Sailor, M. J. *Langmuir* **1997**, *13*, 4652–4658.

[215] Kim, S.; Shin, D. H.; Choi, S.-H. *Appl. Phys. Lett.* **2012**, *100*, 253103–253106.

[216] Jariwala, B. N.; Dewey, O. S.; Stradins, P.; Ciobanu, C. V.; Agarwal, S. *ACS Appl. Mater. Interfaces* **2011**, *3*, 3033–3041.

[217] Rinck Julia,; Schray Dirk,; Kübel Christian,; Powell Annie K.,; Ozin Geoffrey A., *Small* **2015**, *11*, 335–340.

[218] Bürkle, M.; Lozac'h, M.; McDonald, C.; Mariotti, D.; Matsubara, K.; Švrček, V. *Adv. Funct. Mater.* **2017**, *27*, 1701898–1701905.

[219] Puzder, A.; Williamson, A. J.; Grossman, J. C.; Galli, G. *Phys. Rev. Lett.* **2002**, *88*, 097401–097405.

[220] Luppi Marcello,; Ossicini Stefano, *Phys. Status Solidi A* **2003**, *197*, 251–256.

[221] Luppi, M.; Ossicini, S. *Phys. Rev. B* **2005**, *71*, 035340–035355.

[222] Martin, J.; Cichos, F.; Huisken, F.; von Borczyskowski, C. *Nano Lett.* **2008**, *8*, 656–660.

[223] Kang, Z.; Liu, Y.; Tsang, C. H. A.; Ma, D. D. D.; Fan, X.; Wong, N.-B.; Lee, S.-T. *Adv. Mater.* **2009**, *21*, 661–664.

[224] Camilletti, R. C.; Haluska, L. A.; Michael, K. W. United States Patent: 5776235 - Thick opaque ceramic coatings. 1998.

[225] Hiruoka, M.; Sato, K.; Hirakuri, K. *J. Appl. Phys.* **2007**, *102*, 024308–024312.

[226] Kovalev, D.; Gross, E.; Diener, J.; Timoshenko, V. Y.; Fujii, M. *Appl. Phys. Lett.* **2004**, *85*, 3590–3592.

[227] Kovalev, D.; Fujii, M. *Adv. Mater.* **2005**, *17*, 2531–2544.

[228] Carlisle, J. A.; Dongol, M.; Germanenko, I. N.; Pithawalla, Y. B.; El-Shall, M. S. *Chem. Phys. Lett.* **2000**, *326*, 335–340.

[229] Ledoux, G.; Gong, J.; Huisken, F. *Appl. Phys. Lett.* **2001**, *79*, 4028–4030.

[230] Ledoux, G.; Guillois, O.; Porterat, D.; Reynaud, C.; Huisken, F.; Kohn, B.; Paillard, V. *Phys. Rev. B* **2000**, *62*, 15942–15951.

[231] Sinelnikov, R.; Dasog, M.; Beamish, J.; Meldrum, A.; Veinot, J. G. C. *ACS Photonics* **2017**, *4*, 1920–1929.

[232] Sa'ar, A.; Reichman, Y.; Dovrat, M.; Krapf, D.; Jedrzejewski, J.; Balberg, I. *Nano Lett.* **2005**, *5*, 2443–2447.

[233] Resch-Genger, U.; Grabolle, M.; Cavaliere-Jaricot, S.; Nitschke, R.; Nann, T. *Nat. Methods* **2008**, *5*, 763–775.

[234] Spanhel, L.; Haase, M.; Weller, H.; Henglein, A. *J. Am. Chem. Soc.* **1987**, *109*, 5649–5655.

[235] Wang, X.; Qu, L.; Zhang, J.; Peng, X.; Xiao, M. *Nano Lett.* **2003**, *3*, 1103–1106.

[236] Yu, W. W.; Qu, L.; Guo, W.; Peng, X. *Chem. Mater.* **2003**, *15*, 2854–2860.

[237] Derfus, A. M.; Chan, W. C. W.; Bhatia, S. N. *Nano Lett.* **2004**, *4*, 11–18.

[238] Patalay, R.; Talbot, C.; Alexandrov, Y.; Munro, I.; Neil, M. A. A.; König, K.; French, P. M. W.; Chu, A.; Stamp, G. W.; Dunsby, C. *Biomed. Opt. Express* **2011**, *2*, 3295–3308.

[239] Bhattacharjee, S. et al. *Nanoscale* **2013**, *5*, 4870–4883.

[240] Sychugov, I.; Fucikova, A.; Pevere, F.; Yang, Z.; Veinot, J. G. C.; Linnros, J. *ACS Photonics* **2014**, *1*, 998–1005.

[241] Wilcoxon, J. P.; Samara, G. A.; Provencio, P. N. *Phys. Rev. B* **1999**, *60*, 2704–2714.

[242] Bruhn, B.; Qejvanaj, F.; Sychugov, I.; Linnros, J. *J. Phys. Chem. C* **2014**, *118*, 2202–2208.

[243] Beljonne, D.; Curutchet, C.; Scholes, G. D.; Silbey, R. J. *J. Phys. Chem. B* **2009**, *113*, 6583–6599.

[244] Zhou, T.; Anderson, R. T.; Li, H.; Bell, J.; Yang, Y.; Gorman, B. P.; Pylypenko, S.; Lusk, M. T.; Sellinger, A. *Nano Lett.* **2015**, *15*, 3657–3663.

[245] Wang, R.; Pi, X.; Yang, D. *J. Phys. Chem. C* **2012**, *116*, 19434–19443.

[246] Erogbogbo, F.; Chang, C.-W.; May, J.; Prasad, P. N.; Swihart, M. T. *Nanoscale* **2012**, *4*, 5163–5168.

[247] Le, T.-H.; Jeong, H.-D. *Phys. Chem. Chem. Phys.* **2014**, *16*, 18821–18826.

[248] Abdelhameed, M.; Martir, D. R.; Chen, S.; Xu, W. Z.; Oyeneye, O. O.; Chakrabarti, S.; Zysman-Colman, E.; Charpentier, P. A. *Sci. Rep-UK* **2018**, *8*, 3050.

[249] Tamao, K.; Sumitani, K.; Kumada, M. *J. Am. Chem. Soc.* **1972**, *94*, 4374–4376.

[250] Banin, U.; Millo, O. *Annu. Rev. Phys. Chem.* **2003**, *54*, 465–492.

[251] Bakkers, E. P. A. M.; Vanmaekelbergh, D. *Phys. Rev. B* **2000**, *62*, R7743–R7746.

[252] Bakkers, E. P. A. M.; Hens, Z.; Zunger, A.; Franceschetti, A.; Kouwenhoven, L. P.; Gurevich, L.; Vanmaekelbergh, D. *Nano Lett.* **2001**, *1*, 551–556.

[253] Banin, U.; Cao, Y.; Katz, D.; Millo, O. *Nature* **1999**, *400*, 542–544.

[254] Ganesan, P.; Rajadurai, V. S.; Sivanadanam, J.; Ponnambalam, V.; Rajalingam, R. *J. Photoch. Photobio. A* **2013**, *271*, 31–44.

[255] Kathiravan, A.; Panneerselvam, M.; Sundaravel, K.; Pavithra, N.; Srinivasan, V.; Anandan, S.; Jaccob, M. *Phys. Chem. Chem. Phys.* **2016**, *18*, 13332–13345.

[256] Millo, O.; Balberg, I.; Azulay, D.; Purkait, T. K.; Swarnakar, A. K.; Rivard, E.; Veinot, J. G. C. *J. Phys. Chem. Lett.* **2015**, *6*, 3396–3402.

[257] Franceschetti, A.; Zunger, A. *Phys. Rev. B* **2000**, *62*, 2614–2623.

[258] Choi, J.-K.; Jang, S.; Kim, K.-J.; Sohn, H.; Jeong, H.-D. *J. Am. Chem. Soc.* **2011**, *133*, 7764–7785.

[259] Qian, C.; Sun, W.; Wang, L.; Chen, C.; Liao, K.; Wang, W.; Jia, J.; Hatton, B. D.; Casillas, G.; Kurylowicz, M.; Yip, C. M.; Mastronardi, M. L.; Ozin, G. A. *J. Am. Chem. Soc.* **2014**, *136*, 15849–15852.

[260] Jang, E.; Jun, S.; Jang, H.; Lim, J.; Kim, B.; Kim, Y. *Adv. Mater.* **2010**, *22*, 3076–3080.

[261] Kim, T.-H.; Cho, K.-S.; Lee, E. K.; Lee, S. J.; Chae, J.; Kim, J. W.; Kim, D. H.; Kwon, J.-Y.; Amaratunga, G.; Lee, S. Y.; Choi, B. L.; Kuk, Y.; Kim, J. M.; Kim, K. *Nat. Photonics* **2011**, *5*, 176–182.

[262] Shirasaki, Y.; Supran, G. J.; Bawendi, M. G.; Bulović, V. *Nat. Photonics* **2013**, *7*, 13–23.

[263] Hanrahan, M. P.; Fought, E. L.; Windus, T. L.; Wheeler, L. M.; Anderson, N. C.; Neale, N. R.; Rossini, A. J. *Chem. Mater.* **2017**, *29*, 10339–10351.

[264] Aguiar, P. M.; Michaelis, V. K.; McKinley, C. M.; Kroeker, S. *J. Non-Cryst. Solids* **2013**, *363*, 50–56.

[265] Michaelis, V. K.; Keeler, E. G.; Ong, T.-C.; Craigen, K. N.; Penzel, S.; Wren, J. E. C.; Kroeker, S.; Griffin, R. G. *J. Phys. Chem. B* **2015**, *119*, 8024–8036.

[266] Keeler, E. G.; Michaelis, V. K.; Colvin, M. T.; Hung, I.; Gor'kov, P. L.; Cross, T. A.; Gan, Z.; Griffin, R. G. *J. Am. Chem. Soc.* **2017**, *139*, 17953–17963.

[267] Gonzalez, C. M.; Iqbal, M.; Dasog, M.; Piercey, D. G.; Lockwood, R.; Klapötke, T. M.; Veinot, J. G. C. *Nanoscale* **2014**, *6*, 2608–2612.

[268] Palaniappan, K.; Xue, C.; Arumugam, G.; Hackney, S. A.; Liu, J. *Chem. Mater.* **2006**, *18*, 1275–1280.

[269] Freeman, R.; Finder, T.; Bahshi, L.; Willner, I. *Nano Lett.* **2009**, *9*, 2073–2076.

[270] Fang, G.; Xu, M.; Zeng, F.; Wu, S. *Langmuir* **2010**, *26*, 17764–17771.

[271] Vrkoslav, V.; Jelínek, I.; Trojan, T.; Jindřich, J.; Dian, J. *Physica E* **2007**, *38*, 200–204.

[272] Pavesi, L.; Negro, L. D.; Mazzoleni, C.; Franzò, G.; Priolo, F. *Nature* **2000**, *408*, 440.

[273] Digonnet, M. J. F. *Rare-earth-doped fiber lasers and amplifiers*, 2nd ed.; Marcel Dekker,: New York :, 2001.

[274] Palm, J.; Gan, F.; Zheng, B.; Michel, J.; Kimerling, L. C. *Phys. Rev. B* **1996**, *54*, 17603–17615.

[275] Kenyon, A. J.; Chryssou, C. E.; Pitt, C. W.; Shimizu-Iwayama, T.; Hole, D. E.; Sharma, N.; Humphreys, C. J. *J. Appl. Phys.* **2001**, *91*, 367–374.

[276] Han, H.-S.; Seo, S.-Y.; Shin, J. H. *Appl. Phys. Lett.* **2001**, *79*, 4568–4570.

[277] Makarova, M.; Sih, V.; Warga, J.; Li, R.; Dal Negro, L.; Vuckovic, J. *Appl. Phys. Lett.* **2008**, *92*, 161107.

[278] Franzò, G.; Vinciguerra, V.; Priolo, F. *Appl. Phys. A* **1999**, *69*, 3–12.

[279] St. John, J.; Coffer, J. L.; Chen, Y.; Pinizzotto, R. F. *J. Am. Chem. Soc.* **1999**, *121*, 1888–1892.

[280] Wang, X.; Li, P.; Malac, M.; Lockwood, R.; Meldrum, A. *phys. status solidi c* **2011**, *8*, 1038–1043.